NOTICE

The quality of this microform is heavily dependent upon the quality of the original thesis submitted for microfilming. Every effort has been made to ensure the highest quality of reproduction possible.

If pages are missing, contact the university which granted the degree.

Some pages may have indistinct print especially if the original pages were typed with a poor typewriter ribbon or if the university sent us an inferior photocopy.

Previously copyrighted materials (journal articles, published tests, etc.) are not filmed.

Reproduction in full or in part of this microform is governed by the Canadian Copyright Act, R.S.C. 1970, c. C-30.

AVIS

La qualité de cette microforme dépend grandement de la qualité de la thèse soumise au microfilmage. Nous avons tout fait pour assurer une qualité supérieure de reproduction.

S'il manque des pages, veuillez communiquer avec l'université qui a conféré le grade.

La qualité d'impression de certaines pages peut laisser à désirer, surtout si les pages originales ont été dactylographiées à l'aide d'un ruban usé ou si l'université nous a fait parvenir une photocopie de qualité inférieure.

Les documents qui font déjà l'objet d'un droit d'auteur (articles de revue, tests publiés, etc.) ne sont pas microfilmés.

La reproduction, même partielle, de cette microforme est soumise à la Loi canadienne sur le droit d'auteur, SRC 1970, c. C-30.

Canada

Solvent Exchange Drying of Gas Separation Membranes

Amy M. Y. Lui
Department of Chemical Engineering
University of Ottawa

June 21, 1988

ISBN 0-315-46806-8

UNIVERSITÉ D'OTTAWA
UNIVERSITY OF OTTAWA

Acknowledgement

I would like to especially acknowledge and thank my supervisors for their assistance in the completion of this thesis: Dr. F.D.F. Talbot, Professor of Chemical Engineering at the University of Ottawa for assistance, advice and patience; Dr. T. Matsuura, Senior Research Officer at the National Research Council for his insight and knowledge.

I would like to thank Mr. M.R. Margerum for his help using Latex and also his support throughout.

I would also like to acknowledge the expert assistance of all the people in the Chemical Engineering Section and the library staff of the Chemistry Division at the National Research Council.

Contents

List of Tables

List of Figures

Chapter 1

Introduction

This thesis is about gas separation using dry cellulose acetate membranes. Gas separation membranes are generally prepared in a water-wet condition and various techniques have been tested for the removal of water to dryness. It is necessary to keep the asymmetric cellulose acetate membrane structure intact in order to yield a dry membrane suitable for gas separation. The solvent exchange technique is used in this study. The effects of shrinkage temperatures, various solvents, feed gas compositions and operating pressures are investigated. The gas system that was studied was methane-carbon dioxide. The separation factors and permeation coefficients are used as a measure of performance.

1.1 Separation Membranes

Prior to thirty years ago, although known and understood, membrane separations were not used due to marginal efficiency, limited durability, and high costs. The major problems were poor selectivities and/or permeabilities of early membrane materials. Separation using these membrane materials was not practical, because the process with these handicaps was too uneconomical. A low permeation rate makes the process so slow that very large membrane areas would be necessary to get any appreciable amounts of permeate, thus creating high capital costs. Selectivity is also very important. To cite an example, the enrichment of U^{235} was expensive because the barriers used had very low selectivities, thus requiring many energy intensive stages. As a consequence, very large surface areas, often in multistage configurations, were required to provide acceptable levels of enrichment at acceptable flow rates. Multistage configurations created an extra expense

of interstage compression that was required to raise the pressure of the permeate stream before it entered the subsequent stage of the separation unit. In addition, it was necessary to find a good physical support for a large surface area of a thin membrane. From basic theory, the permeation rate (the rate at which a gas permeates through the membrane) increases with pressure (the driving force for the separation process). It is important to have a thin membrane, since a thick one requires a higher pressure for a reasonable permeation rate, since permeation rate is inversely proportional to the thickness.

Major breakthroughs in membrane research occurred in the 1950's and 1960's. Charles Reid et al. [68] found that cellulose acetate–acetone solutions produced a membrane that would allow a separation of fresh water from seawater with a relatively good selectivity. However, reasonable permeation rates were only achieved at high pressures, due to the thickness of the membrane. Loeb and Sourirajan developed an asymmetric cellulose acetate membrane [36,71] 500 times more permeable to water than Reid's membrane. These high flux membranes consisted of two layers, a thin separating or rejecting layer and a larger porous supporting layer. They were the beginning of the reverse osmosis industry.

1.2 Applications of Membranes

In the last three decades, there have been many companies active in membrane development. Companies such as Filmtec (Dow), UOP, Hydranautics, Toray, Toyobo, DuPont and Monsanto have been manufacturing membranes for a variety of applications [94]. Until recently, most of these applications were in the liquid separation field. In the last decade, it has been shown that gas separation using membranes is both practical and economical [35].

Membranes have been used in many areas. They have been applied to toxic waste filtration, salt and chlorine production, and seawater desalination. More recently, membrane applications include gas extraction and reclamation (separation), metals recovery, the design of controlled-release drug capsules, protein harvesting, monoclonal antibody production, food and beverage purification, and ionic transport in battery cells [65].

1.3 Gas Separation Membranes

Observations of transport of gases and vapors in polymeric membranes date back to the early 1800's [79]. Thomas Graham was the first to report a partial separation of gases in 1866. This gas separation was performed by means of different permeation velocities of various gases through a membrane [25].

In the early 1940's, gas diffusion through membranes was used to enrich the isotope U^{235} in uranium from 0.71 % to about 3.0 % by weight. This was done using large gaseous diffusion facilities for the isotopic enrichment of UF_6 [28]. It was extremely expensive, but there were no practical alternatives [95]. Membrane separations discussed in this thesis are different from barrier separations used in the uranium enrichment plant at Oak Ridge, Tennessee. In barrier separation, gases of differing molecular weights are separated by differing gaseous diffusion rates within the porous media.

The separation of gases was one of the first applications conceived for membranes. However, the same problem of poor selectivity and low permeation rates occurred. Also, once a good wet membrane with a good permselectivity (permeability and selectivity) towards salt was found, they often resulted in poor dried membranes. Liquid separation membranes are designed with respect to salt rejection (i.e. a good/practical membrane for the liquid case is where salt rejection is high). These wet membranes usually have a high water content, with water remaining within the pore structure. To make a dry membrane for gas separation (a wet membrane cannot be used for this application) the water must be removed. A good method of drying the wet membrane was necessary, where the pore structure would be retained. If the wet membrane was left to air-dry, the water would evaporate, leaving a collapsed pore structure. The pore structure must be retained since that is what allows permeation as well as the selectivity. This will be discussed to a greater extent later.

Gas separation membranes are expected to be considerably improved in the future as membranes specifically designed for gas separation become available, as opposed to membranes adapted from liquid reverse osmosis membranes [3].

1.4 Advantages of Membrane Separation

Until recently, gas separation using membranes was not ready for competition with other processes such as distillation, physical adsorption, chemical

absorption, and direct conversion processes [35]. Nevertheless, the above techniques can be quite expensive to maintain and operate, since they usually require large and complex process plants. Thus, much effort was expended to improve alternate separation techniques, the area of membranes being one of them. Although gas separation is still considered as a relatively new field of membrane technology and much research is devoted to this area, it now ranks as one of the most important membrane applications [65]. Research has made membrane processes competitive with other gas separation methods. It is now a method of choice.

Henis and Tripodi [27] point out some reasons why it is often the method of choice. The strongest advantages of membrane systems are compactness, flexibility and simplicity. They are no more likely to fail mechanically than a heat exchanger (they are similar in many ways) and have no moving parts, thus they require minimal operator attention. They are modular [40] offering more flexibility in design and operation. Units can be replaced, if they fail, without much change to the overall process output. Membrane systems are able to handle changing capacity requirements easily by turning sections on or off as needed. This fact is important economically as a plant can be enlarged as necessary by adding new units. This arrangement also is attractive for plant retrofitting. Since they are usually smaller in size and more modular than the old equipment, they fit into existing plant structures, not requiring new construction [94]. Start-up and shutdown time is also very short. They are less energy intensive and more economical to operate.

1.5 Requirements for Gas Separation

Henis and Tripodi [27] discuss improvements to membrane systems since the 1950's. Membrane systems had to fulfill the following requirements in order to become competitive:

- Membranes had to exhibit a higher gas flux of three to four orders of magnitude over those existing at the time.
- A reasonably high selectivity was needed (at least > 20).
- Membranes had to be able to operate at pressures around 2000 to 3000 psi(13.800 and 20.684 MPa).

- Membranes had to maintain their properties and function in the presence of a variety of contaminants, at varying concentrations and over a reasonable range of temperatures (between 0 to 100 °C).
- Membranes had to be compatible with large scale modules and seals, have systems with optimized flow and distribution of gases to the membrane, and remain stable in process environments.

These goals have been met in the last 30 years.

According to Baldus and Tillman [4], membrane technology might be most advantageously employed:

- when only moderate purity and recovery rates are sufficient.
- when large concentrations of the components to be separated are in the feed gas.
- when the feed gas is available at the needed pressure or when the retentate is needed at high pressure.
- when the components of the feed gas do not alter or destroy the membrane.
- when a membrane is available with a sufficient selectivity towards gases to be separated.

1.6 Applications of Gas Membranes

Stookey et al. [82] list how membranes have been applied to many commercial gas separation processes. Among the most important are CO_2 separations:

- *Carbon Dioxide for EOR Flood:* Carbon dioxide is recovered from gases produced in EOR (enhanced oil recovery) floods for recycle.
- *Pipeline Natural Gas:* Moisture and carbon dioxide are removed from natural gases to upgrade them to pipeline or fuel specification [14].
- *Landfill Gas:* Salable methane is recovered by removing carbon dioxide and water from biogas generated by anaerobic decomposition of wastes in sanitary landfills.

- *Digester Gas:* As with landfill gas processing, digester off-gas can be upgraded to salable or usable fuel by carbon dioxide removal.

Studies have shown that membrane technology can separate effectively at both high and low carbon dioxide concentrations [24,12]. It has also been suggested that a membrane separation unit could be used in conjunction with another type of separation unit. Using a membrane separation unit as a pretreatment stage to remove bulk carbon dioxide from a gas stream could allow a smaller, cheaper absorption unit (Benfield type) [74] to carry out the final carbon dioxide removal. Since only half to two-thirds of the carbon dioxide content need be removed by a membrane unit in the combined case, a small membrane unit would be sufficient. Estimates of cost usually indicate that the combined systems would be more economical than either an absorption or a membrane unit alone [35].

Laverty and O'Hair [35] discuss using membrane technology for the removal of carbon dioxide, specifically in the area of offshore removal of carbon dioxide from natural gas. This illustrates many of the advantages of membrane processes. Carbon dioxide occurs in natural gas and many of the North Sea fields possess appreciable amounts of it (e.g. the Sleipner field in the Norwegian sector). Methane is lost when the carbon dioxide is vented. To reduce operating costs, a separation system is required to minimize the amount of methane lost.

There are various reasons for removing the carbon dioxide offshore at the well heads. Meeting the transmission standards is one reason, another is that carbon dioxide can be corrosive in the presence of water. By separating the carbon dioxide at the well head, the bulk of gas that needs to be transported is reduced, thus reducing the amount of compression power required to land the gas. This would also result in a reduction in the pipeline size for natural gas with extremely high carbon dioxide content.

Separation of carbon dioxide from the associated hydrocarbon gases from oil fields using EOR techniques is another offshore use. Carbon dioxide is injected at high pressures and depths into oil reservoirs to stimulate the recovery of oil. After some time, carbon dioxide begins to emerge with the hydrocarbon gases typically recovered with the oil. The carbon dioxide must be relatively pure to be effective in this application [27]. Recovery and recompression of the carbon dioxide for reinjection greatly reduces the cost of applying EOR offshore. Bulk removal is especially important where EOR techniques are used.

Another reason for using a membrane process offshore is that the area available for a purification plant is limited and membranes are ideal for

these situations. The constraints of the platform construction also limit the weight of the plant. Membrane separation units are modular in design and are more compact than absorption plants. Membrane systems can easily accommodate additional units in parallel or series to adapt to changing feed composition and flow rate of the associated gas from the field [72]. They also have negligible start up times and require little maintenance, thus making the use of membrane separation units not only suitable but competitive for offshore deployment.

1.7 Economics

Among the reasons membranes have been used for gas separations are simplicity and reduced operating costs. Thus, economics are very much another consideration in the design. Reverse osmosis consumes much less energy than other processes, only about a third to one half as much energy compared to multistage flash distillation [65]. The capital costs are comparable with other plants, membranes being generally better for small scale applications. The economics are especially attractive when the gas is already at high pressure.

The two most important economic factors are feed (or permeate) compression power and the membrane area. These two factors are inversely proportional since for a larger membrane area a lower operating pressure is required to obtain the same flux. Thus there is an optimal operating scheme for a given set of conditions for a particular separation [72].

The potential sales of membrane products, technologies and systems in 1985 were about $500 million. They are projected to total $2 billion by 1995. Similarly, membrane gas separation systems is expected to grow from $25 million in 1985 to $500 million in 1995. There are two basic applications for the separation of carbon dioxide (sweetening natural gas and reuse in tertiary oil recovery) and if commercialized to their full potential they could have a dollar value of more than 150 million a year [94].

1.8 Solvent Exchange Technique

The term solvent exchange refers to exchanging water within the pores with solvents. Various solvents can be used and the number of different solvents used for this process can also vary. Most often one, two or three solvents are used for this process. The objective of solvent exchange is to keep the

pores of the membrane intact while changing the medium within from a polar to a non-polar substance. The membrane is then allowed to air dry. When the substance within the pore is polar, the pores would collapse upon evaporation of the substance.

Research in the area of solvent exchanging is necessary. Although the solvent exchange technique has been known for many years, the actual solvents which give the best results are still unknown. The actual method needs optimization as to the number of steps each solvent should be replaced in, how many solvents are needed, solvents with what properties yield the best results, and how long should the membranes be immersed in each solvent before the system reaches equilibrium. In this thesis, work has been done towards answering these questions.

Chapter 2

Literature Review

2.1 Areas of Research

Research for gas separation has been concentrated in several areas. One is to find the adequate materials which the membrane can be made, since separation technology tends to be very site or application specific [94]. There are hundreds of materials available, each with its own structural and chemical characteristics. The key is to find a material with good selectivity, productivity and durability. Usually, polymers are used. Among the most promising are cellulose acetate, polysulfones with a silicone rubber coating and some polyamides. However, cellulose acetate still remains the standard to which "best" membrane performance is compared [8]. Inorganic materials such as ceramics, steel and carbon are also being looked at to handle some rigorous industrial environments [83].

Research is also done to determine the type of membrane which performs best. The types vary in the way they were made. The types most widely used are cellulose acetate Loeb-Sourirajan membranes, silicone rubber coated Loeb-Sourirajan polysulfone membranes or Ward-Riley composite membranes [3]. For gas separation there is the additional problem of finding an optimum method for drying the membrane. Simple air drying results in very poor gas separation membranes. The solvent exchange drying technique is being investigated in this thesis.

The configuration of the separation module is important. Membranes in the form of flat sheets provide a very low surface area to permeator volume ratio, so they are not acceptable. In the past, plate and frame or tube in shell modules were used but were found to be quite expensive. Hollow fiber and flat sheet spiral wound membranes are the chief competitors in

industry at present. Sufficient surface area is necessary to provide a high permeation rate [79]. Both of the above meet this criterion. Hollow fibers are said to have three times more surface area. The spiral wound types can be mounted vertically or horizontally. Essentially, both do the same job and the one used depends on the application [64], the goal being to find a configuration that compactly and inexpensively support the large surface area of a thin membrane. Presently, both of these configurations are used in gas separations.

Practical applicability of reverse osmosis has been greatly limited by the availability of a membrane suitable for a particular purpose. The appropriate membrane could, however, be formulated on a rational basis if the mechanism of transport through the membrane was properly understood. This understanding is also important for membrane and system specifications and predictability of their performances, which are fundamental to reverse osmosis engineering [48]. A firm cause and effect relationship must therefore be known. The number of ways in which a permeant gas can interact with a membrane are many and therefore it is difficult to formulate a single explanation of the complex transport processes. Researchers have developed a number of phenomenological and physicochemical models for membrane transport. There are two major competing theories, pore flow and diffusive flow. The first is called the Surface-Force-Pore-Flow mechanism and the second is the Solution-Diffusion model.

A major problem with membrane technology is the reproducibility of results. The rejection rate in membrane production can be as high as fifty percent. Statistical work and optimization using factorial design has been done to identify areas of large variation. If these variations could be reduced, then membranes would not be wasted when they do not meet requirements [9,26]. Many authors have designed their experiments statistically to minimize the number of experimental tests required and to facilitate data analysis [8,9].

One of the goals of current research and development is to develop membranes that can operate in harsh environments (i.e. higher temperatures or concentrated chemical environments). Other goals still remain to be higher permeability (productivity) and selectivity (purity) [64].

A major area of research is making and drying membranes. Cellulose acetate membranes for water desalination must be stored in water to maintain their permeation performance. However, for gas permeation, the membranes must be dried properly; otherwise they will lose their permeation properties due to plastic creep of the soft material under pressure.

Also, they lose these properties when the microporous sublayer collapses and thus increases the thickness of the skin layer. Gas separation membranes are generally still prepared in a water-wet condition, and various techniques have been tested for the removal of water to dryness [41]. Carefully controlled direct-drying techniques were tried but were found to be quite unsatisfactory. It resulted in the destruction of the membrane structure, which is critical for gas separation. In the next few sections these various areas will be discussed in further detail.

2.2 Models

2.2.1 Various Models Suggested

As mentioned above, there are several approaches towards understanding the basic mechanisms, several papers exist in this area. Irreversible thermodynamics and the Finely-Porous are two of the approaches. However, most of the approaches fall into two categories, porous and non-porous. " In the first case, the membrane is considered as a bundle of capillaries where the flow is determined by the application of Poiseuille's equation. The other case involves dissolution of the components in the membrane followed by diffusion through the membrane." [48]. These principle approaches and the extent of their usefulness are discussed further.

Irreversible Thermodynamics The first practical model was developed by Kedem and Katchalsky [31]. This model was for transfer of non-electrolytes through membranes and was extended to electrolytes. It is an elegant model and works well when the structure of the membrane is not known and the molecular mechanisms of transport processes within the membrane are not fully understood. However, the parameters are not related to any physical characteristics, since this approach treats the membrane as a " black box ".

Solution-Diffusion This model was developed by Lonsdale et al. [38] in 1965. It only uses two parameters. The solute and the solvent dissolve in the membrane material and then permeate through the membrane by diffusion through the homogeneous nonporous surface layer.The solubilities and diffusivities of solvent and solute are the important parameters in this model. The problem with this model is that it does not consider the structure of the membrane. It also breaks down for high concentrations of

solute. It is the most used model in module design due to the simplicity of the calculations necessary. And it gives a reasonable estimation.

Finely-Porous This model is based on a porous membrane structure. It combines diffusion with viscous flow through the pores. It is somewhat more complicated than the Solution Diffusion model since it uses three parameters. Using this model an average pore size can be calculated [29].

Surface Force-Pore Flow The Surface Force-Pore Flow model follows the basic framework of the Finely-Porous model. This model considers both the nature of the solution as well as that of the surface in contact. Reverse osmosis is the combined result of preferential sorption of one of the constituents of the feed solution at the membrane– solution interface, and mass transport by fluid permeation under pressure through the capillaries of the microporous membrane. An appropriate chemical nature of the membrane surface and the physical structure in terms of the appropriate number and size of pores are needed for a practical separation process. Because this model explains the mechanism more fully than the above, it is also more elaborate and complicated. It requires more parameters to describe the mechanism.

2.2.2 Surface Force Pore Flow Model

The surface force pore flow mechanism is used to represent the gas separation by permeation under pressure through asymmetric reverse osmosis membranes. In this mechanism, transport equations are developed for flow through a porous structure of the membrane surface. Pore size distribution on the membrane surface is represented by a normal distribution function. This model can predict the permeability coefficient of pure gases through various asymmetric membranes satisfactorily [66].

A similar transport model is applied to the membrane for the separation of gas mixtures, assuming that the component of the mixture permeate through the membrane independently of one another. The comparison of experimental and predicted values of the total permeation rate and the separation factor show fairly good agreement [47]. However, disagreements exist in some cases, indicating the need for modification to the model.

Gas Transport Through Porous Membranes Using this Model Symbols in this section are defined in the nomenclature. For the devel-

opment of transport equations, it is assumed that pores on the surface of an asymmetric porous membrane are equivalent to capillary tubes. The gaseous flow through these capillaries is governed by four flow mechanisms Knudsen, slip, viscous and surface flows. The first three mechanisms are considered as pore flow, which does not involve interaction forces between the gas and the membrane material. It is assumed that Knudsen flow occurs in the pores of radii >0 to 0.05 λ, slip flow occurs in the pores of radii 0.05 λ to 50 λ, and the viscous flow occurs in the pores of radii larger than 50 λ. Where the mean free path of a gas is,

$$\lambda = \left(\frac{\mathbf{R}T}{\sqrt{2}\pi d^2 N \bar{P}}\right) \tag{2.1}$$

Surface flow does involve interaction forces and is applicable to all pore sizes. The variation in pore sizes is represented by a single equivalent normal distribution,

$$N(R) = \left(\frac{N_t}{\sqrt{2\pi}\sigma}\right) exp\left(-\frac{1}{2}\left(\frac{R-\bar{R}}{\sigma}\right)^2\right) \tag{2.2}$$

A transport equation reported by Rangarajan et al. [66] is used to calculate the gas permeability coefficient based on the above.

$$A_G = A_1(G_1 I_1 + G_2 I_2 + G_3 I_3) + A_2 \frac{I_4}{I_5}\bar{P} \tag{2.3}$$

where (for each component i)

$$(I_1)_i = \frac{1}{(2\pi)^{1/2}\sigma}\int_{R=0}^{0.05\lambda_{12}} R^3 \exp\left[-\frac{1}{2}\left(\frac{R-\bar{R}_i}{\sigma}\right)^2\right] dR \tag{2.4}$$

$$(I_2)_i = \frac{1}{(2\pi)^{1/2}\sigma}\int_{0.05\lambda_{12}}^{50\lambda_{12}} R^3 \exp\left[-\frac{1}{2}\left(\frac{R-\bar{R}_i}{\sigma}\right)^2\right] dR \tag{2.5}$$

$$(I_3)_i = \frac{1}{(2\pi)^{1/2}\sigma}\int_{50\lambda_{12}}^{R_{max}} R^4 \exp\left[-\frac{1}{2}\left(\frac{R-\bar{R}_i}{\sigma}\right)^2\right] dR \tag{2.6}$$

$$(I_4)_i = \frac{1}{(2\pi)^{1/2}\sigma}\int_{R=0}^{R_{max}} R^2 \exp\left[-\frac{1}{2}\left(\frac{R-\bar{R}_i}{\sigma}\right)^2\right] dR \tag{2.7}$$

$$(I_5)_i = \frac{1}{(2\pi)^{1/2}\sigma}\int_{R=0}^{R_{max}} R \exp\left[-\frac{1}{2}\left(\frac{R-\bar{R}_i}{\sigma}\right)^2\right] dR \tag{2.8}$$

and

$$(G_1)_i = \left(\frac{32\pi}{\bar{\pi}V_i RT}\right)^{1/2} \tag{2.9}$$

$$(G_2)_i = \frac{\bar{\pi}}{M_i \bar{c}_i} \tag{2.10}$$

$$(G_3)_i = \frac{\pi \bar{P}}{S\eta_{12}RT} \tag{2.11}$$

Where G's are physicochemical constants and I's are defined quantities of integrals dependent on the porous structure.

The i's stand for gas component i and the second subscripts indicate the phase. 1 is the bulk or feed condition, 2 is the surface condition and 3 represents the permeate condition. Additionally,

$$\bar{P}_i = \frac{X_{i2}P_2 + X_{i3}P_3}{2} \tag{2.12}$$

$$\bar{c}_i = \left(\frac{SRT}{\pi M_i}\right)^{\frac{1}{2}} \tag{2.13}$$

According to this development, a membrane can be characterized by the average pore radius, $\bar{R}$, the standard deviation, σ, and by two additional parameters A_1 and A_2. Setting the parameters A_1 and A_2 as

$$A_1 = \frac{N_t}{S\delta} \tag{2.14}$$

$$A_2 = \frac{RT\rho_{app}k^2}{2000\tau C_R \delta^2 S} \tag{2.15}$$

The quantity A_1 is related to the effective membrane thickness and the total number of pores, and therefore should remain constant irrespective of the gas for any given membrane. The quantity A_2 is related to the adsorption equilibrium, the mobility of the sorbed gas species and the membrane pore structure. The value of A_2 for various gases are related to that of a reference gas,

$$(A_2)_i = (A_2)_{ref}\phi_i \tag{2.16}$$

The parameter ϕ_i, is the relative surface transport coefficient and can be found listed in past literature for various gases [66]. The effective mean pore radius $\bar{R}$ is found by adding a radius correction factor, δ_i, which is also found in past literature.

$$\bar{R}_i = \bar{R}_{ref} + \delta_i \tag{2.17}$$

The deviation, σ, remains constant for a given membrane.

These four characteristic parameters are used to calculate the permeation rate and the separation factor of a gas mixture with respect to the characterized membrane. Here are steps using equation 2.3 to calculate A_G for any gas in the membranes characterized by helium data.

- Calculate λ using equation 2.1.
- Evaluate integrals I_1 through to I_5.
- Evaluate G_1, G_2 and G_3.
- Substitute A_1, $G's$, $I's$ and A_2 into equation 2.3 to obtain the value of A_G.

The product permeation rate can be calculated from the fluxes, J_i of each component of the gas mixture.

$$J_1 = (A_G)_1(P_2X_{12} - P_3X_{13}) \tag{2.18}$$

$$J_2 = (A_G)_2(P_2X_{22} - P_3X_{23}) \tag{2.19}$$

$$[PR] = \sum J_i \tag{2.20}$$

The separation factor, S_{12} defined as:

$$S_{12} = \frac{X_{13}/X_{23}}{X_{11}/X_{21}} = \frac{X_{13}/X_{23}}{X_{12}/X_{22}} \tag{2.21}$$

X_{13} = mole fraction of gas 1 in the permeate
X_{23} = mole fraction of gas 2 in the permeate
X_{23} = $(1 - X_{13})$ for a binary situation

These terms have been defined for all calculations as:

X_{13} = mole fraction of CO_2 in product gas
X_{23} = mole fraction of CH_4 in product gas
X_{12} = mole fraction of CO_2 in feed gas
X_{22} = mole fraction of CH_4 in feed gas

The separation factor can be calculated from X_{13} and the feed composition. X_{13} is obtained by solving a complicated cubic equation derived from the individual flows. Further details of the equations are in papers by Mazid et al. and Rangarajan et al. [47,66]. Thus to predict the separation factor and the permeation rate, first $\bar{R}$, σ, A_1 and A_2 using the permeability of a reference gas through the membrane must be obtained. These reference parameters are then used to evaluate the characteristic parameters with respect to each component of the gas mixture. These evaluated parameters are subsequently used to predict the separation factor and the permeation rate for a gas mixture for the characterized membrane.

2.3 Materials Selection

For a particular membrane gas separation, the selection of a polymer involves a compromise between permeability and selectivity. Generally the most permeable polymers are the least selective ones. Good membranes should have high surface porosity with minimal pore diameters, but the pore diameter generally increases with increasing porosity [90]. There are a large number of permeability data reported in the literature confirming this inverse correlation between selectivity and permeation rate [37].

As mentioned above, the application of membrane separation is very site or material specific. Membranes with widely differing properties and characteristics are therefore needed for various applications. Principle considerations leading to the selection of the appropriate membrane for a particular process [90] are:

1. the mechanism of separation:
   - based on large differences in the permeating molecular sizes (sieve effect).
   - based on charges of the separating substances (electrochemical effect).
   - based on differences in solubilities of materials in the membrane phase because of the physicochemical nature of the substances (e.g. polarity, H-bonding).
2. the permeation properties (flux and rejection of substances) of the membrane.
3. mechanical and chemical stability of the membrane.

4. compatibility of the materials being processed with the membrane (e.g. membrane fouling or scaling).

Once a polymer is chosen, inherent membrane productivity and its selectivity can be altered by varying the polymer structure. Usually there is an interaction of permeability and selectivity, and thus both parameters must be considered when altering the structure.

Another consideration is whether the polymer should be rubbery or glassy. The term rubbery refers to a material that is above its glass transitional state. Glassy refers to the same material when it is below its glass transitional state. Cellulose acetate and polysulfone are glassy materials at room temperature. Their glass transition temperatures are 60 °C and 180 °C respectively [19]. Notice that glassy polymers do not exist in equilibrium, and thus prior history, such as fabrication techniques determines their properties [10]. Glassy materials have a higher selectivity and, with the invention of asymmetric membranes, can be produced thin enough to produce a relatively high permeation rate. Some glassy polymers actually have permeation rates exceeding the high permeabilities previously associated only with rubbery polymers. However, these same glassy materials exhibit low selectivities. This suggests that within the domain of glassy materials, there may exist some with both high selectivity and permeability or that glassy polymers can be tailored to a larger extent. Simple structural variation gives a broad range of permeability and selectivity properties of glassy materials. This makes glassy polymers extremely attractive and they will likely be the materials of choice in the future generation [34].

Currently most membrane products are based on highly selective glassy polymers in the form of asymmetric membranes. (If not made in this form, the glassy materials would not be as permeable as rubbery materials.) Cellulose acetate membranes in either spiral wound or hollow fiber forms are considered as "simple" membrane structures. These membranes require careful drying methods to prevent damage to the thin skin layer during removal of the water. Water is present due to gelation in the membrane formation process. Drying methods have been investigated and have been evaluated using gas separation (H_2-CO, H_2-CH_4, H_2-N_2, CO_2-CH_4) [11,13]. These drying methods will be discussed further in the next section.

Caulking, silicone rubber occlusion of pore defects, can be used to eliminate some of the requirements of solvent exchange. Caulking is used basically for polysulfone membranes which are applied to the same types of systems as the cellulose acetate ones [27,6].

These two asymmetric membrane systems are the major competitors

for gas separation systems. The two basic materials widely used therefore are, cellulose acetate and polysulfone. Cellulose acetate membranes are used in certain areas because of the ease and costs to manufacture them. They also have resistivity against common concentrations of chlorine pretreatment. Other areas preclude their use because of their susceptibility to hydrolysis and biological degradation [90]. Pan reported excellent performance of cellulose acetate membranes in obtaining hydrogen recovery and acid gas separation (SO_2). At 25 °C, the membrane has a H_2-CH_4 selectivity of about 100. At 10 °C, the cellulose acetate membrane has an effective CO_2-CH_4 selectivity of 36 [61,60]. Polysulfone is able to withstand higher temperatures. It can operate in temperatures of at least 100 °C [64]. It also has good chemical resistivity [90].

The determination of gas separation on a polymeric membrane material can be done using gas chromatography. The retention volume is the strength of gas adsorption. Experiments done at the University of Ottawa showed that cellulose acetate (CA-398) is a good membrane material for the separation of carbon dioxide-methane mixtures [96]. This finding was confirmed by experiments done by Ellig et al. [16]. He showed that separation factors were good for polyethersulfone, polysulfone, sulfolene, cellulose acetate and 3-methylsulfolene. Out of all these, only cellulose acetate gave high flux rates.

2.4 Making and Drying

2.4.1 Non-cellulosic Membranes

As mentioned in the materials selection section, classes of polymers other than cellulose acetate have also been used for gas membranes. Rubbery polymers used to make membranes resulted in high permeation rates with low selectivities. They did not have the problem of drying since there was no pore structure to retain. However, they had a tendency to distend (distort mechanically) under higher pressure differences. Ward et al. [92,93], used block copolymers (using two polymers) for gas permeation membranes. They combined a rubbery polymer such as silicone with a glassy polymer, polycarbonate. They were able to produce an ultrathin silicone/polycarbonate membrane by spreading the solution on a water surface between two plastic blocks and then moving the blocks apart. A nitrogen permeation rate of 8.6 $\times 10^{-2}$ $cm^3(STP)/cm^2$-s-cmHg and an O_2 /N_2 selectivity of 2.3 was reported for a 1000 Åthin film.

In 1979, Henis and Tripodi [27] used polysulfone as a polymer material. They found difficulty in producing reproducible hollow fibers free of imperfections. "Skin layer fine pores with diameters larger than those of the penetrant gas molecules effect a viscous or pore flow through the membranes, which reduces drastically their separation capabilities."[19]. They found that the control of surface porosity is possible by changing casting and coagulation conditions or by post-treatment of the membrane according to Henis and Tripodi [27]. They also separated the problem of surface porosity and the actual preparation of the polysulfone fibers by applying a thin layer of silicone rubber inside the fiber pores using vacuum coating.

However, it has been shown that the separation factor of a He/Kr mixture is higher for a cellulose acetate membrane than a silicone rubber membrane. Also, the preference to the permeation of these gases can be reversed completely [55].

Other methods of membrane preparation include compression molding at high temperatures [10]. It is possible to create pores in a polymer film by after treatment, i.e. mono or biaxially stretching the film (Celgard, Goretex Porefion) or bombarding the film with neutron-induced nuclear fragments (Nucleopore) [90].

2.4.2 Cellulosic Membranes

The first asymmetric membrane for gas separation was produced by Gantzel and Merten [22]. They dried cellulose acetate membranes with an acetyl content of 39.4 % by quick-freezing and vacuum sublimation at $-10\,^{\circ}C$. They obtained high N_2 permeation rates of 3.1×10^{-6} $cm^3(STP)/cm^2$-s-cmHg and a He-N_2 separation factor of 34.

Vos and Burris [89] used a surface active agent to dry cellulose acetate membranes. The membrane was first soaked in an aqueous surfactant solution, which reduced the surface tensions of the water polymer and was then left in atmosphere to be air dried. They were able to keep the pores intact. Stern et al. [81], using this method of preparation, was able to obtain 4.7×10^{-7} $cm^3(STP)/cm^2$-s-cmHg at 30 °C for nitrogen permeation.

Using successive solvent exchange steps and air-drying an integral asymmetric cellulose acetate blend, Schell [73] obtained a permeation rate for nitrogen of 4.8×10^{-6} $cm^3(STP)/cm^2$-s-cmHg at 25 °C. The separation factor obtained foe He-N_2 separation was 68.

Agrawal [78] investigated the effects of operating pressure and temperature, nature of gas and the pore size on membrane surface using freeze

dried porous cellulose acetate membranes. He studied the permeation of helium, hydrogen, methane, ethylene, nitrogen and argon. The membrane was immersed in −80 °C isopentane followed by vacuum drying overnight at the same temperature, then at −10 °C. He found the freeze drying technique preserves the porous structure of the membrane to a certain extent but not completely.

According to Manos [41], solvent exchange methods were costly and time consuming due to the multiple steps necessary. Polymers with high surface tensions also reacted poorly to this drying process. This showed that although the method had the ability to dry the membranes, it still needed much improvement.

Manos [41,42], applied for a U.S. patent in 1978 for an improved method of solvent exchange. This method was used to dry any semi-permeable membrane which relies mostly on its physical structure for its performance, including asymmetric membranes. Basically, it consisted of contacting the water-wet membrane with at least one replacement liquid and then removing it from the membrane. The term water-wet in this case was understood to mean that a major part, that is, at least 50 weight percent, of the liquid with which the membrane is wet is water. The invention worked best when the liquid in the membrane was pure water. "The replacement liquid consisted of a homogeneous solution of (a) a major portion of at least one organic solvent substantially immiscible with water and (b) a minor portion of at least one organic solvent substantially miscible with water."[41]. This replacement liquid was inert to the membrane and to the components of the wetting liquid to avoid depreciation of membrane properties. Also, it was capable of penetrating the membrane, had a low viscosity and a small molar volume. Contacting was continued until water was completely removed. This was done by repeatedly contacting with different batches of the same replacement liquid. Manos claims that this can also be done by further contacts with a water miscible solvent alone. (Note: it is believed that Manos meant "immiscible" here.) Water could be removed from a replacement liquid by simple decanting or centrifuging. The replacement liquid was removed by contacting the liquid-wet membrane with another organic solvent or a series of solvents. This was to obtain a membrane wet with a liquid which could be evaporated without significant effect on the permselective properties of the resulting dry membrane. Specifically, this last solvent had a low surface tension, had to be non-polar and water-immiscible, and had to be capable of penetrating the membrane.

Rangarajan used a procedure described by Pageau and Sourirajan [59]

to make gas membranes. He obtained different porosities by either shrinking them at different temperatures or by varying the composition of the casting solution and the conditions of membrane making. Polysulfone membranes were then dried in air while cellulose acetate membranes were either freeze dried or solvent exchanged and then air dried. For the solvent exchange process he used a combination of ethylene glycol and methanol or used methanol alone. Although he felt that the solvent exchange procedure still needed to be established he realized that the mechanical stability of the membranes obtained by different solvent exchange procedures were affected. He studied the performance of the dried membranes by measuring the permeation rates of hydrogen, helium, methane, nitrogen, ethylene and argon through asymmetric membranes made of cellulose acetate, hydrolyzed cellulose acetate propionate, and polysulfone. These experiments were conducted at room temperature for various operating pressures. This work led to the development of a model for the permeation of single gases through porous membranes [66]. His model characterized a membrane in view of pore structure and the surface transport of nitrogen. This characterization was then used to predict the performance of permeability with any gas.

Mazid et al. [47] used the same treatment and extended the model further to deduce expressions for fluxes of component gases in a mixture of two gases and relationships between separation factors and membrane characterization are derived. He used the same method as above to produce a cellulose acetate membrane. He measured the permeation rates of pure helium as a function of operating pressure as reference gas for membrane characterization. Helium was used instead of nitrogen because there is less interaction with the membrane material and higher reliability of the helium permeation data due to its higher permeability. The permeation and separation data of H_2-CH_4 mixtures were obtained at different operating pressures with different feed compositions.

Minhas et al. [49] investigated the effect of various solvents used in the solvent exchange drying process on its performance in the separation of H_2-CH_4 gas mixtures. The separation factor and the product permeation rate were also shown to be affected by process variables such as operating pressure and the hydrogen mole fraction in the feed gas mixture. Again, Minhas used helium as a reference gas for characterization. He found a wide variation in both separation factors and permeation rates and contributed the variation to different solvents used. The membrane dried with the combination of isopropyl alcohol and hexane in the solvent exchange process

performed the best. He also found that the number of stages involved in the drying process significantly affected the performance. It was found that for membranes dried using the combination of isopropyl alcohol and hexane, the two stage process worked best. He reported a separation factor of 28.0 and a permeation rate of 0.150 $\times 10^{-4}$ kmol/m^{2}s for two stage isopropyl alcohol-hexane at 2224.9 kPa. The feed gas mixture contained 0.883 mole fraction of hydrogen.

Many variables involved in the formation of membranes have been identified. Evaporation period as well as conditions like room temperature and relative humidity during the evaporation period need to be carefully controlled, since they were found to affect membrane performance. Asymmetric cellulose acetate membranes must be treated in hot water (tempering or shrinking) in order to close imperfections in the active layer or to change the structure of the polymer matrix, thus improving the selectivity [67]. The shrinkage temperature is an important variable. Finally, the membrane drying method is an extremely important variable. The solvents used and the number of stages used can result in wide variations, as shown by Minhas.

Chapter 3

Experimental

This section describes the preparation and drying of cellulose acetate membranes. A polymer solution is mixed, cast on a glass plate and gelled in cold water. The membrane is then immersed in a water bath at various shrinkage temperatures. The solvent exchange technique involved immersion of the membrane in two solvents. The membrane is then air dried to produce a gas separation membrane which is placed in a testing cell. A gas mixture is fed into the cell. The flux of the retentate and the composition determined using a gas chromatograph is monitored and is used to evaluate the membranes. The membranes used in this study were made by the National Research Council.

3.1 Membrane Preparation

A solution was made of the following components (weight%): cellulose acetate (Eastman 398-3) 17%, acetone (A.C.S. standard) 69.2%, magnesium perchlorate (Anachemia, A.C.S. standard) 1.45%, and distilled water 12.35% [59]. The solution was cooled and stored at a constant temperature of 10 °C. The casting room was kept at a constant temperature of 30 °C. The relative humidity of the room was maintained at 65%. This was to keep the rate of acetone evaporation constant.

The solution was then cast with a metal bar (doctor blade) onto a glass plate to produce a thin uniform film. The metal bar left a gap between the glass plate and the blade. The film, still on the glass plate, was gelled in distilled ice water after sixty seconds of solvent evaporation time. The film was left in the gelation bath for one hour after which time it was either stored in fresh distilled water or cut into coupons immediately. This step is

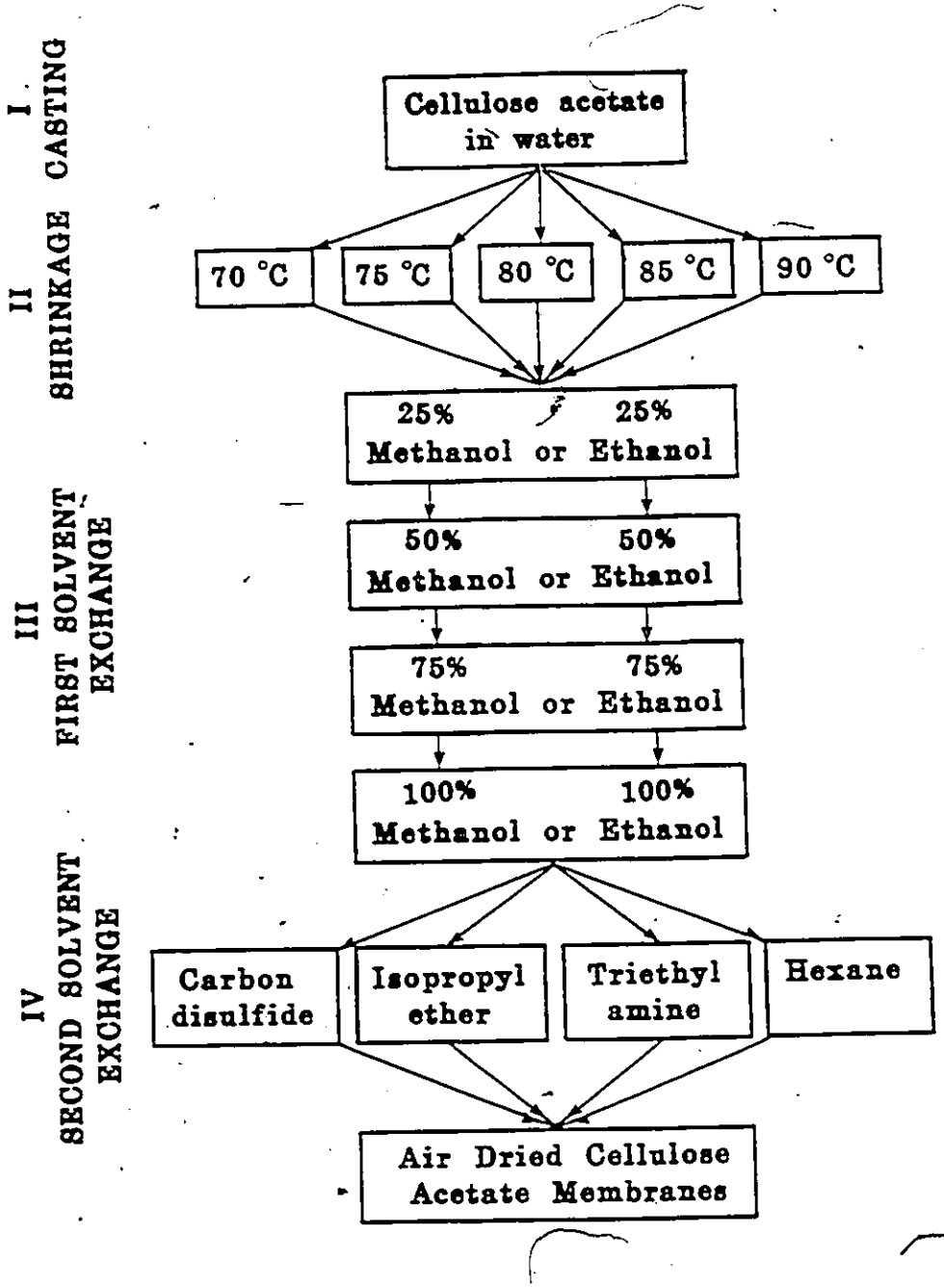

Figure 3.1: Schematic Diagram for the Preparation of Dry Cellulose Acetate Membranes by the Solvent Exchange Technique.

called casting and is represented by stage I of Figure 3.1. At this stage, the membranes were very stable and could be kept immersed in water for up to a year without adverse effects [87]. The pores result from water displacing solvent and/or additive held within the polymer solution as it solidifies. A network of pores through the membrane was formed by the solvent being replaced by the water in the bath. Membranes made in this way become asymmetric in structure. The cross-section may be divided into two distinct regions: a thin, dense skin layer on the one side which gives the membrane its selectivity (ability to separate); underneath the skin a porous support layer exists to give mechanical strength to the membrane.

The wet membranes were cut into circles of 3 inch diameter, called coupons. Usually, 6 to 25 coupons were cut from each membrane sheet. The circles were cut so that pin holes, air bubbles, rips, tears and any other kinds of irregularities were avoided. The membranes produced were approximately 0.15 mm thick.

Stage II (Figure 3.1) is shrinking and was accomplished in the following manner. The coupons were shrunk by immersion into a water bath at different temperatures (70–90 °C) for ten minutes. They were shrunk at various temperatures in order to obtain different average pore sizes and pore size distributions. The coupons were selected randomly for each temperature so that the differences due to location of the coupon and differences from different membrane sheets were masked.

The coupons were then dried using a multiple-stage solvent exchange drying technique. The shrunken coupons were selected randomly and divided so that two coupons from each temperature would be allocated for each solvent combination. The remaining coupons were left to be wet tested (see Section 3.2).

In this drying technique, water in the membrane is first replaced by a water miscible solvent (called the "first solvent") which is a non-solvent for the membrane material. This is seen as stage III of Figure 3.1. The first solvent is then replaced by a second solvent which is volatile, stage IV in Figure 3.1. The second solvent is subsequently air evaporated to obtain the dry membrane. A number of different solvents were used. First solvents used were methanol and ethanol, and second solvents were hexane, carbon disulfide, triethyl amine and isopropyl ether (to provide a variation in boiling points and solvent molecular size). Thus, eight solvent combinations were employed. All solvents were from BDH Chemicals, and met A.C.S. specifications under the category of analytical reagents.

The replacement of water in the membrane by the first solvent was

done by successive immersion, for twenty four hours, in first solvent–water solutions which were progressively more concentrated in the first solvent. Four stage replacement was used, with 25, 50, 75 and 100 volume% aqueous solutions of the first solvent. Once the water was completely replaced by the first solvent, the coupons were immersed in 100% second solvent for a period of twenty four hours. The coupons were removed from the second solvent in a fume hood. Each coupon was taken out of the solvent, placed between two filter papers, and then placed in a dessicator with silica gel. Handling of coupons was minimized to avoid damage. Gloves or tongs were used as protective measures for harmful solvents. All the solvent exchanges were done at room temperature.

Coupons were left to be dried at room temperature for at least two weeks, seen as the last part of Figure 3.1. This was simply a set period and no actual tests were done to check that the solvents were completely evaporated or not. The use of different solvents in the drying procedure resulted in membranes with a further difference in average pore sizes and pore size distributions.

3.2 Wet Membrane Testing

Wet membrane testing involved obtaining pure water permeation rates and salt (NaCl) separation data for coupons that were shrunk at different temperatures, before they were solvent exchanged. The testing was done using liquid reverse osmosis cells. The standard for pure water permeation rates and salt separation cellulose acetate membranes was established at NRC laboratories [88] by taking an average of several results for a particular salt concentration (3500 ppm) in the feed at a particular operating pressure (1724 kPa). Pure water permeation rate versus separation factor was plotted and compared to the standard curve. The purpose of wet membrane testing is to show whether there is any significant deviation of permeation rate or separation factor of membranes from standard cellulose acetate membranes.

3.3 Gas Testing Equipment

The equipment and the experimental procedure have been reported previously [66]. A detailed diagram of the flat sheet (coupon) gas testing cell is shown in Figure 3.2. The characteristic dimensions were as follows: The

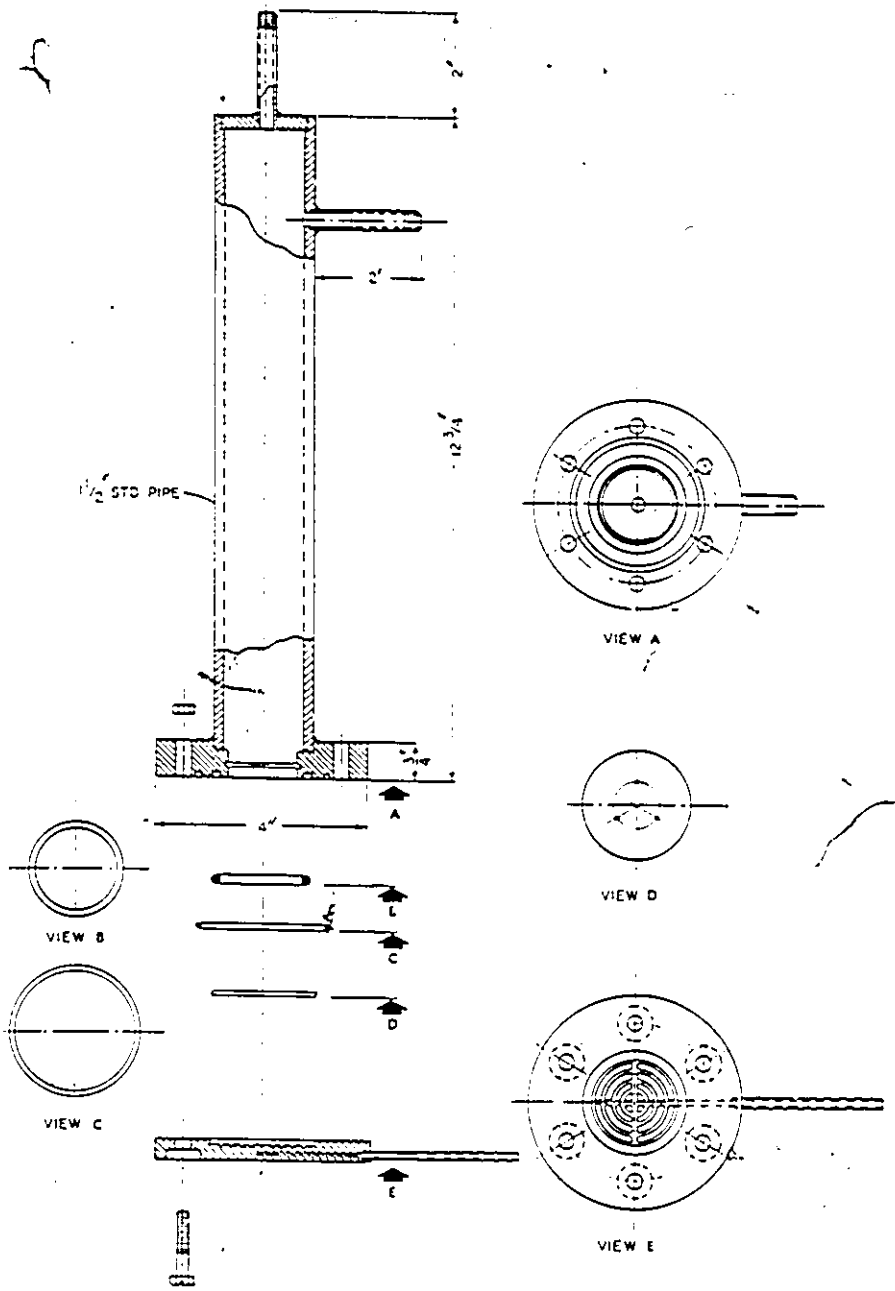

Figure 3.2: Gas Testing Equipment.

upper part of the cell, part (A), consisted of a 1 $\frac{1}{2}$ in. standard pipe size of # 18-8 stainless steel. This basic chamber had a height of 12 $\frac{3}{4}$ in. and was connected to an inlet and outlet, each being $\frac{1}{8}$ in. stainless steel tubes 2 in. long. The lower part of the cell, part (E), was basically a stainless steel disc of 4 in. diameter attached to an outlet. Also a small stainless steel porous disc, part (D), from Pall (Canada) ltd. was necessary to give support to the coupons. Within the gas system, eight of these gas cells were used as shown in Figure 3.3. They were all connected using 316 stainless steel $\frac{1}{8}$ in. piping and stainless steel swagelok valves and fittings.

3.4 Installation of Coupons

The gas cells were detached from the system at the inlet of part (A). Each cell was disassembled by removing the six bolts on the bottom of part (E). The surface of part (E) and the lower surface of part (A) was cleaned with acetone. The two O rings were removed from the lower surface of part (A) and were also cleaned with acetone. Using three small pieces of tape, a 7cm diameter filter paper was attached to parts (D) and (E). A coupon was selected randomly for testing; coupons with visible pinholes or rips were discarded. The coupon was placed on top of the attached filter paper with the skin layer facing up. Using a second filter paper to hold the coupon in place, the coupon was attached using six small pieces of tape. Note that the second filter paper was not attached. Part (A) with the O rings in place was put on top of the lower part. This was done so that the direction of the inlet on part (A) faced away from the direction of the outlet on part (E). Once the upper part of the cell was placed on the coupon, it was not moved again to prevent tearing of the coupon. Bolts were replaced and tightened. The cell was reconnected into the gas system. This was done for seven of the eight cells (One cell was left empty so that gas flowing through it was considered as feed gas.) Helium was passed through the apparatus at 345 kPa. and all fittings were checked for leaks using a leak detection solution. Flowrates were checked to ensure that none of the coupons were broken. A broken coupon was obvious due to extremely high permeation flows, not measurable with the bubble meters. If a broken coupon was found, that particular cell was removed and the coupon replaced. Once no leaks were found at 345 kPa., the pressure was increased to 689 kPa. and again tested for leaks and broken coupons. This was also done at 1034, 1379, 1724 and 2068 kPa. At 2068 kPa., the helium gas was allowed to flow through for approximately 2-3 hours. The flow to the feed line was then shut off. The

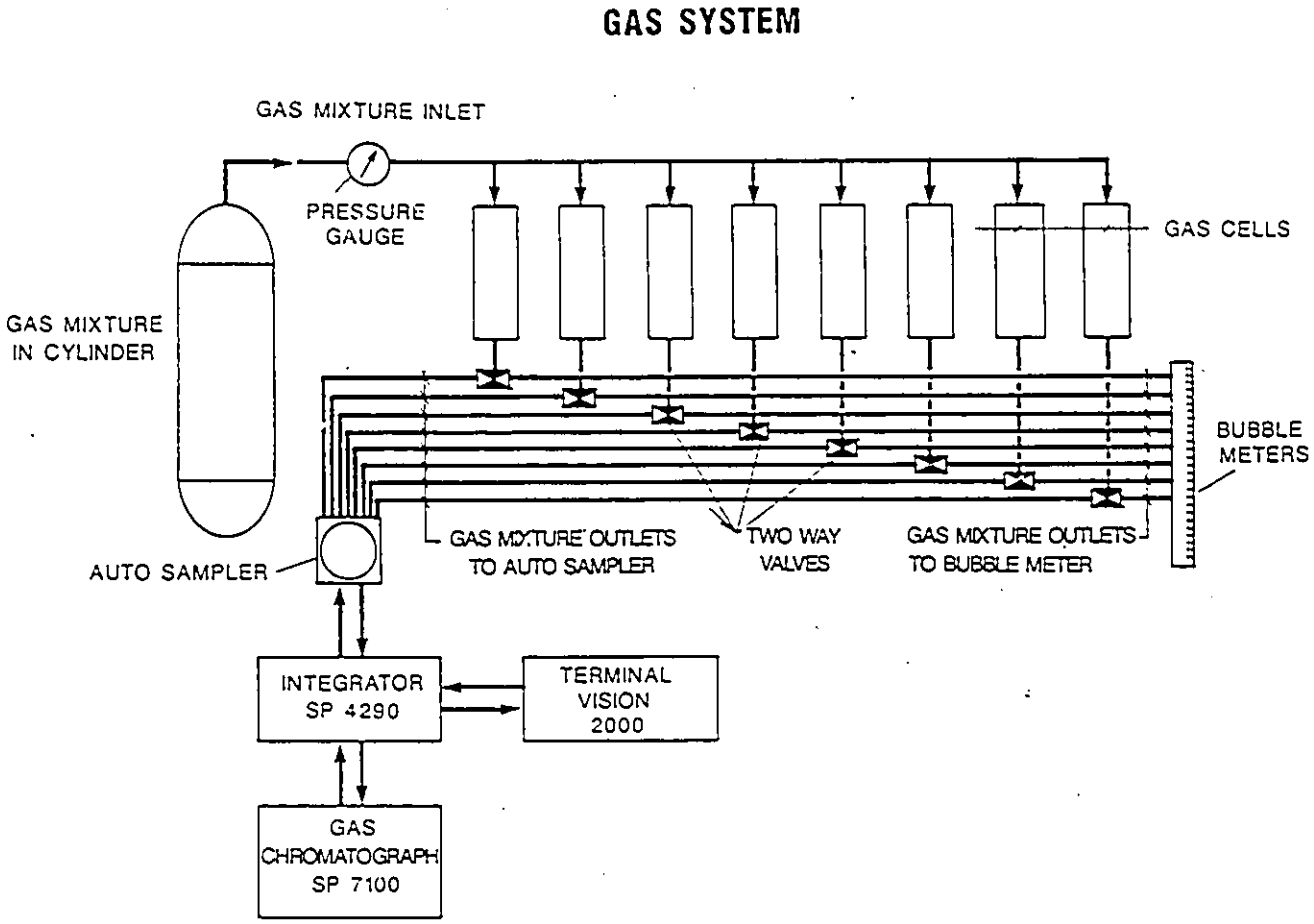

Figure 3.3: Gas System Used.

gas was released from the cells and the coupons were left to relax overnight at atmospheric pressure.

3.5 Test Procedure

All the cells were isolated from the feed gas line. The gas cylinder was opened to 345 kPa and all cells were flushed with the feed gas mixture of carbon dioxide and methane, or the pure components. This was done by opening the inlet valve to allow feed gas into the cell, and then closing it. The outlet valve was opened to allow gas to escape. When the gas stopped flowing out, this valve was closed so that air would not flow back into the cell. This procedure was repeated once more before the feed gas was allowed to saturate the cell. The mole fraction of carbon dioxide in the feed gas was varied from 0.9 to 0.1. Pure carbon dioxide, methane and helium gases were measured for permeation rate only. All the experiments were conducted at room temperature and the feed pressure was varied in the range of 345 to 2068 kPa. This is considered to be the operating pressure. At each pressure, the feed gas mixture or pure component was allowed to flow until the system reached steady state, approximately 30 to 45 minutes. The permeate flow was measured by soap bubble meters and analyzed using a Spectra-Physics SP7100 gas chromatograph equipped with a Porapak Q column. The gas chromatograph was connected to a Spectra-Physics SP4290 integrator which was connected to a terminal, using the Labnet software package (Figure 3.3). The accuracy of the analysis of the same sample from the gas chromatograph was $\pm$ <1.0%. All of the gases (pure and mixed by vendor) were obtained from Matheson Canada with a specific purity of 99.9%.

Chapter 4

Results and Discussion

The results are presented and discussed in the following manner. The experimental test conditions and variables are given. General trends derived from average results are qualitatively discussed. These trends are discussed and are shown in the specific case of the membrane shrunk at 70 °C with a solvent combination of methanol–IPE. A pore formation mechanism is proposed and experimental evidence is presented to support this hypothesis.

4.1 Experimental Data

All of the experimental variables studied are listed below.

The membrane formation variables are:

Temperature: 70, 75, 80, 85, 90 °C
First Solvent: methanol, ethanol
Second solvent: carbon disulfide (CS_2), isopropyl ether (IPE), triethyl amine (TEA), hexane

When the coupons were tested, they were each given a coupon number. The first number stands for the set number. Six sets of experiments were conducted. Each set was tested with three pure gases, five gas mixtures at six different operating pressures. The second number stands for the cell number. In Table 4.1, it is shown how the coupon number is related to the membrane formation variables (shrinkage temperature, first solvent and second solvent).

The operating variables used are:

Pure Gases: helium, methane, carbon dioxide

Gas Mixtures: 10, 20, 50, 80, 90 % CH_4(remaining is CO_2)
Pressure: 255, 345, 689, 1034, 1379, 1724, 2068 kPa
(37, 50, 100, 150, 200, 250, 300 psia)

The results are shown in Tables B.1 to B.24 in the appendix. The purpose of the study was to explore solvent drying, to detect trends and to identify areas of promise for future studies. From the data, permeation coefficients and separation factors were calculated as measures of membrane performance. The permeation coefficient is defined as the flux divided by the area of the membrane and operating pressure. The separation factor is calculated using Equation 2.21.

Runs with pure gases comprising of helium, methane and carbon dioxide at six different pressures were used to evaluate the membrane characteristics. Results using helium gas at six different pressures were used to determine the four characteristic parameters needed to use the Surface-Force-Pore-Flow model. Results using the other two gases were used to reveal that the two gases have different transport mechanisms. They were also used as an indication of the two possible extremes for this particular gas system.

Runs with gas mixtures of methane and carbon dioxide at six different pressures were used to measure separation factors and permeation coefficients to evaluate the effects of solvent exchange with various solvents. These values were also compared to the values predicted using the Surface-Force-Pore-Flow model.

4.2 Collective Membrane Results

The average results generally indicate that the separation factor increases with a decrease in permeation coefficient; the relationship is shown in Figure 4.1. Because separation is related to the pore size of the membrane, one can assume that at lower permeation coefficient values pore size is small and contributes to gas separation. It is because of this that one can discard the methanol–CS_2 membranes (1-5 and 5-7); they have unusually high permeation coefficients and low separation factors. A separation factor of one indicates no separation, thus one can conclude that these two membranes do not have a suitable pore size.

Because of the large amount of data and its inherent scatter, it was decided to evaluate the main variables using average values obtained in the experiments. Preliminary examination indicated that it was best to con-

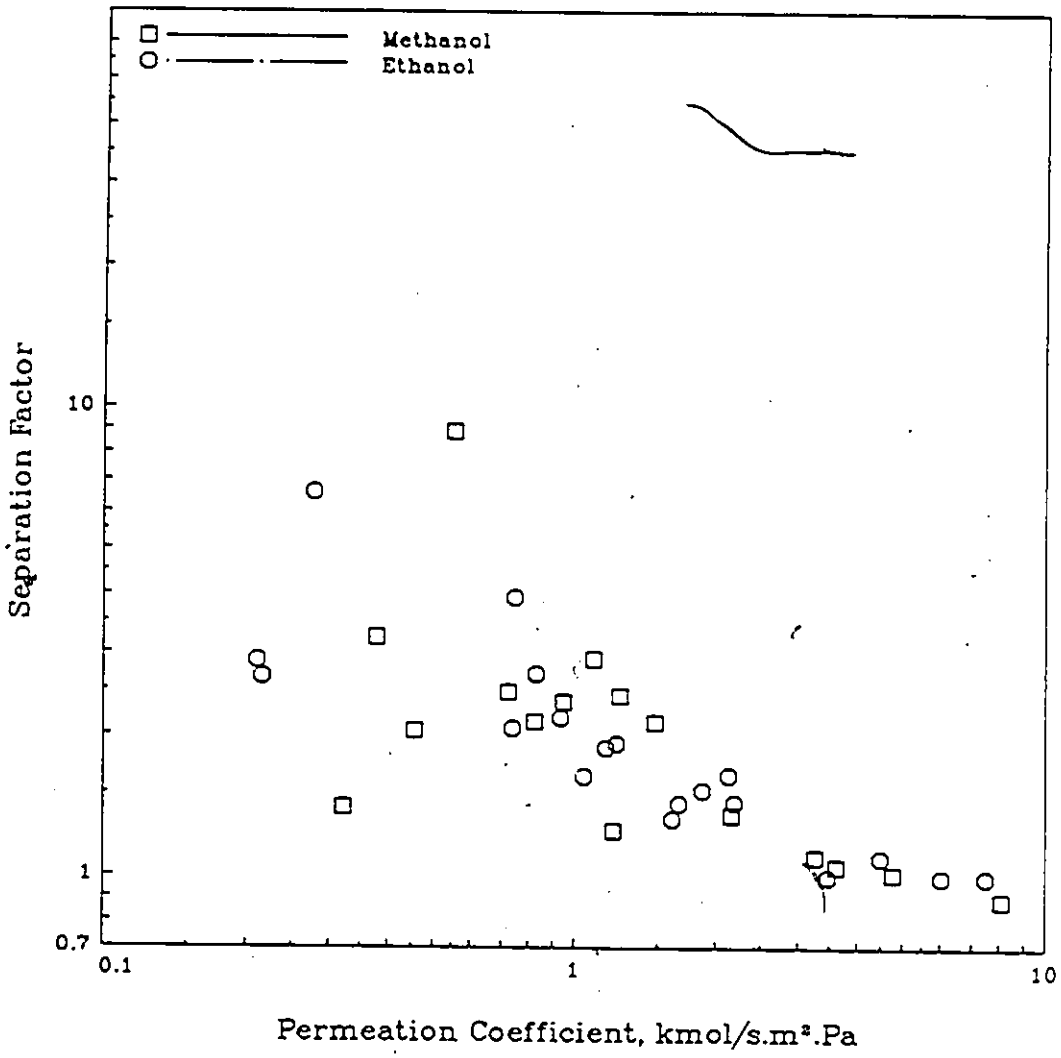

Figure 4.1: Permeation Coefficient $\times 10^{11}$ versus Separation Factor.

sider each membrane separately and determine its average response (i.e. separation factor and permeation coefficient). This reduction in data is summarized on twelve figures, Figures 4.3 through 4.13, six for each first solvent system. Separation factors and permeation coefficients were plotted for each solvent system as a function of temperature, pressure and composition. The average values of permeation coefficient do not include results from pure gas runs. This approach was useful in identifying trends within each first–second solvent membrane.

For the methanol–hexane combination, all permeation coefficients for the membranes shrunk at a particular shrinkage temperature were summed and divided by the total number of points to give the average permeation coefficient. This was plotted in Figure 4.2 and is represented by the square symbol. Similarly, the other curves would be averages at each particular temperature for the other solvent combinations. Averages of all the data were taken in this way and are presented in Figures 4.2 through 4.13. The curves within the figures are there only to connect the points to make them more visible, and are not in any way a model or a fit.

The major variables in the experimental design were shrinkage temperature and drying solvent combination. This is confirmed if one examines Figures 4.2 through 4.7 for the methanol system and Figures 4.8 through 4.13 for the ethanol system. The important observation from these figures is the order of the curves on the figure. If one excludes the methanol–CS_2 membranes in Figures 4.2 to 4.7, the remaining results indicate that the higher the boiling point of the second solvent the greater the permeation coefficient and the less the separation factor. This is observed for both first–solvent systems. This observation will be discussed later.

Figure 4.2 shows that the shrinkage temperature is an important variable, especially for the solvent combinations methanol–IPE and methanol–TEA. At the lower shrinkage temperature, the solvent combination methanol–TEA gave a very low permeation value which then increased with the shrinkage temperature. The corresponding separation factor decreased with an increase in shrinkage temperature, Figure 4.3. There is a steep drop in the permeation coefficient for methanol–IPE at 90°C. This may be due to that the shrinkage temperature being too high, which leads to a collapse in the pore structure. The pore radius that is left is small and non-functional, hence a low flowrate and a low separation factor was observed. The other two second solvents had similar but weaker trends.

In Figure 4.4, it is seen that there is only a slight increase in permeation coefficient with pressure. All average values of permeation coefficient were

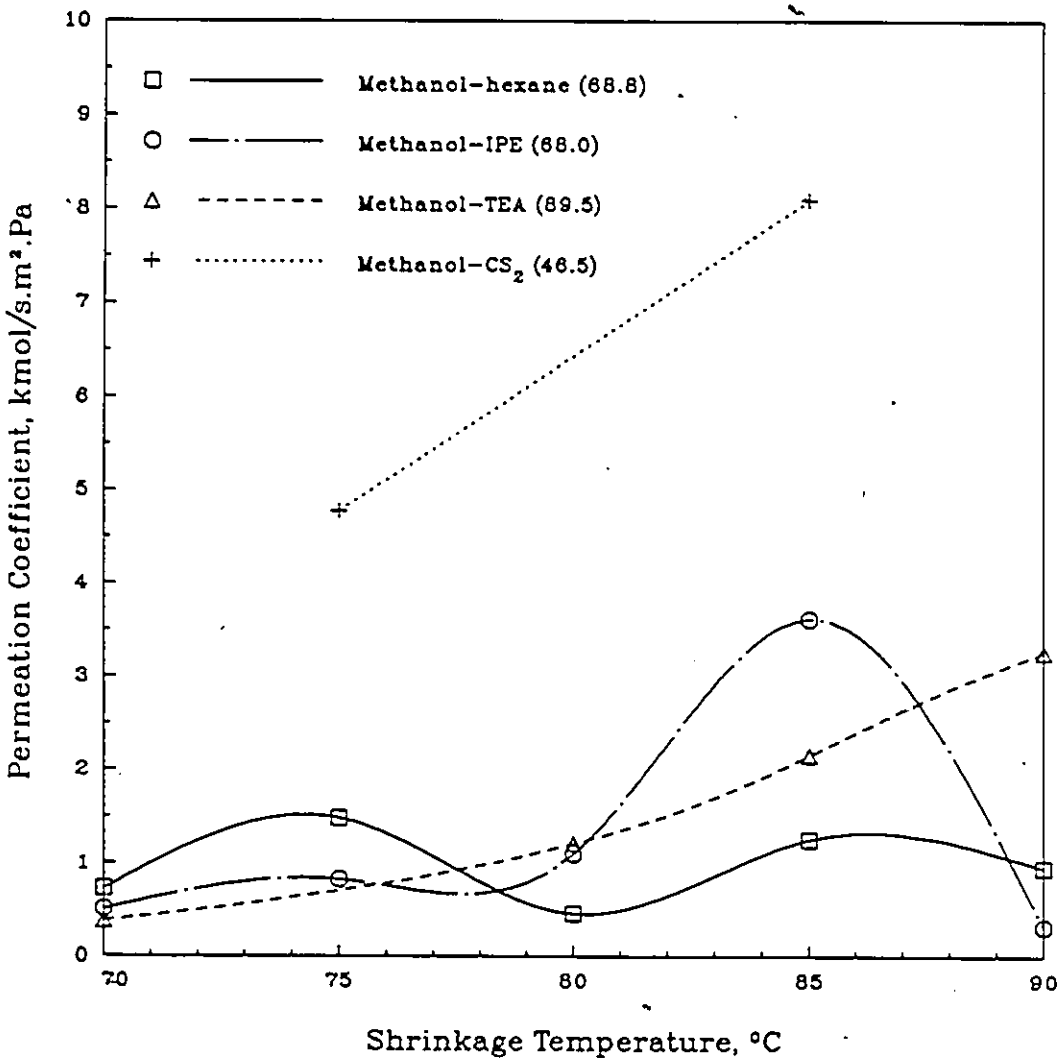

Figure 4.2: Average Permeation Coefficient $\times 10^{11}$ versus Shrinkage Temperature for Methanol Solvent Membranes. The numbers within the brackets indicate the second solvent boiling point.

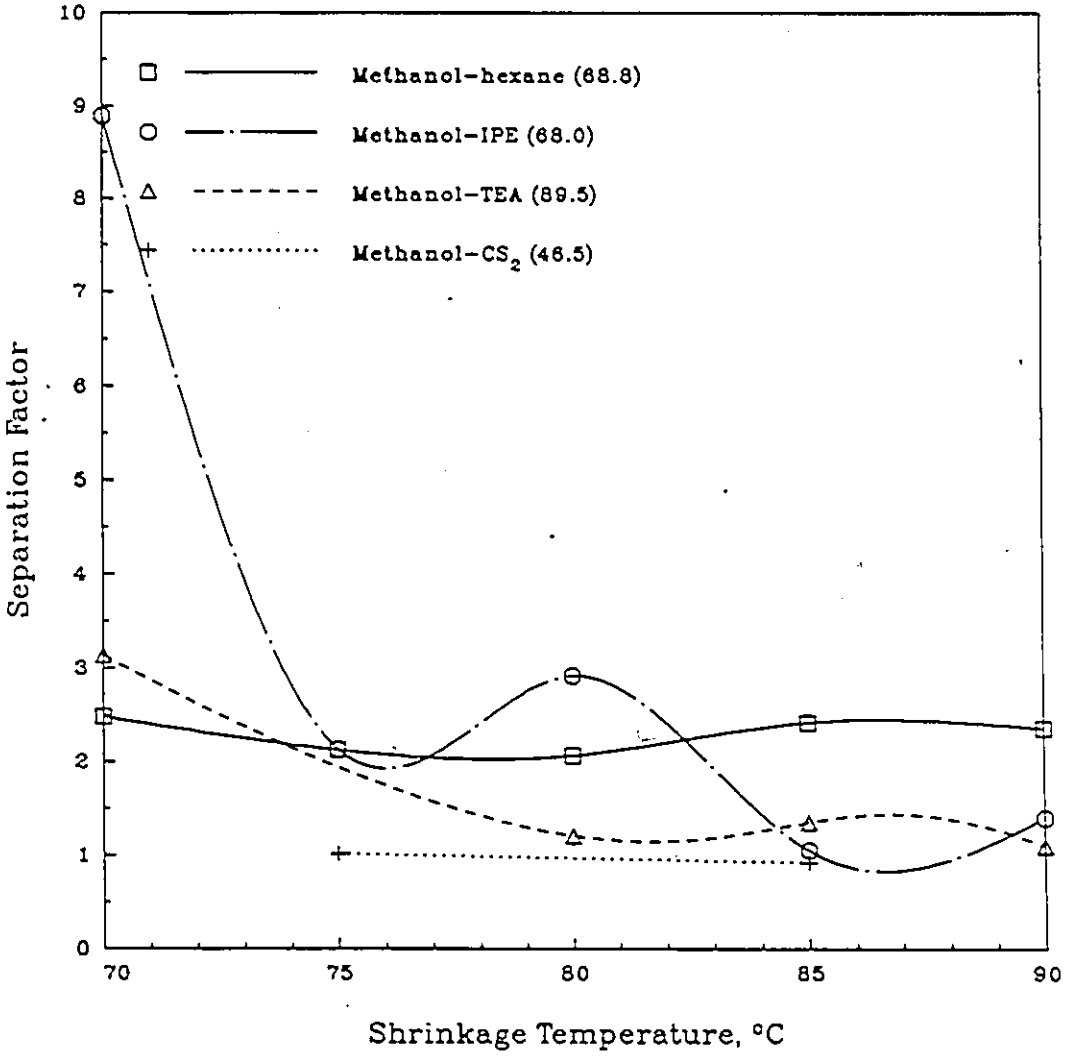

Figure 4.3: Average Separation Factor versus Shrinkage Temperature for Methanol Solvent Membranes. The numbers within the brackets indicate the second solvent boiling point.

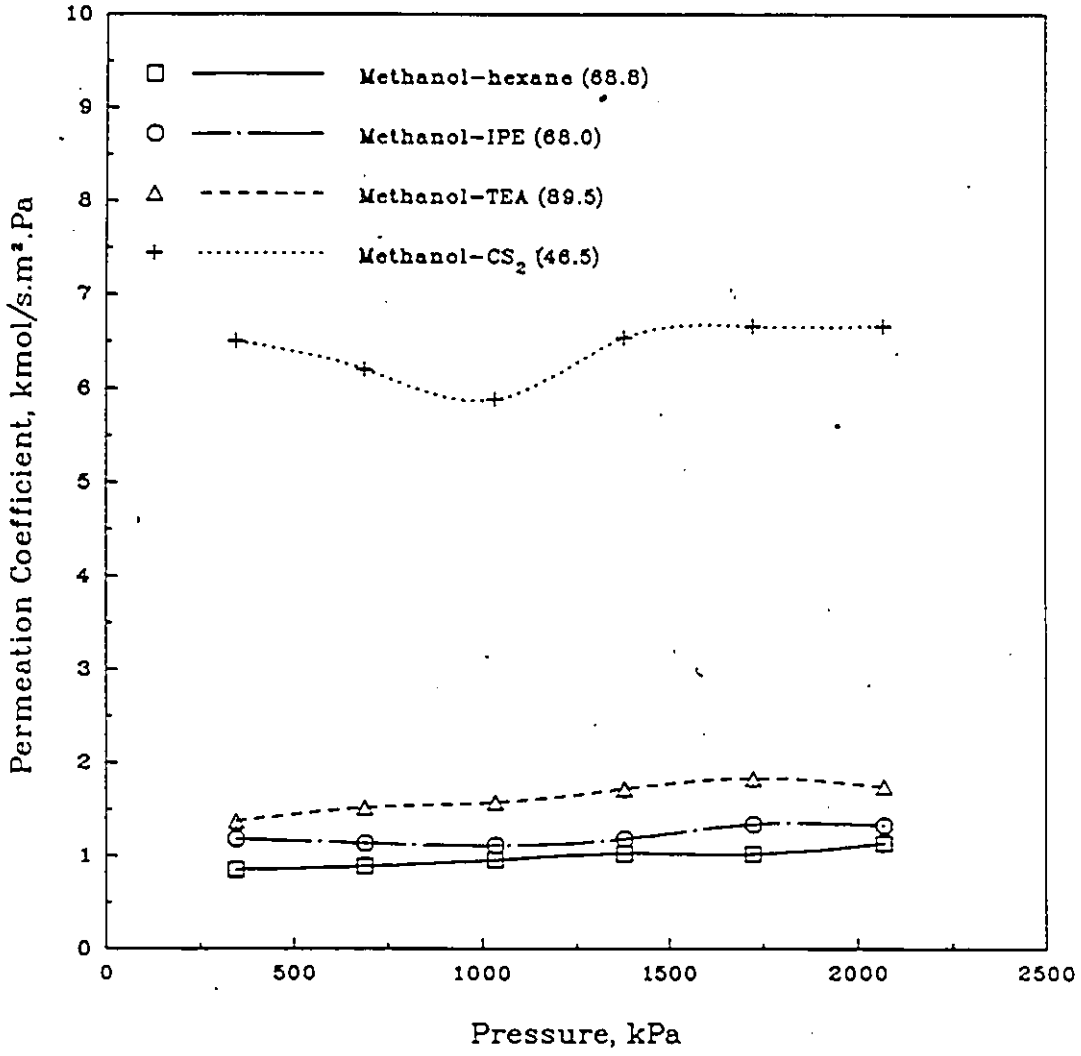

Figure 4.4: Average Permeation Coefficient $\times 10^{11}$ versus Pressure for Methanol Solvent Membranes. The numbers within the brackets indicate the second solvent boiling point.

approximately the same, around 1.0×10^{-11} kmol/s.m^2.Pa. The separation factor decreased with an increase in pressure, Figure 4.5.

Figures 4.6 and 4.7, show that both permeation coefficient and separation factor decrease slightly with an increase in mole percent methane. This small change may be due to the plasticization of the membrane by carbon dioxide [51] (more plasticization occurs with a higher concentration of carbon dioxide gas in the feed gas, CO_2–membrane interaction).

Figures 4.8 through 4.13 contain experimental results for ethanol as the first solvent. Comparing Figures 4.8 and 4.9, the trend of a high permeation coefficient with a low separation factor and vice-versa is apparent for the combinations with hexane and TEA as the second solvents. The permeation coefficient increased and the separation factor decreased with shrinkage temperature.

The permeation coefficients increased slightly and the separation factors decreased with an increase in pressure shown in Figures 4.10 and 4.11.

In Figures 4.12 and 4.13, both permeation coefficients and separation factors decreased with the increase in mole percent methane, the exception being the ethanol-TEA membrane where they increased.

Figures 4.2 and 4.3 for methanol and Figures 4.8 and 4.9 for ethanol indicate the extent of the variation of separation factor and permeation coefficient with shrinkage temperature. Generally, as the temperature is increased the permeation coefficient increases and the separation factor decreases. This indicates an increase in pore size. This observation is consistent for the methanol membranes but may not be true for the ethanol membranes. For example, the ethanol–CS_2 membranes may go through a maximum at 80 °C and the ethanol–IPE membranes may exhibit an increase in separation factor and decrease in permeation coefficient as the shrinkage temperature increases.

Two solvent combinations produced the best membranes with respect to permeation coefficient and separation factor; methanol–IPE and ethanol–hexane. Membranes shrunk at 70 °C were the best in each series. The trend of results indicate that a lower shrinkage temperature might even produce a better membrane.

4.3 Single Membrane Results

The individual membrane results of the specific case of membrane 1-1 (methanol–IPE, 70 °C) are discussed below. This membrane was one of the best membranes produced in the study. The variation with pressure

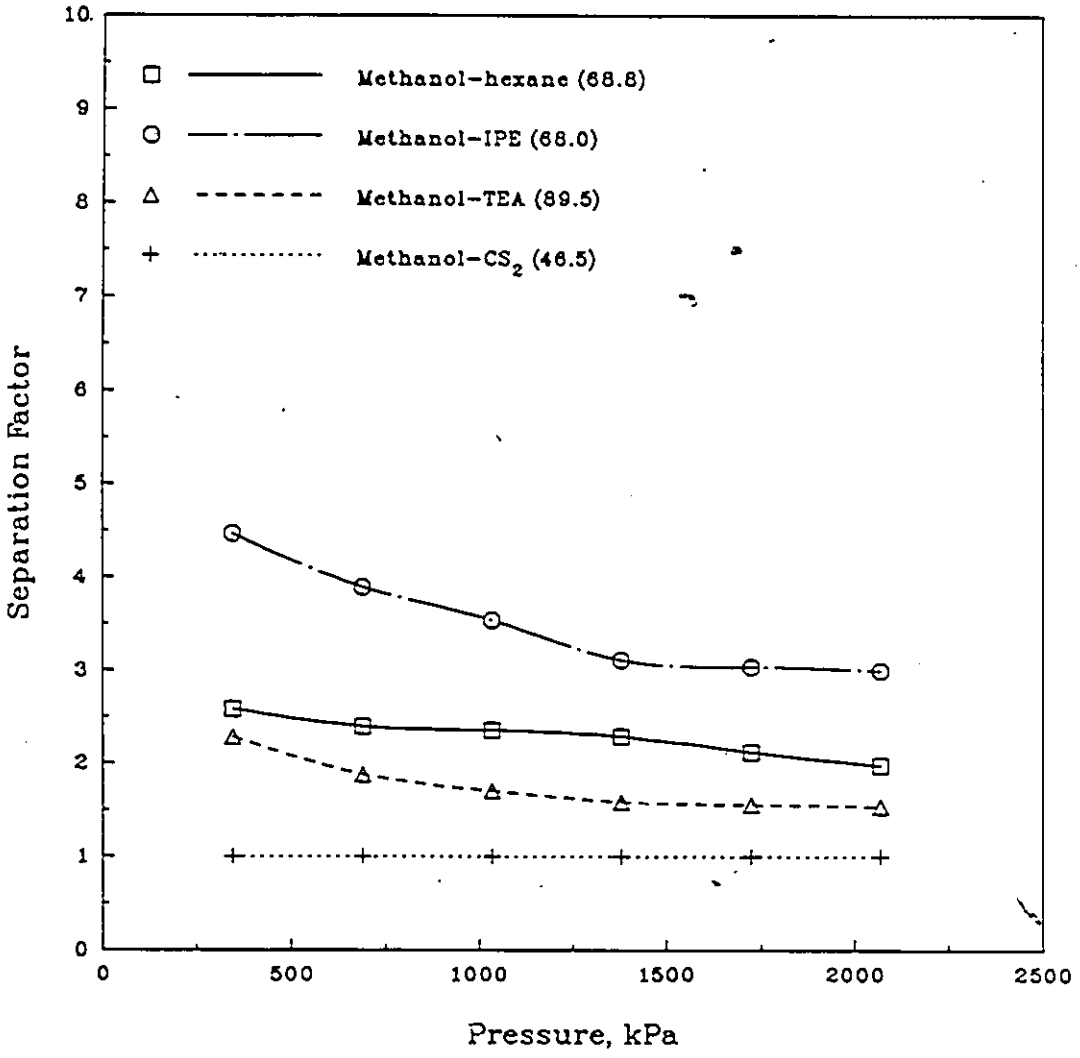

Figure 4.5: Average Separation Factor versus Pressure for Methanol Solvent Membranes. The numbers within the brackets indicate the second solvent boiling point.

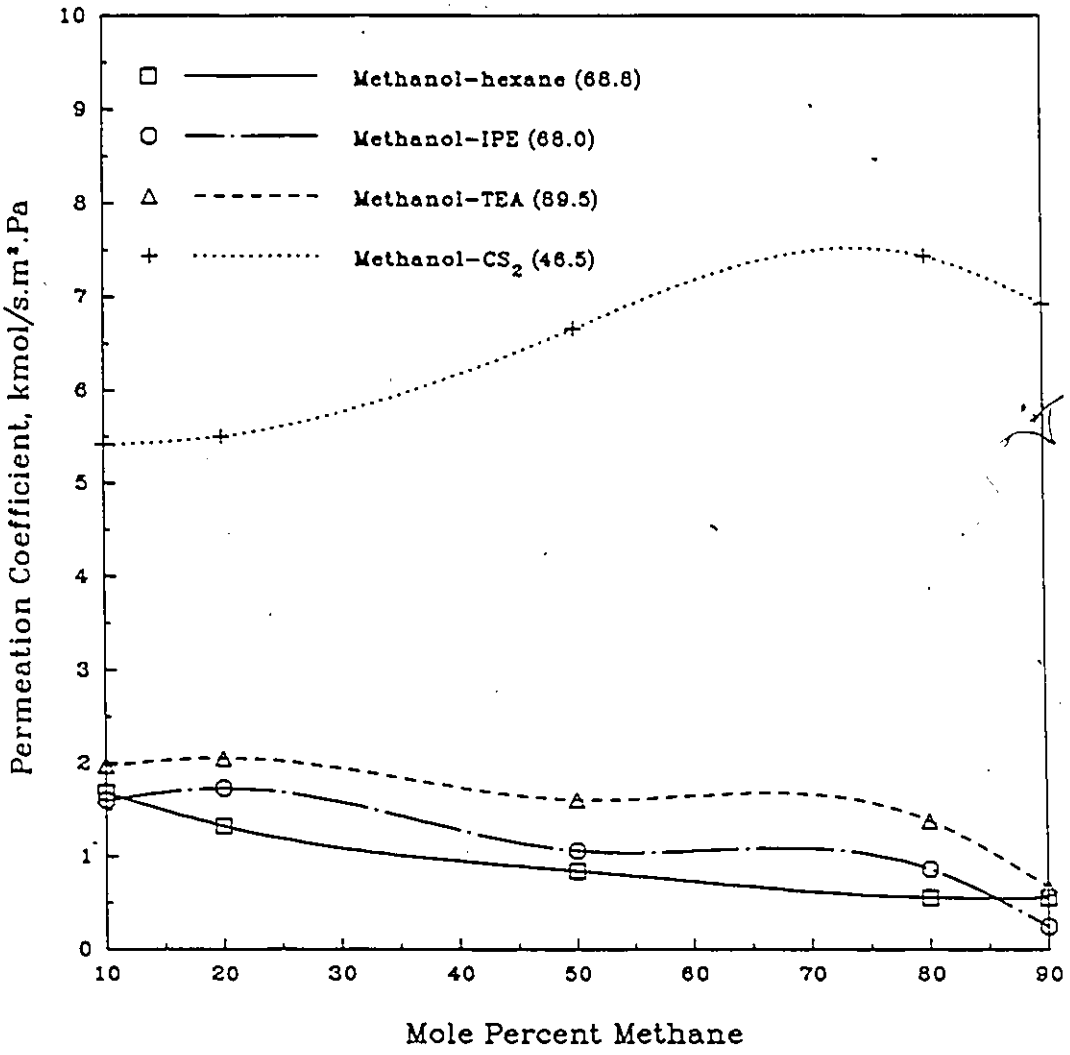

Figure 4.6: Average Permeation Coefficient $\times 10^{11}$ versus Mole Percent Methane for Methanol Solvent Membranes. The numbers within the brackets indicate the second solvent boiling point.

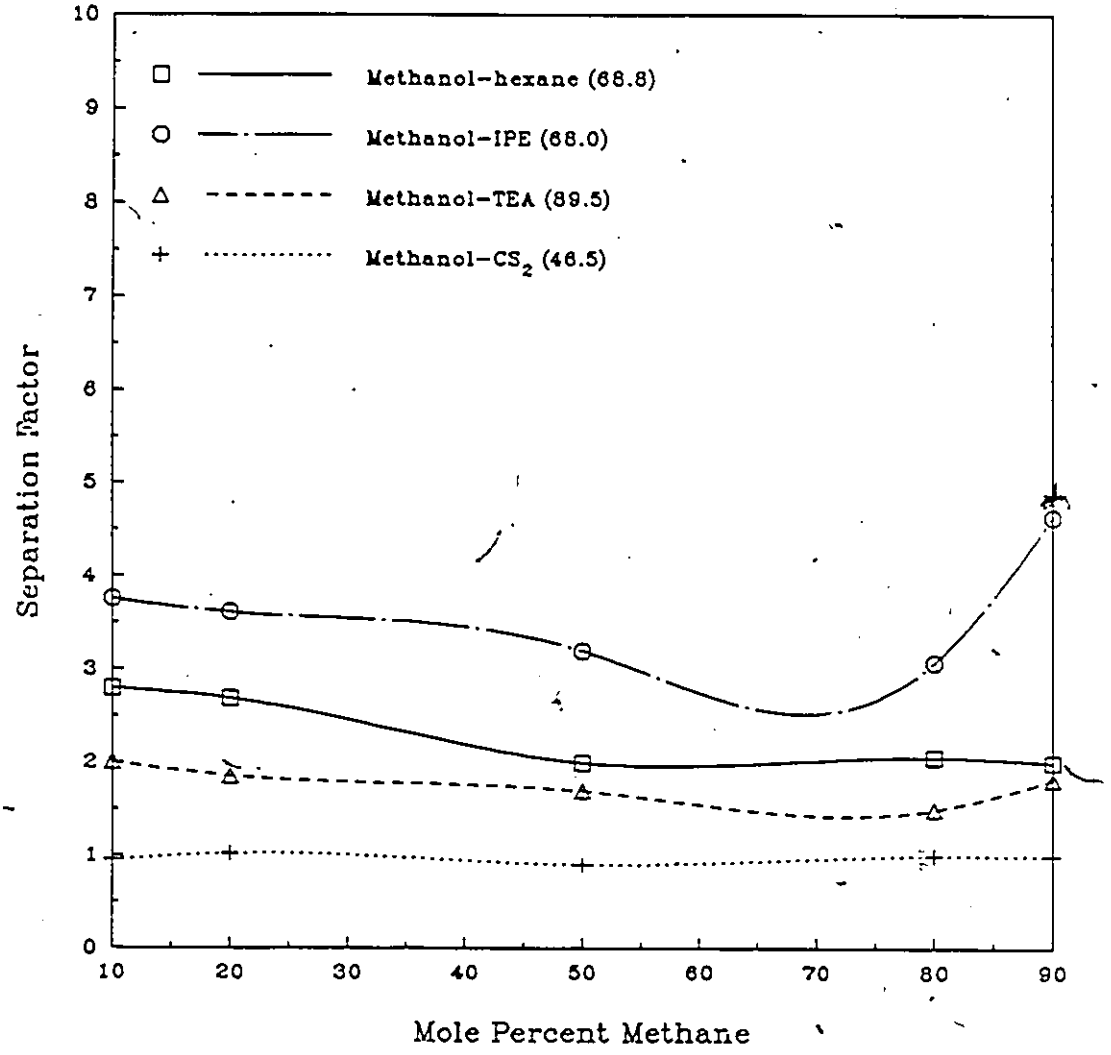

Figure 4.7: Average Separation Factor versus Mole Percent Methane for Methanol Solvent Membranes. The numbers within the brackets indicate the second solvent boiling point.

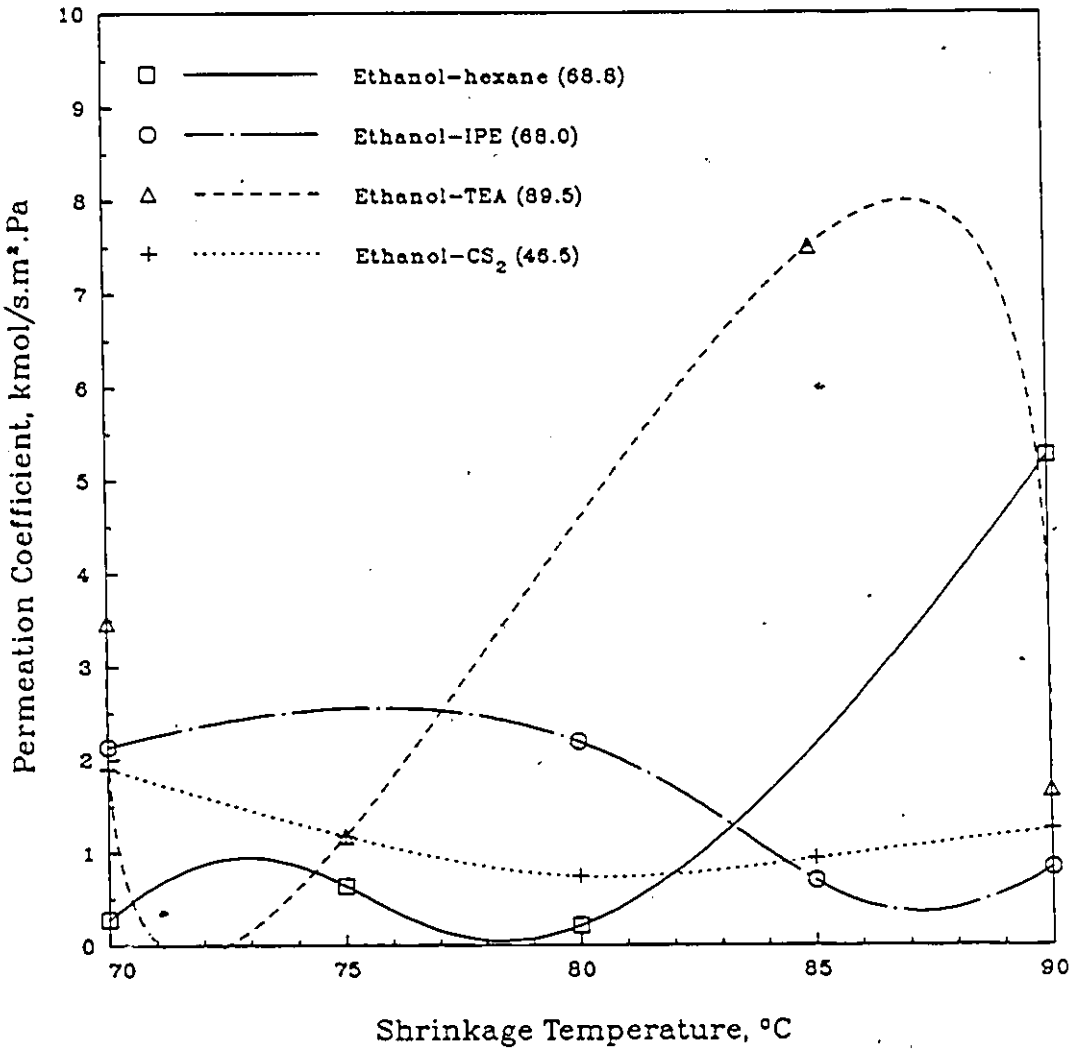

Figure 4.8: Average Permeation Coefficient $\times 10^{11}$ versus Shrinkage Temperature for Ethanol Solvent Membranes. The numbers within the brackets indicate the second solvent boiling point.

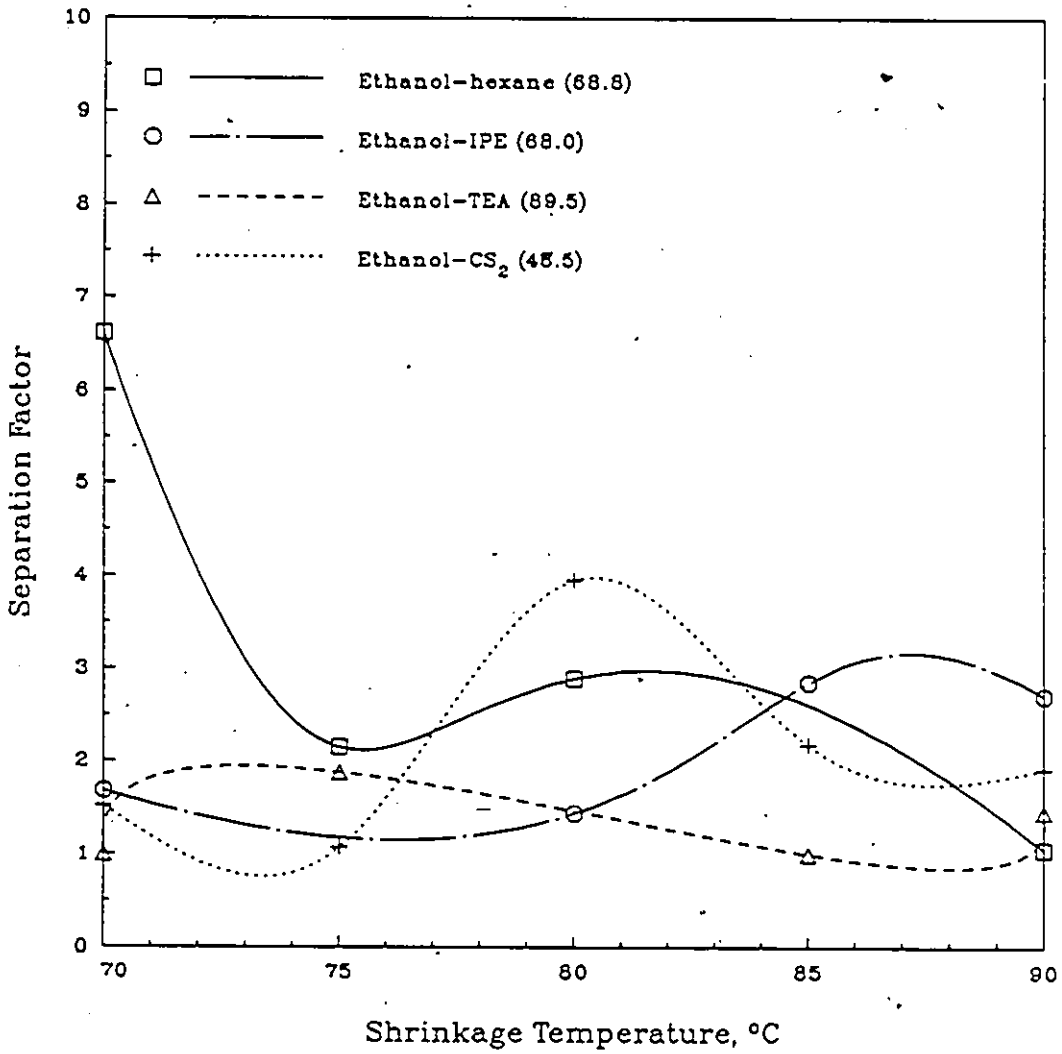

Figure 4.9: Average Separation Factor versus Shrinkage Temperature for Ethanol Solvent Membranes. The numbers within the brackets indicate the second solvent boiling point.

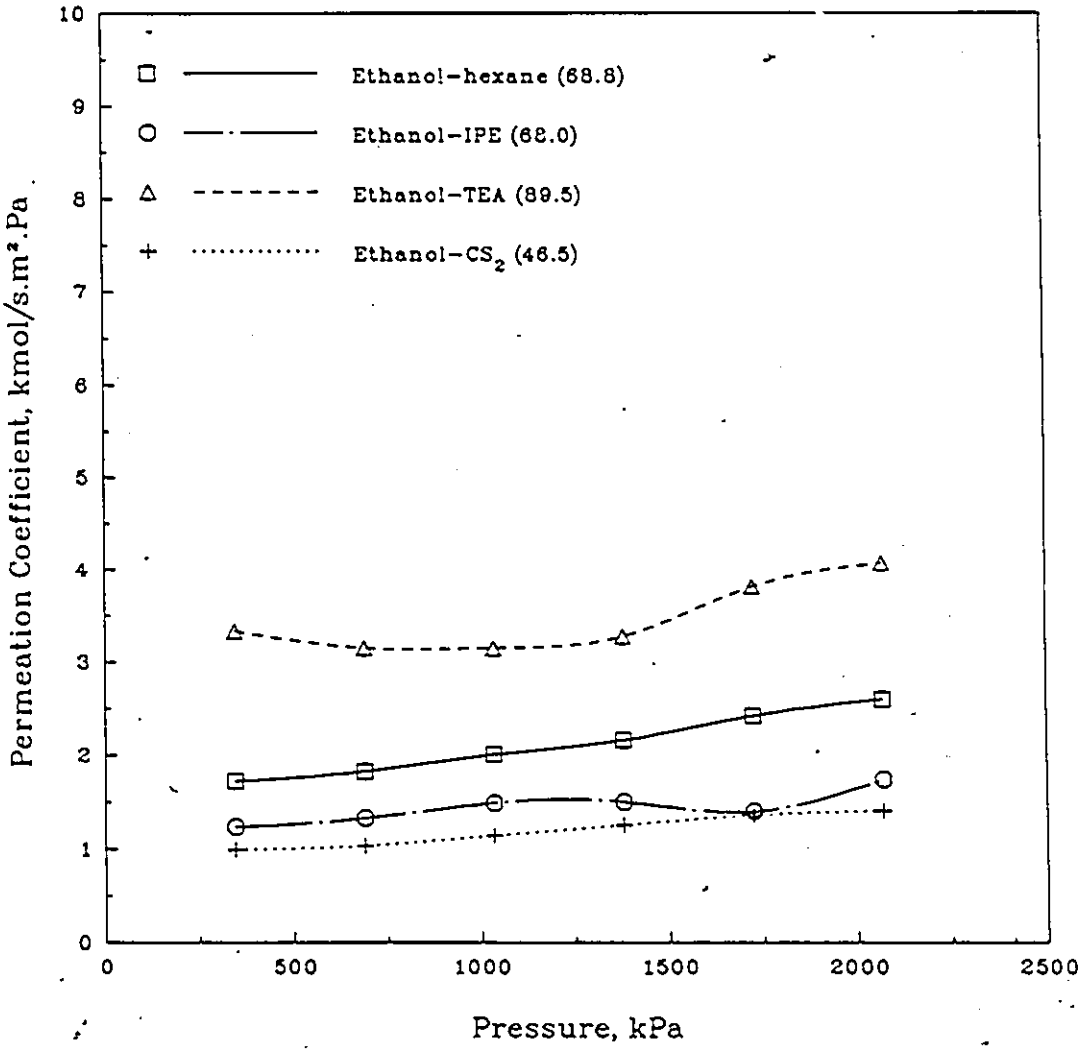

Figure 4.10: Average Permeation Coefficient $\times 10^{11}$ versus Pressure for Ethanol Solvent Membranes. The numbers within the brackets indicate the second solvent boiling point.

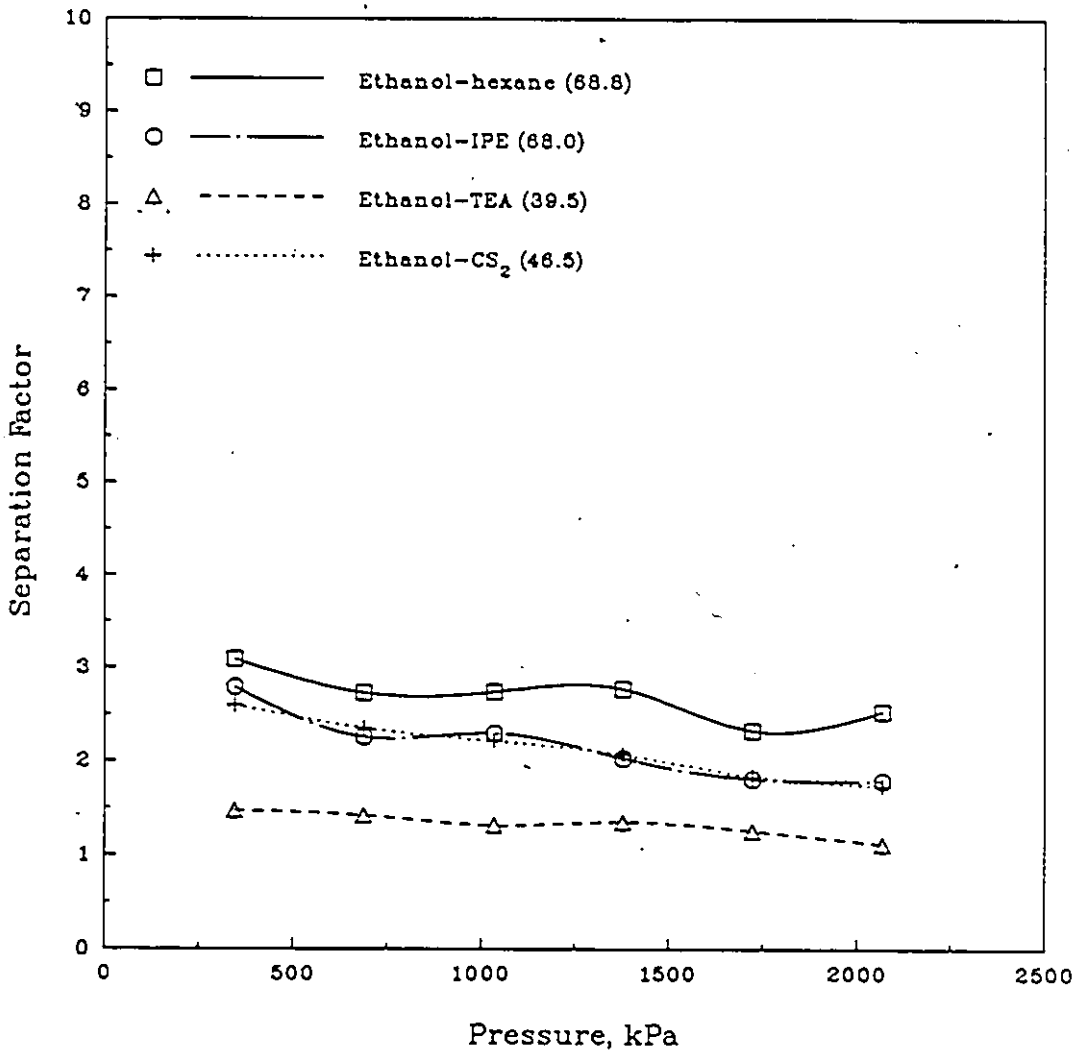

Figure 4.11: Average Separation Factor versus Pressure for Ethanol Solvent Membranes. The numbers within the brackets indicate the second solvent boiling point.

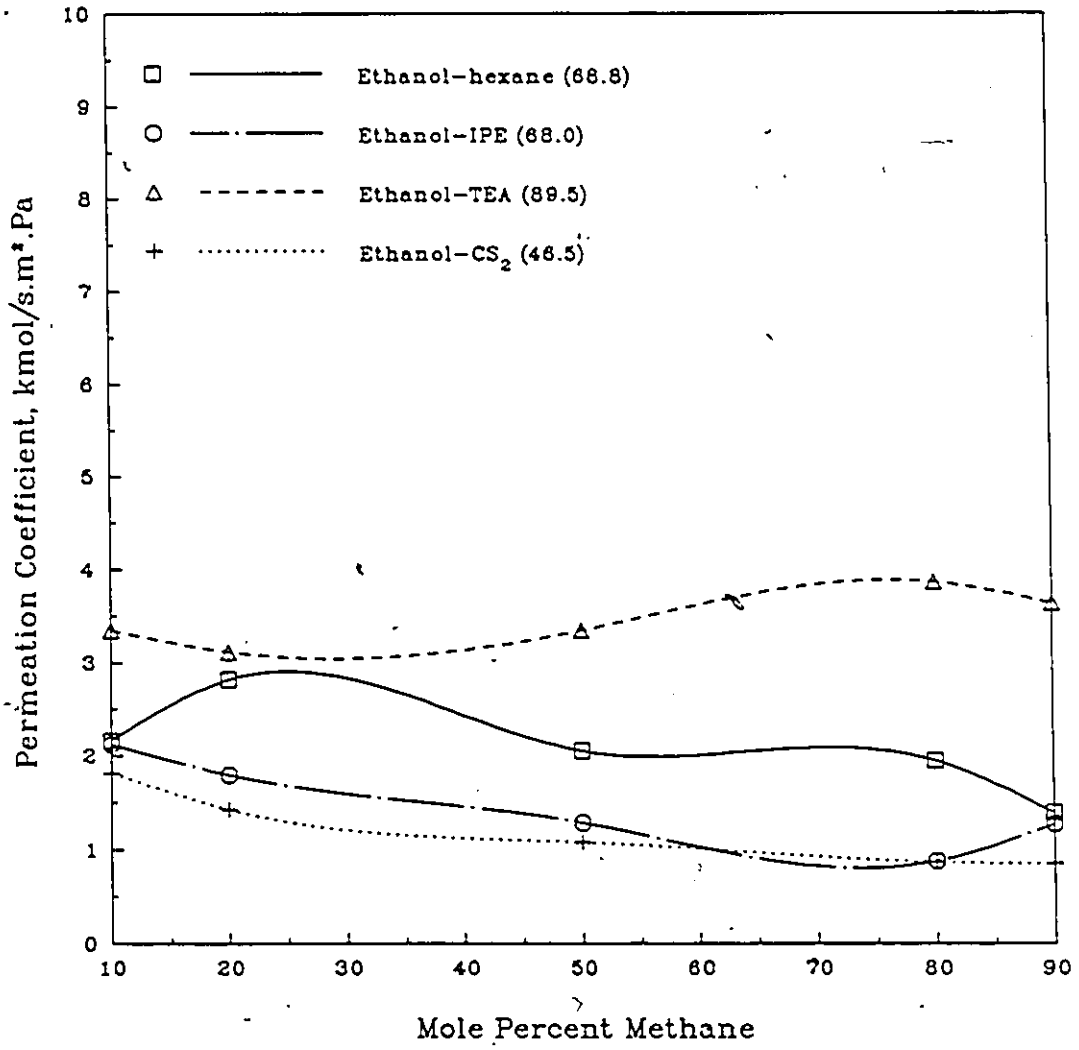

Figure 4.12: Average Permeation Coefficient $\times 10^{11}$ versus Mole Percent Methane for Ethanol Solvent Membranes. The numbers within the brackets indicate the second solvent boiling point.

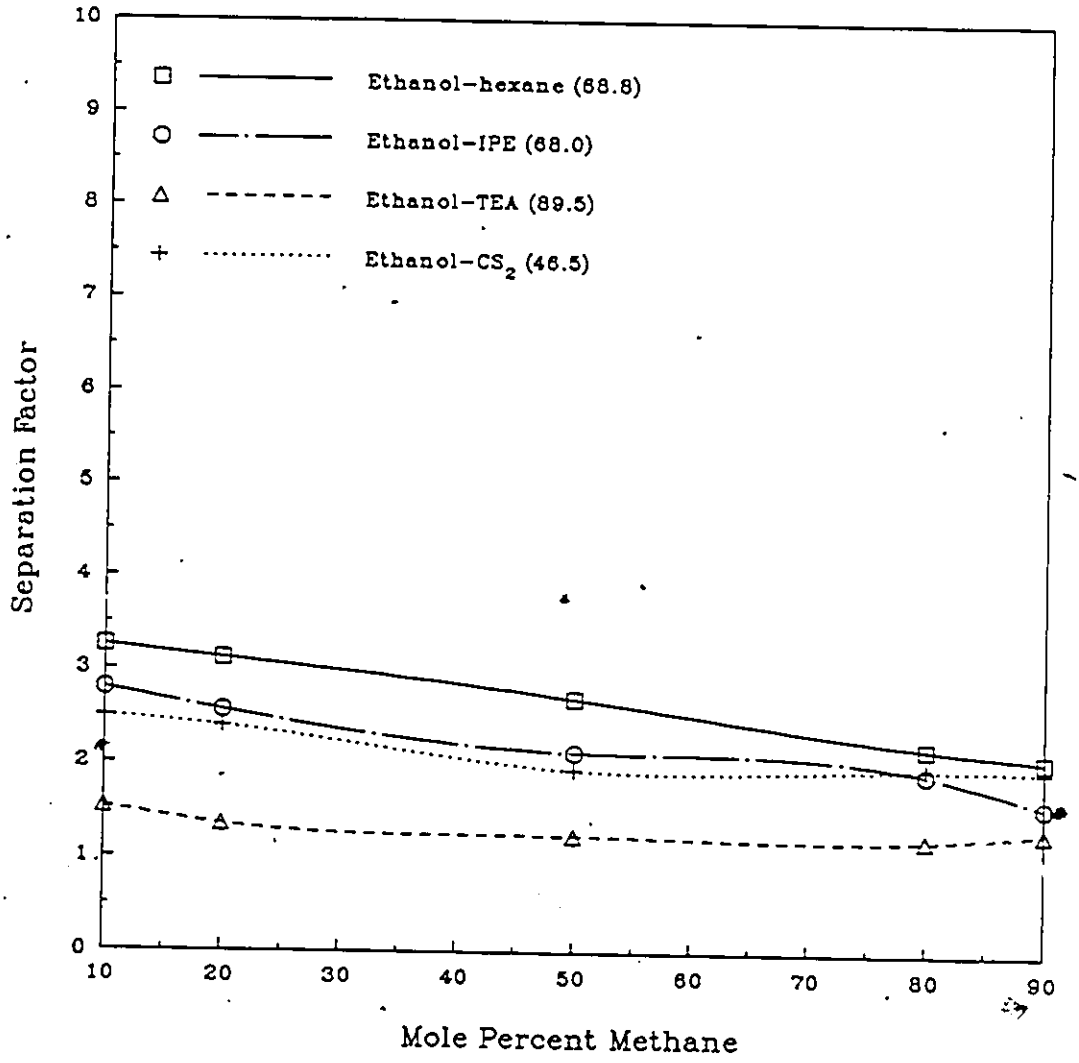

Figure 4.13: Average Separation Factor versus Mole Percent Methane for Ethanol Solvent Membranes. The numbers within the brackets indicate the second solvent boiling point.

and composition of separation factors and permeation coefficients are shown in Figures 4.14 through 4.17. The other solvent combinations show similar trends with higher degrees of variability. In Figure 4.14, the permeation coefficient either increased or stayed constant with increasing pressure. It is observed that the permeation coefficient of carbon dioxide is greater than that of methane and increases with increasing pressure. Methane has a much lower permeation coefficient which does not increase with pressure. Permeation coefficients for mixtures of the pure gases fall between the pure component curves. These results indicate that the mechanism for carbon dioxide transport through the membrane is different from that of methane.

In Figure 4.15, the variation of the permeation coefficient is large for pure CO_2 (i.e. 0 % CH_4). The permeation coefficient is very close to zero for pure CH_4.

The results plotted in Figure 4.16 indicate that the separation factor decreases with increasing pressure. The results plotted in Figure 4.17 the separation factor is independent of gas composition.

Minhas et al. [52] studied the separation of the same gases using solvent dried cellulose acetate membranes and did similar experiments. He found that the permeabilities of both pure carbon dioxide and methane increased with increasing feed pressure. The rate of increase in the carbon dioxide case was greater due to carbon dioxide interaction (plasticization) with cellulose acetate. The membrane is not damaged and this effect is reversible. Due to the above, the separation factor, defined as the ratio of carbon dioxide to methane permeabilities at a particular pressure, will increase with an increase in pressure. The permeabilities of individual components in the mixtures were found to be different from those of the pure components. The fact that the presence of one component will influence the other components must be taken into account.

Another possible explanation of the decrease in separation factor with an increase in pressure is that the pressure exerted on the membrane results in a stretching of the pores or a loosening of the polymer matrix. This in turn allows more gas to flow through (higher permeation coefficients) and a loss in separation (lower separation factors).

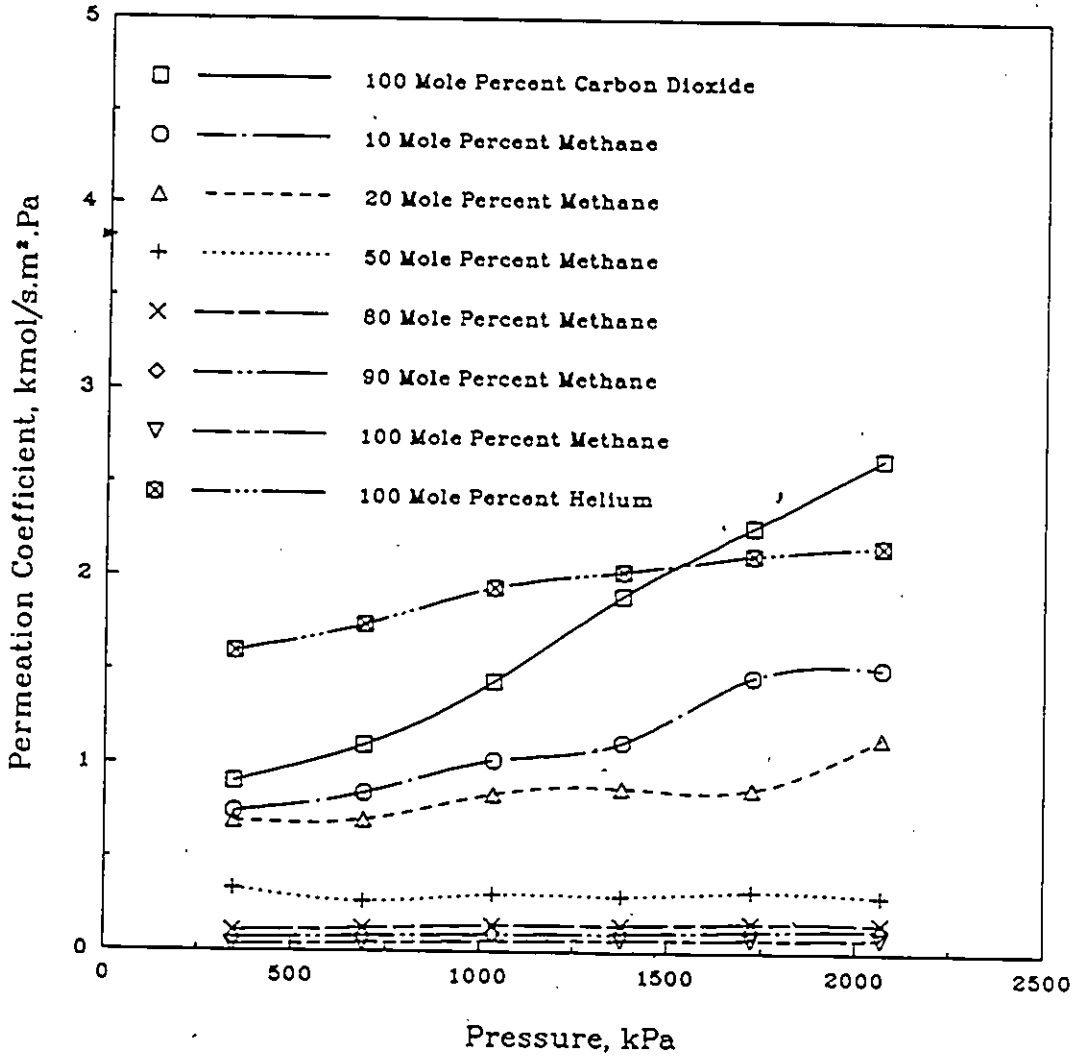

Figure 4.14: Permeation Coefficient $\times 10^{11}$ versus Pressure for the Methanol -IPE Solvent Combination at a shrinkage temperature of 70 °C.

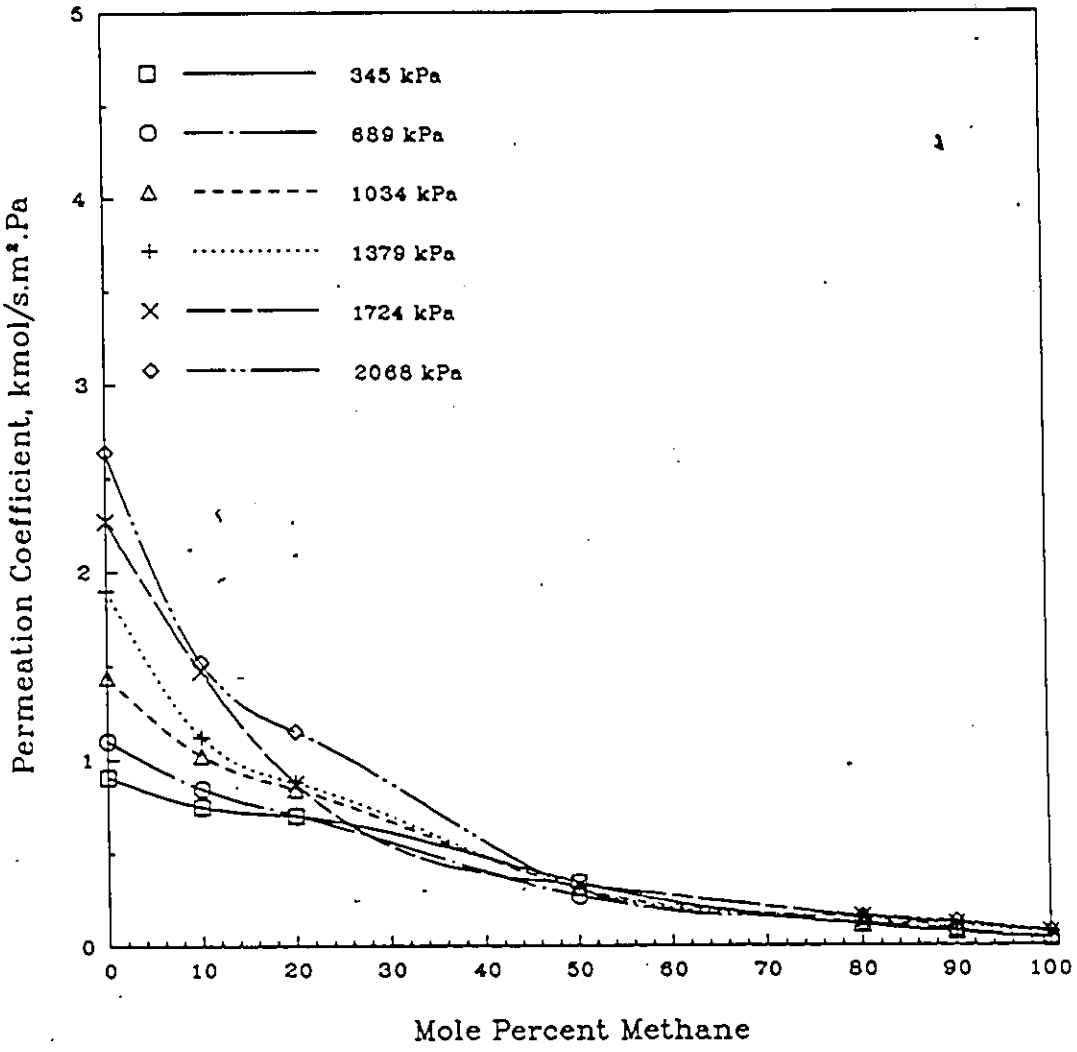

Figure 4.15: Permeation Coefficient $\times 10^{11}$ versus Mole Percent Methane for Methanol–IPE Solvent Combination at a shrinkage temperature of 70 °C.

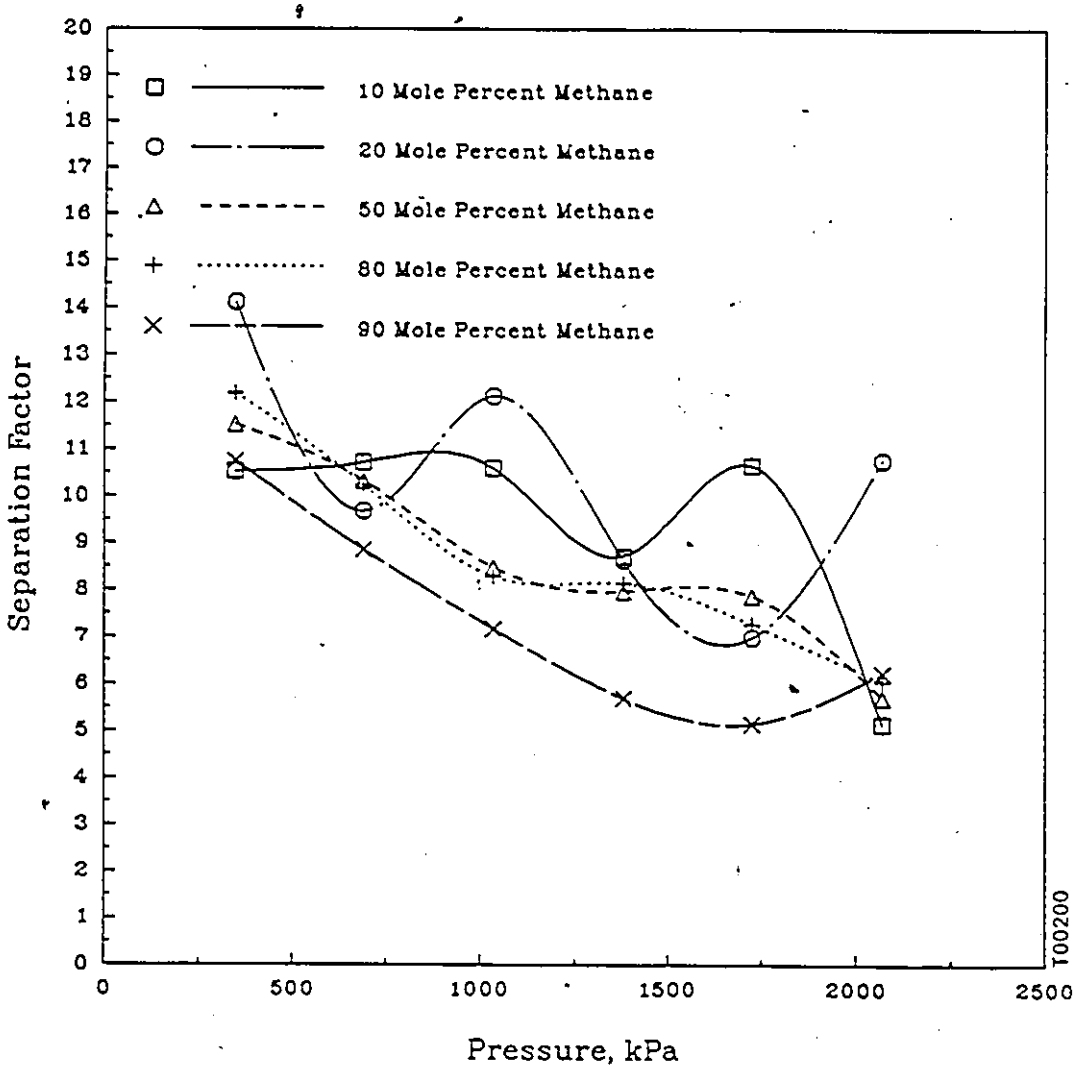

Figure 4.16: Separation Factor versus Pressure for Methanol–IPE Solvent Combination at a shrinkage temperature of 70 °C.

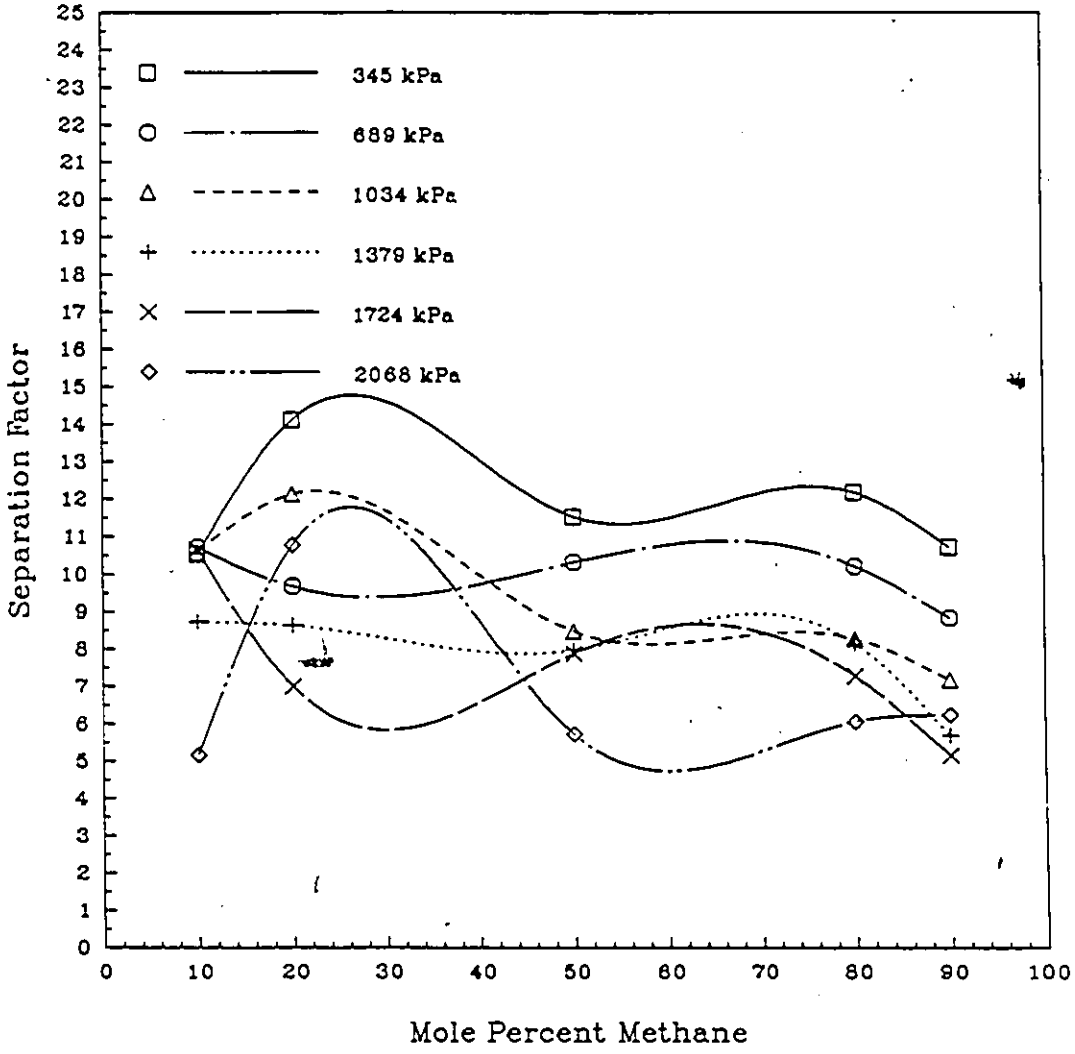

Figure 4.17: Separation Factor versus Mole Percent Methane for the Methanol–IPE Solvent Combination at a shrinkage temperature of 70 °C.

4.4 Pore Formation Mechanism

4.4.1 Theory

It is conjectured that the pores on the membrane surface changes during shrinking and the solvent exchange process. The term pore size refers to the size of the pore on the surface of the membrane. Figure 4.18 shows four stages with their corresponding pore sizes. It is assumed that pore sizes are identical (i.e. there is little or no variation of pore size in making the membrane sheets) on coupons before they are shrunk. By varying the temperature of the water bath in which the coupons are shrunk, different water-wet membrane pore sizes are created. The higher the bath temperature the smaller the resulting pore size.

- Pore size (I) corresponds to the pore size on the water wet membranes that have been shrunk at various temperatures.
- Pore size (II) corresponds to the pore size of the membranes after the replacement of water by the first solvent.
- Pore size (III) corresponds to the pore size of the membrane after the replacement of the first solvent by the second solvent.
- Pore size (IV) corresponds to the pore size of the evaporated and dry membrane.

Lui [39] describes the pore formation mechanism using the following five basic assumptions.

1. The separation factor increases with a decrease in pore size (IV) (pore size on the surface of the dry membrane).
2. The pore size on the water-wet membrane (pore size (I)) decreases with an increase in the shrinkage temperature.
3. The pore size on the membrane after first solvent replacement, (pore size (II)), increases with an increase in the molecular size of the alcohol.
4. There is a critical value of pore size (II) from which the smallest pore size (IV) is produced. Pore size (IV) becomes larger as the deviation from this critical pore size (II) gets large.

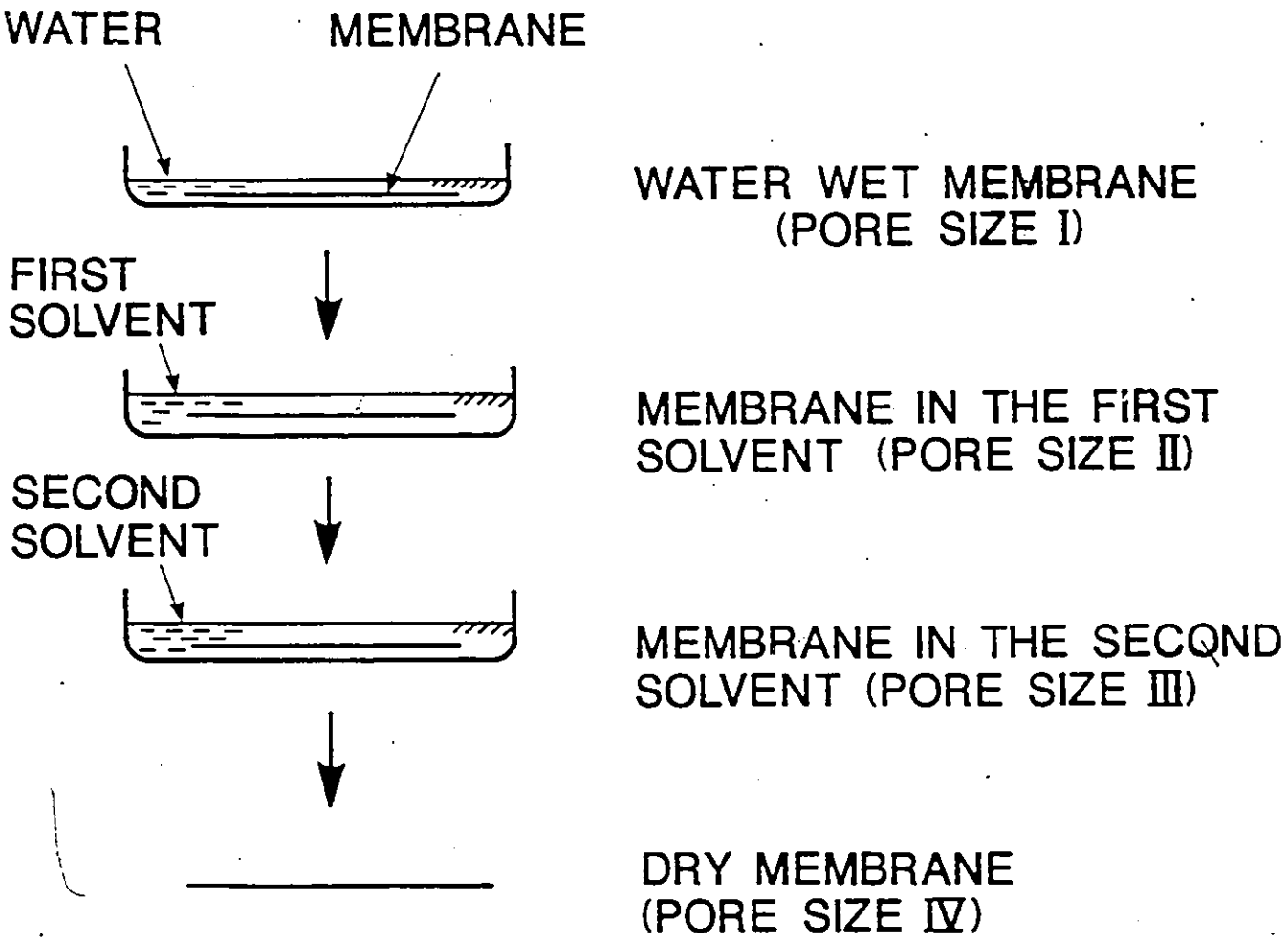

Figure 4.18: Four Stages Affecting Pore Sizes.

5. The critical value of pore size (II) depends on and is unique to the second solvent and this value increases with an increase in the boiling point of the second solvent.

In Figure 4.19, seven membranes are shown with different pore sizes. As shrinkage temperature increases, pore size (II) decreases. For a particular first solvent, pore size (I) has the same relative sizes as pore size (II). Also seen is membrane 4 which corresponds to the membrane with the smallest pore size (IV). This is where the highest separation factors were observed. For a particular second solvent, there is a unique critical pore size (II). These critical pore sizes increase with an increase in boiling point of the second solvent. Any deviation from the critical value leads to a larger pore size (IV). Also, the ranges of pore size (IV) are classified into four patterns, α, β, γ and δ.

The pore size on the membrane surface (active layer) is responsible for selecting the flow mechanism of gas transport. It is the surface flow mechanism that is significantly responsible for the separation of gases [47]. This mechanism takes place in all pore sizes however, when the pore size becomes smaller, the surface flow contribution becomes greater. Thus separation increases as the size of the pores decrease. Nguyen et al. [44] found that cellulose acetate materials formed small agregate pores in unshrunk membranes and that the pore size determined using the Surface-Force-Pore-Flow model indicated a decrease of pore size with shrinkage temperature increase, explaining the second assumption. Farnand et al. [17,18] has reported that for a given membrane, separation in a water system was greater than that of a methanol system, which in turn was greater than that in an ethanol system. These results can be interpreted in terms of pore radius as $R_{\text{ethanol}} > R_{\text{methanol}} > R_{\text{water}}$. Essentially, a small increase in the pore size was found when water was replaced by methanol and a larger increase when replaced by ethanol.

The presence of a critical pore size (II) implies that there are two opposing effects on the final pore size. At the critical pore size (II) the resulting pore size (IV) is the minimum attainable with a specific second solvent. For the pore size (II) greater or less than the critical, the resulting pore size (IV) is greater. This first effect can be explained as follows. Pores within the membrane shrink proportionally when the same second solvent is evaporated thus, a decrease in pore size (II) will result in a decrease in pore size (IV). The other effect is explained in the following. It is known that when a capillary pore of a small diameter is filled by a liquid a negative pressure prevails in the pore and a force is exerted on the capillary wall to decrease

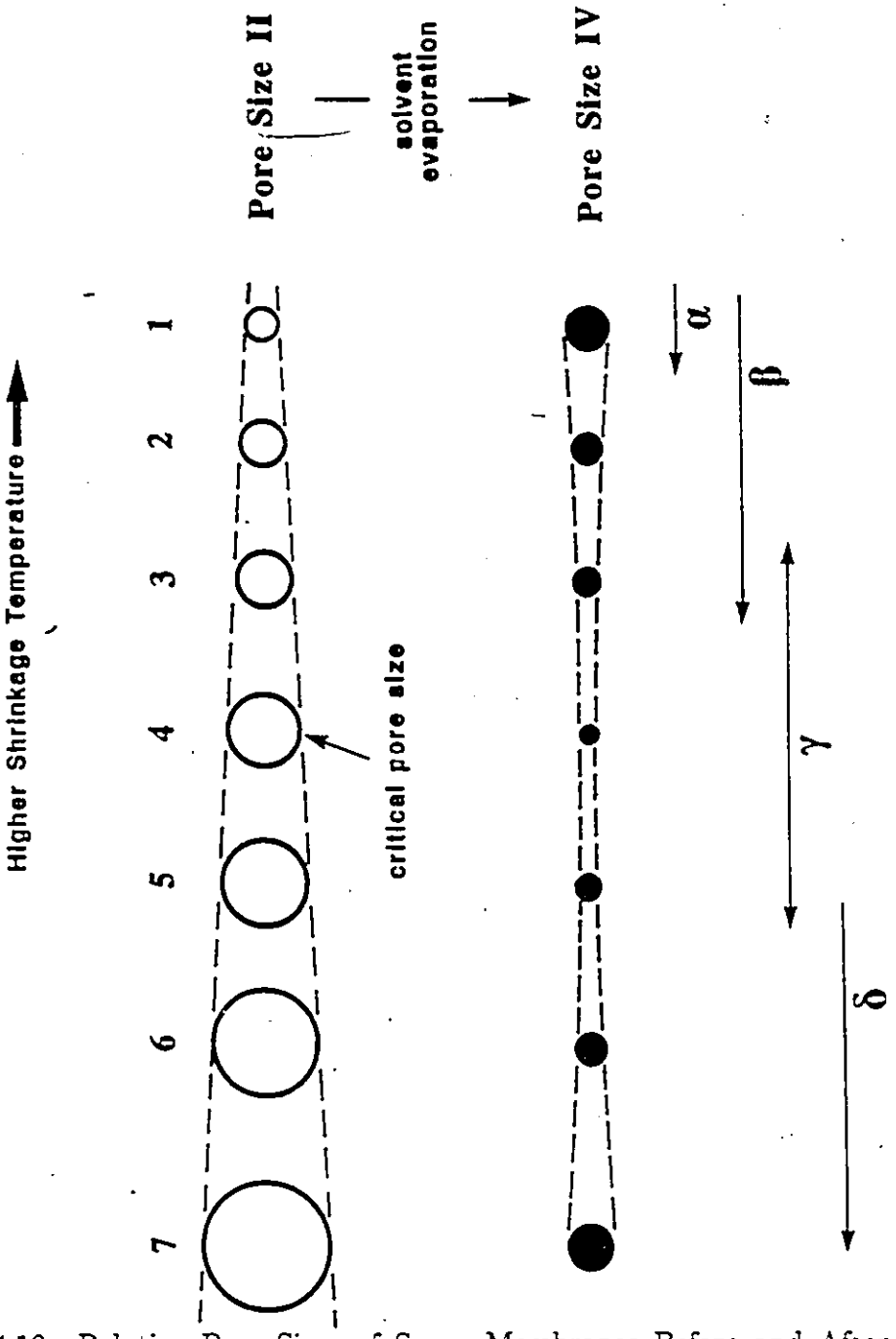

Figure 4.19: Relative Pore Sizes of Seven Membranes Before and After Solvent Evaporation.

the pore size [53]. This is particularly true when the liquid can wet the membrane surface effectively. When the liquid is taken away rapidly under these circumstances, the pore size is reduced, and the pore may completely collapse. When the liquid is removed slowly, on the other hand, the pore size may retain the initial value. Briefly, the degree of the reduction in the pore size depends on the speed of removing the liquid from inside the pore. This speed further depends on the diffusion rate of the liquid through the pore which is governed by the size of the pore. When the pore size is large, the liquid diffusion rate in the pore is rapid and the degree of pore size reduction is greater. The pore filling liquid corresponds to the second solvent and is removed by evaporation in this work. Thus we may expect a larger degree of pore size reduction resulted from a larger pore size (II) according to the above mechanism.

Furthermore, when the boiling point of the second solvent increases, the driving force applied on the second solvent to be removed from the pore is lowered. Therefore, in order to obtain a sufficiently high diffusion rate, the pore size must be larger. As a consequence, the same degree of pore size reduction can be achieved only for a greater pore size (II). This results in the shift of the critical value in the pore size (II) to a greater value.

As a consequence of this mechanism one would expect the separation factor to exhibit a maximum and the permeation coefficient to exhibit a minimum with respect to shrinkage temperature. The location of these curves on a plot would depend on the molecular size of the first solvent and the boiling point of the second solvent. For a given first solvent the maximum separation factor would shift to the left with increasing boiling points of the second solvent. Different first solvents for the same second solvent would shift the maximum to the right going from methanol to ethanol.

4.4.2 Experimental Evidence of Theory

In the following section, the results will be discussed in terms of the above mechanism proposed by Lui. It is proposed that second solvents with low boiling points gave smaller pores and hence a lower permeation coefficient (as stated in assumption 5) [39]. Noting that the IPE and hexane solvents have similar boiling points, seen in Figure 4.6, the hexane and IPE curves have a lower permeation coefficient than the TEA curve. In Figure 4.7, higher separation factors occur with lower second solvent boiling points (i.e. IPE (68.0 °C) has a higher value than TEA (89.5 °C)). This also follows the general rule that permeation is low for a high separation factor.

The orders of the second solvents were the same as in Figures 4.4 and 4.5.

Figure 4.9 shows the separation factor results obtained for ethanol as the first solvent. According to assumption 2, a shrinkage temperature increase can be represented by a decreasing scale of pore size (I). Since only one first solvent was used this scale can also be represented by a decreasing pore size (II). Also from Figure 4.9, the critical pore size (II) of CS_2 which results in the highest separation factor, and hence the smallest pore size (IV), according to assumption one, occurs around 80°C. CS_2 has a boiling point of 46.5°C. The boiling point is 68.8°C for hexane, and the shrinkage temperature at which the highest separation factor occurred was below 70°C. Extrapolating further, the highest separation factor for TEA occurred below 70°C, and TEA boiling point is 89.5°C. The exception is ethanol–IPE with a boiling point of 68.0°C. The highest separation should occur at a shrinkage temperature below or around 70°C. This appears not to be the case for ethanol–IPE. An analysis of variance in the Appendix Errors, was performed showing that shrinkage temperature was a significant variable in spite of scatter in the data. The trend is that the shrinkage temperature at which the highest separation factor is obtained shifts from a higher value to a lower one as the boiling point of the second solvent is increased. This is consistent with assumptions 4 and 5.

As postulated above, the lower second solvent boiling points yield lower permeation coefficients. This is shown very effectively in Figure 4.10. This order is inverted for separation factor and follows the general rule, as shown in Figure 4.11.

The third assumption can be tested by plotting separation factors versus pore size (II) for both first solvents, for the same second solvents. Figures 4.20 to 4.22 are actual data where the operating conditions are 10 mole percent methane in feed at an operating pressure of 345 kPa absolute. Data from Minhas et al. [52], using isopropanol as the first solvent, has been added to these graphs to further show the effect of first solvent molecular size. This data was collected with an operating pressure of 2200 kPa absolute. Isopropanol is the largest molecule, then the ethanol molecule is larger than methanol, and in the same way, pore size (II) is larger for the isopropanol case then ethanol and methanol, in that order. This is illustrated in Figure 4.20, which shows separation factors for isopropanol, ethanol and methanol for the second solvent CS_2. A range of pore size (II) exists for each first solvent, since a range of shrinkage temperatures are used. The critical pore size (II) which leads to the highest separation factor is produced at a shrinkage temperature around 80 °C for isopropanol

as the first solvent. The critical pore size (II) which leads to the highest separation factor when the membrane is dried, is in the middle of the range covered by ethanol, see Figure 4.20. The constant separation factors obtained for methanol as the first solvent is understandable when the pore size (II) of these membranes are significantly less than those of ethanol. Similarly Figures 4.21 through 4.22 refer to different second solvents and show similar trends.

The shapes of separation factor for methanol and ethanol are represented in Figure 4.23. These shapes are classified into four patterns α, β, γ and δ which were illustrated in Figure 4.19. The combinations of solvents determine the shape of the curves. The patterns are defined as:

1. Pattern α: (Methanol–CS_2) The membrane pore size (II) is the smallest. However, there is little pore size reduction during the solvent evaporation process and as a result the largest pore size (IV) is produced.

2. Pattern β: (Methanol– IPE and Ethanol–Hexane) The pore sizes (II) are on the right side of the critical pore size. The pore size (IV) decreases as the shrinkage temperature decreases.

3. Pattern γ: (Ethanol–CS_2) The pore sizes (II) passes the critical pore size. The pore size (IV) decreases as the shrinkage temperature decreases.

4. Pattern δ: (Ethanol-IPE) The pore size (II) is on the left side of the critical pore size. The pore size increases as shrinkage temperature decreases.

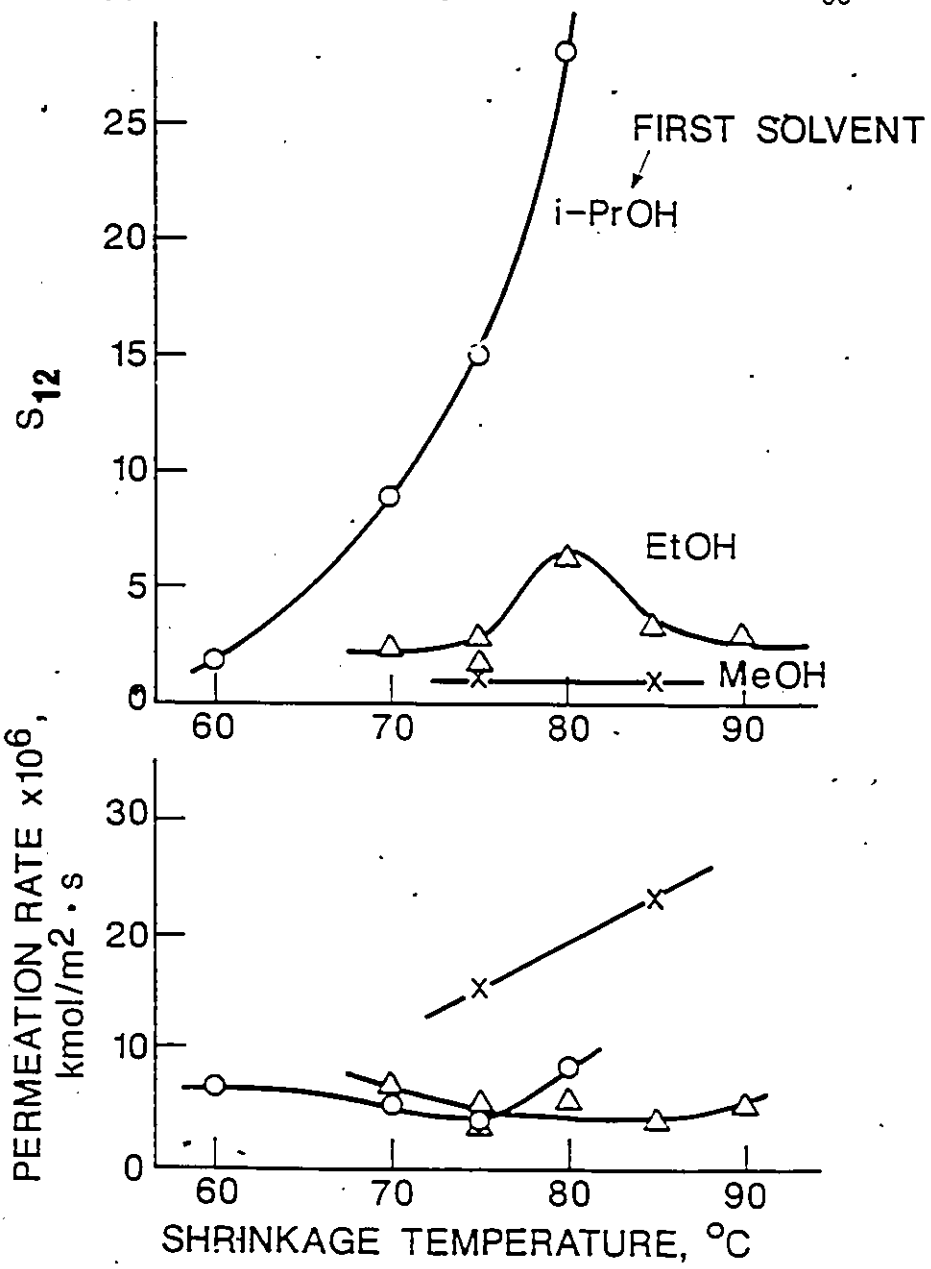

Figure 4.19: The Effect of Shrinkage Temperature and First Solvent on the Separation Factor for Carbon Disulfide as Second Solvent.

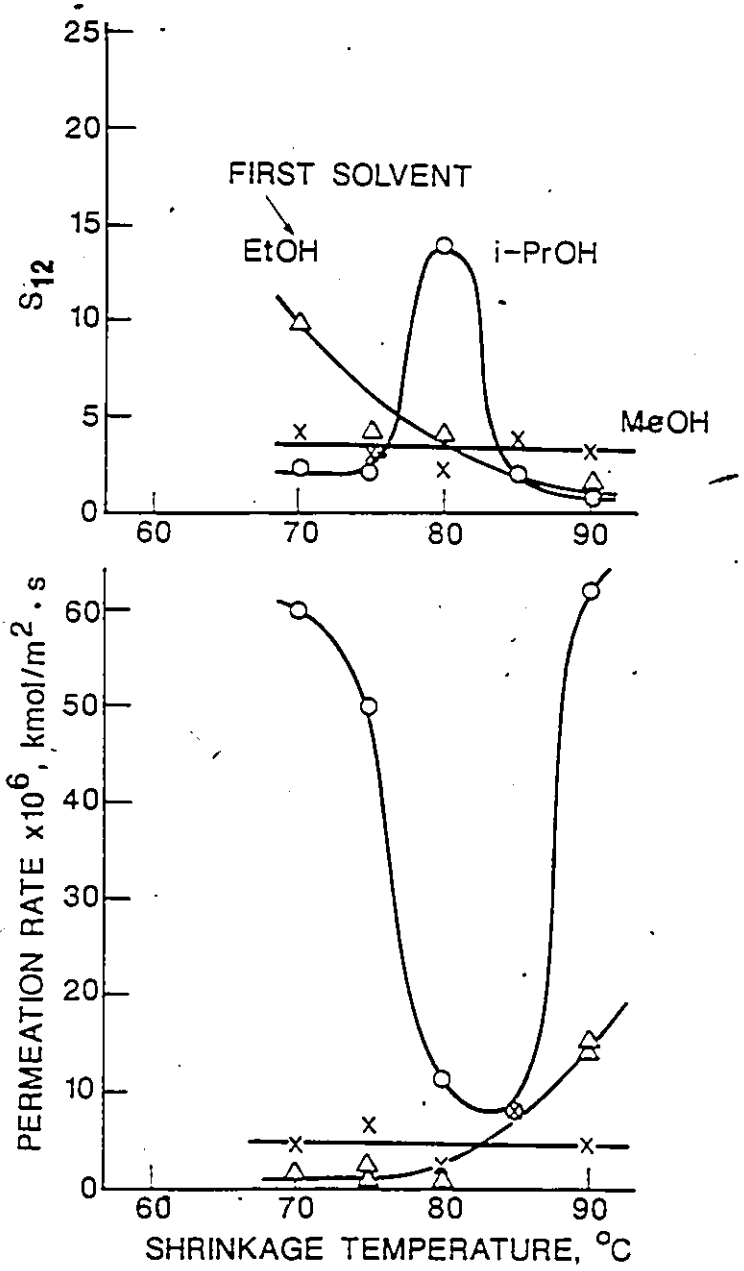

Figure 4.20: The Effect of Shrinkage Temperature and First Solvent on the Separation Factor for Hexane as Second Solvent.

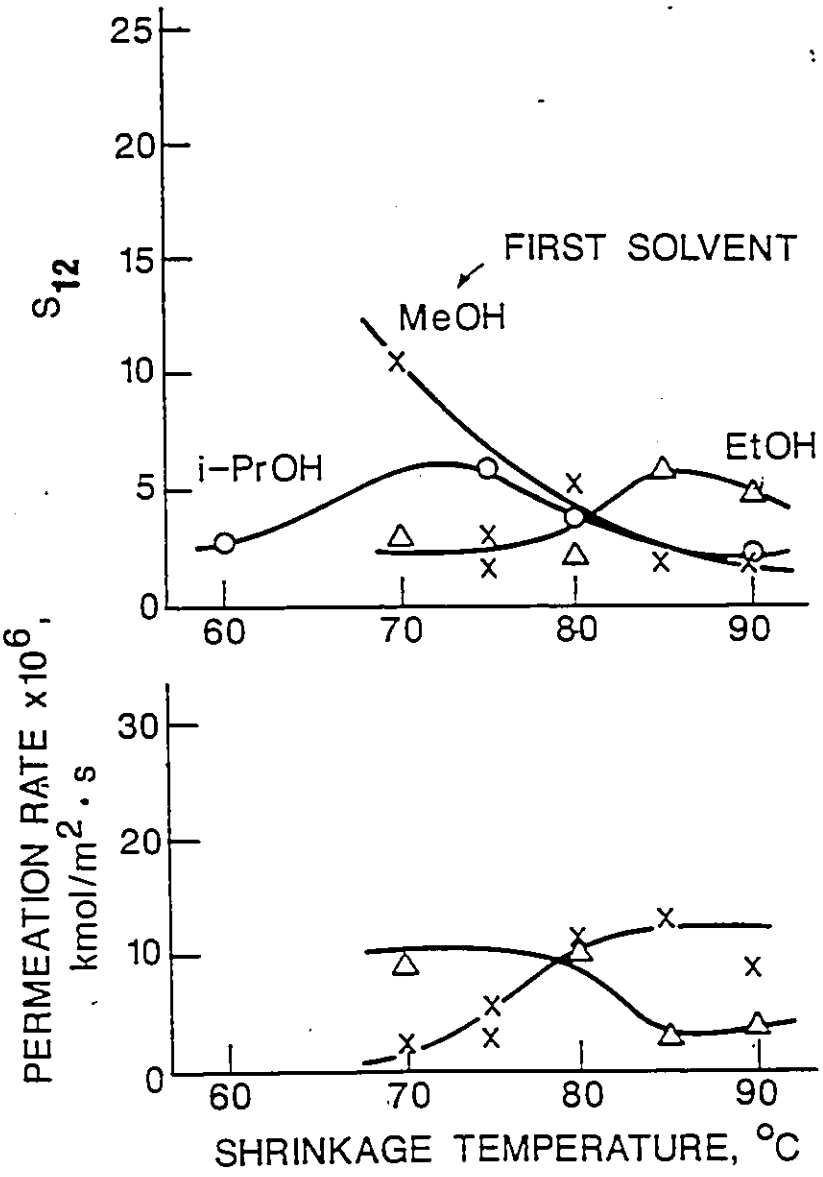

Figure 4.22: The Effect of Shrinkage Temperature and First Solvent on the Separation Factor for Isopropyl Ether as Second Solvent.

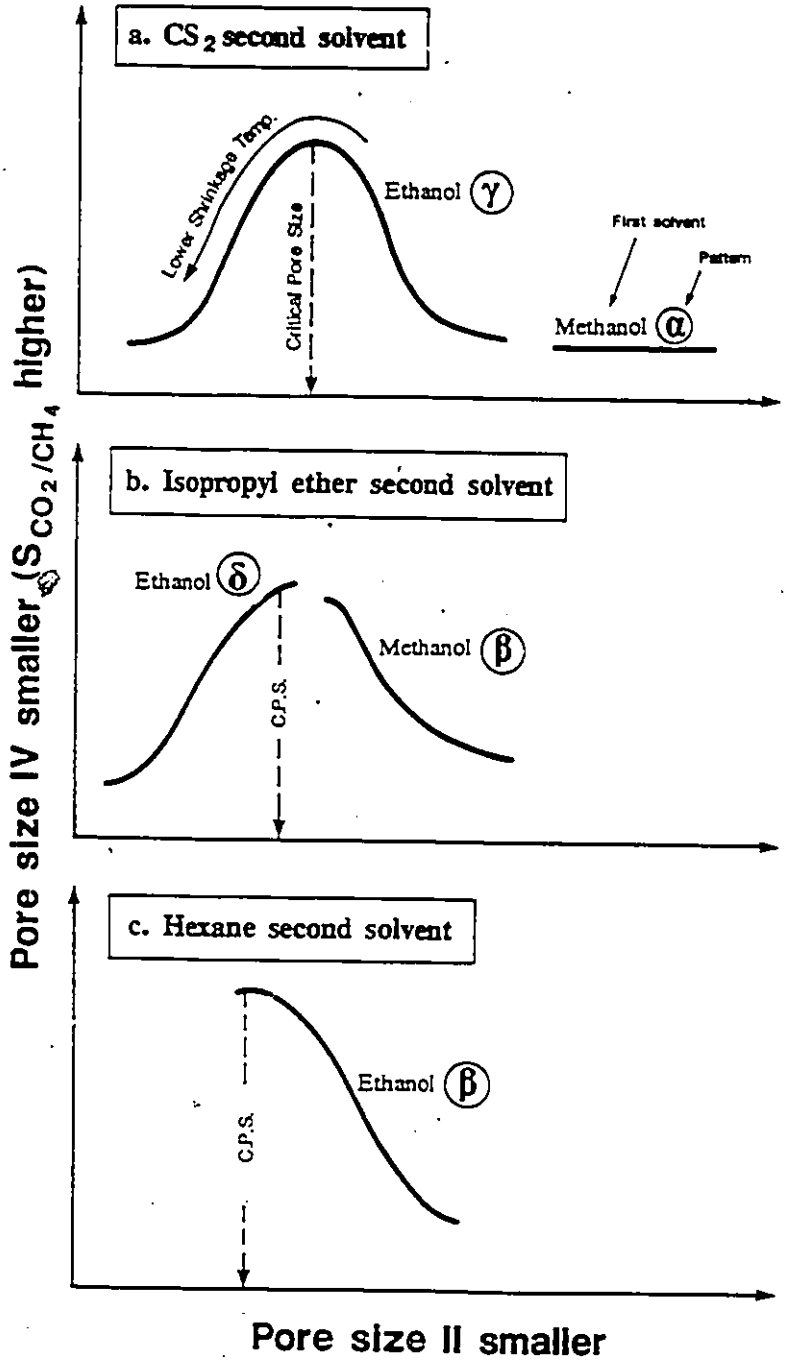

Figure 4.23: Patterns of Various Solvent Combinations

Table 4.1: Coupon Numbers

First Solvents Used	Shrinkage Temperature °C	Second Solvents Coupon Numbers			
		CS_2	IPE	TEA	hexane
Methanol	70	–	1-1	1-4	2-8
	75	1-5	1-2	–	6-7
	80	–	4-6	1-3	5-3
	85	5-7	4-7	4-3	2-4
	90	–	4-4	4-5	5-6
Ethanol	70	6-3	2-3	6-6	2-6
	75	5-5,6-2	2-5	6-8	1-6,4-1
	80	2-7	–	–	5-1
	85	6-4	1-8	6-1	–
	90	5-4	2-2	5-2	6-5,4-2

Chapter 5

Conclusions

Over the range of variables tested, the following conclusions can be drawn. Average responses of separation factor and permeation coefficient of each membrane revealed trends adequately. Shrinkage temperature, first and second solvents were major variables. The results indicated that separation factor varies inversely with the permeation coefficient. Methanol–IPE and ethanol–hexane are the solvent combinations that produced the best membranes. Generally, as shrinkage temperature increased, permeation coefficient increased and separation factor decreased.

The membrane methanol–IPE with a shrinkage temperature of 70 °C was one of the best membranes. Results show that permeation of CO_2 is greater than CH_4 and increases much more as pressure is increased. Separation factor decreased with increased pressure.

The results seem to support the proposed mechanism. A critical value of pore size (II) on the surface of the first solvent membrane exists. This critical value is achieved through shrinking and first solvent replacement. It also results in the smallest pore size (IV) on the surface of the final dry membrane which gives the highest separation factor. The critical pore size depends mainly on the boiling point of the second solvent, and to a lesser extent on the molecular size of the first solvent.

Chapter 6

Recommendations

The experiments should be done in a more defined manner. Perhaps a factorial design could be used to determine the amount of error. Shrinkage temperatures at a lower range should be investigated (i.e. at a temperature lower than 70 °C). Other solvents, using the solvent exchange technique, could be used to further confirm the theory proposed. A specific solvent composition such as methanol–IPE should be thoroughly investigated so as to eliminate the solvent exchange as a variable and to understand fully the effects of shrinkage temperature and to confirm the theory proposed.

Bibliography

[1] J.P. Agrawal and S. Sourirajan, "Helium Separation by Cellulose Acetate Membranes," *J. Appl. Polym. Sci.*, **13**, 1065 (1969).

[2] J.P. Agrawal and S. Sourirajan, "High Flux Freeze–Dried Cellulose Acetate Reverse Osmosis Membranes as Microporous Barriers in Gas Permeation and Separation," *J. Appl. Polym. Sci.*, **14**, 1303 (1970).

[3] R. W. Baker and I. Blume, "Permselective Membranes Separate Gases," *Chemtech*, 4, 232 (1986).

[4] W. Baldus and D. Tillman, "Conditions Which Need to be Fulfilled by Membrane Systems in Order to Compete with Existing Methods of Gas Separation," *Membr. as Sep. Enrich.*, **62**, 26 (1986).

[5] B. Baum, W. Holley,Jr. and R.A. White, "Membrane Separation Processes," *P. Meares Ed.*, Elsevier, New York 187 (1976).

[6] W.A. Bollinger, D.L. MacLean and R.S. Narayan, "Separation Systems for Oil Refining and Productions," *Chem. Eng. Prog.*, **27**, Oct. (1982).

[7] K. Chan, L. Tinghui, T. Matsuura and S. Sourirajan, "Effect of Shrinkage on Pore Size and Pore Size Distribution of Cellulose Acetate Reverse Osmosis Membranes," *Ind. Eng. Chem. Prod. Res. Dev.*, **23**, 124 (1984).

[8] M.C. Chan and J.W. McCutchan, "Method for the Development of a High Performance Reverse Osmosis Membrane," *Proc. 6th Inter. Symp. Fresh Water from the Sea*, **3**, 173 (1978).

[9] E.S.K. Chian and H.H.P. Fang, "Constrained Optimization of Cellulose Acetate Membrane Using Two–Level Factorial Design," *J. Appl. Poly. Sci.*, **19**, 251 (1975).

[10] J.S. Chiou, Y. Maeda and D.R. Paul, "Gas Permeation in Polyethersulfone," *J. Appl. Polym. Sci.*, **33**, 1823 (1987).

[11] A.B. Coady and J.A. Davis, "CO_2 Recovery by Gas Permeation (Separation Techniques)," *Chem. Eng. Prog.*, **78**, 44 (1982).

[12] T.E. Cooley and W.L. Dethloff, "Field Tests Show Membrane Processing Attractive," *Chem. Eng. Prog.*, **81**, 45 (1985).

[13] T.E. Cooley, "Spiral Wound Membrane CO_2 Removal Process for the Wellhead," *Presented at AIChE Spring National Meeting*, Anaheim, Calif., (1984).

[14] T.E. Cooley and A.B. Coady, "Removal of H_2S and/or CO_2 From a Light Hydrocarbon Stream by Use of Gas Permeable Membrane," *United States Patent*, **4130403**, Dec. 19 (1978).

[15] U. Eickmann and U. Werner, "Gas Separation Using Porous Membranes," *Ger. Chem. Eng.*, **8**, 186 (1985).

[16] D.L. Ellig, J.B. Althouse and F.P. McCandless, "Concentration of Methane from Mixtures with Carbon Dioxide by Permeation through Polymeric Films," *J. Membrane Sci.*, **6**, 259 (1980).

[17] B.A. Farnand, F.D.F. Talbot, T. Matsuura and S. Sourirajan, "Reverse Osmosis Separations of Some Organic and Inorganic Solutes in Methanol Solutions using Cellulose Acetate Membranes," *Ind. Eng. Chem. Proc. Des. Dev.*, **22**, 179 (1983).

[18] B.A. Farnand, F.D.F. Talbot, T. Matsuura and S. Sourirajan, "Reverse Osmosis Separations of Some Organic and Inorganic Solutes in Ethanol Solutions with Cellulose Acetate Membranes," *I&EC Research*, **26**, 1080 (1987).

[19] H. Finken, "Asymmetric Membranes for Gas Separations," *Materials Science of Synthetic Membranes*, **Chapt. 11**, 245 (1985).

[20] H.L. Frisch and S.A. Stern, "Diffusion of Small Molecules in Polymers," *CRC Critical Reviews in Solid State and Materials Sciences*, **11**, 123 (1981).

[21] P.K. Gantzel and U. Merten, "Method and Apparatus for Gas Separation by Diffusion," *U.S. Patent 3,415,038*, Dec. (1968).

[22] P.K. Gantzel and U. Merten, "Gas Separations with High-Flux Cellulose Acetate Membranes," *Ind. Eng. Chem. Proc. Des. Dev.*, **9**, 331 (1970).

[23] E.R. Gilliland, R.F. Baddour and J.L. Russell, "Rates of Flow Through Microporous Solids," *A.I.Ch.E.J.*, 4, 90 (1958).

[24] C.S, Goddin, "Pick Treatment for High Carbon Dioxide Removal," *Hydrocarbon Proc.*, 61, 125 (1982).

[25] T. Graham, "On the Absorption and Dialytic Separation of Gases by Colloid Septa," *Philos. Magazine and Journal of Sci.*, **32**, 401 (1866).

[26] H.E. Grethlein, "Statistical Design of Experiments for Optimizing the Casting Variables for Cellulose Acetate Membranes," *Reverse Osmosis Synth. Membr.*, 111 (1977).

[27] J.M.S. Henis and M. K. Tripodi, "The Developing Technology of Gas Separating Membranes," *Science*, **220**, 11 (1983).

[28] S.T. Hwang and K. Kammermeyer, "Membranes in Separations," Wiley, New York, Chapt. 13 (1975).

[29] G. Jonsson and C.E. Boesen, *Desalination*, **17**, 145 (1975).

[30] S.M. Jordan, W.J. Koros and G.K. Fleming, "The Effects of CO_2 Exposure on Pure and Mixed Gas Permeation Behaviour: Comparison of Glassy Polycarbonate and Silicone Rubber," *J. Membrane Sci.*, **30**, 191 (1987).

[31] O. Kedem and A. Katchalsky, "Thermodynamic Analysis of the Permeability of Biological Membranes to Nonelectrolytes," *Biochim. Biophys. Acta*, **27**, 229 (1958).

[32] S. Kimura and S. Sourirajan, "Concentration Polarization Effects in Reverse Osmosis Using Porous Cellulose Acetate Membranes," *Ind. Eng. Chem. Proc. Des. Dev.*, 7, 41 (1968).

[33] S. Kimura and S. Sourirajan, "Mass Transfer Coefficients for Use in Reverse Osmosis Process Design," *Ind. Eng. Chem. Proc. Des. Dev.*, 7, 539 (1968).

[34] W.J. Koros, B.J. Story, S.M. Jordan, K. O'Brien and G.R. Husk, "Material Selection Considerations for Gas Separation Processes," *Presented at AIChE Spring National Meeting*, New Orleans, LA (1986).

[35] B.W. Laverty and J.G. O'Hair, "Applications of Membrane Technology in the Gas Industry," *Membr. Gas Sep. Enrich.*, **62**, 291 (1986).

[36] S. Loeb and S. Sourirajan, "Sea Water Demineralization by Means of an Osmotic Membrane," *ACS Adv. in Chem. Ser.*, **38**, American Chemical Society, 117 (1963).

[37] H.K. Lonsdale, "Reverse Osmosis and Gas Separations," *Industrial Membrane Technology*, 55 (1982).

[38] H.K. Lonsdale,U. Merten and R.L. Riley, "Transport Properties of Cellulose Acetate Osmotic Membranes," *J. Appl. Polym. Sci.*, **9**, 1341 (1965).

[39] A. Lui, F.D.F. Talbot, A. Fouda, T. Matsuura and S. Sourirajan, "Studies on the Solvent Exchange Technique for Making Dry Cellulose Acetate Membranes for the Separation of Gaseous Mixtures," *J. Appl. Polym. Sci.*, In press, (1988).

[40] D.L. MacLean and T.E. Graham, "Hollow Fibers Recover Hydrogen," *Chem. Eng.*, **87**, No. 4, 54 (1980).

[41] Manos, "Membrane Drying Process," *U.S. Patent*, 4080743, Mar. (1978).

[42] Manos, "Gas Separation Membrane Drying with Water Replacement Liquid," *U.S. Patent*, 4080744, Mar. (1978).

[43] S.L. Matson, J. Lopez and J.A. Quinn, "Separation of Gases with Synthetic Membranes," *Chem. Eng. Sci.*, **38**, No. 4, 503 (1983).

[44] T.D. Nguyen, K. Chan, T. Matsuura and S. Sourirajan, "Effect of Shrinkage on Pore Size and Pore Size Distribution of Different Cellulosic Reverse Osmosis Membranes," *Ind. Eng. Chem. Proc. Des. Dev.*, **23**, 501 (1984).

[45] T. Matsuura and S. Sourirajan, "Reverse Osmosis Transport Through Capillary Pores Under the Influence of Surface Forces," *Ind. Eng. Chem. Proc. Des. Dev.*, **20**, 273 (1981).

[46] T. Matsuura, personal communication.

[47] M.A. Mazid, R. Rangarajan, T. Matsuura and S. Sourirajan, "Separation of Hydrogen-Methane Gas Mixtures by Permeation Under Pressure through Porous Cellulose Acetate Membranes," *Ind. Eng. Chem. Proc. Des. Dev.*, 24, 985 (1985).

[48] M.A. Mazid, "Review: Mechanisms of Transport through Reverse Osmosis Membranes," *Sep. Sci. Tech.*, 19, 357 (1984).

[49] B.S. Minhas, T. Matsuura and S. Sourirajan, "Solvent–Exchange Drying of Cellulose Acetate Membranes for Separation of Hydrogen–Methane Gas Mixtures," *ACS Symposium Series 154*, American Chemical Society, Washington, D.C., 451 (1985).

[50] B.S. Minhas, T. Matsuura and S. Sourirajan, "Characterization of Dry RO Membranes and Predictability of Their Performance for the Separation of H_2/CH_4 Mixtures," *Ind. Eng. Chem. Proc. Des. Dev.*, Submitted (1986).

[51] B.S. Minhas, S.P. Wang and M.B. Sherwin, "Effect of Process Variables on Cellulose Acetate Membrane Performance for Separation of Carbon dioxide–Methane Mixtures," *Proceedings of the International Membrane Conference on the 25th Anniversary of Membrane Research in Canada*, 213 (1986).

[52] B.S. Minhas, T. Matsuura and S. Sourirajan, "Formation of Asymmetric Cellulose Acetate Membranes for the Separation of Carbon Dioxide–Methane Gas Mixtures," *I&EC Research*, 26, 2344 (1987).

[53] K.J. Mysels, *Introduction to Colloid Chemistry*, Interscience, N.Y., 129 (1959).

[54] K.C. O'Brien, W.J. Koros and G.R. Husk, "Influence of Casting and Curing Conditions on Gas Sorption and Transport in Polyimide Films," *Polym. Eng. and Sci.*, 27, 211 (1987).

[55] M. Ohno, T. Morisue, O. Ozaki, H. Heki and T. Miyauchi, "Separations of Rare Gases by Membranes," *Radiochem. Radioanal. Letts.*, 27, 299 (1976).

[56] H. Ohya, Y. Imura, T. Moriyama and M. Kitaoka, "A Study on Pore Size Distribution of Modified Ultrathin Membranes," *J. Appl. Polym. Sci.*, 18, 1855 (1974).

[57] H. Ohya, H. Konuma and Y. Negishi, "Posttreatment-Effects on Pore Size Distribution of Loeb-Sourirajan-Type Modified Cellulose Acetate Ultrathin Membranes," *J. Appl. Polym. Sci.*, **21**, 2515 (1977).

[58] H. Ohya, A. Mase, Y. Negishi and K. Matsumoto, "Gas Permeation Characteristics of Dried Asymmetric Cellulose Acetate Membranes by Alcohol Exchange Treatment," *Maku*, **11** 169 (1986).

[59] L. Pageau and S. Sourirajan, "Improvement of Porous Cellulose Acetate Reverse Osmosis Membranes by Change of Casting Conditions," *J. Appl. Polym. Sci.*, **16**, 3185 (1972).

[60] C.Y. Pan, "Gas Separation by High-Flux, Asymmetric-Hollow Fiber Membrane," *A.I.Ch.E.J.*, **32**, 2020 (1986).

[61] C.Y. Pan, "Gas Separation by Permeators with High-Flux Asymmetric Membranes," *A.I.Ch.E.J.*, **29**, 545 (1983).

[62] C.Y. Pan and H.W. Habgood, "Gas Separation by Permeation, Part II: Effect of Permeate Pressure Drop and Choice of Permeate Pressure," *Can. J. Chem. Eng.*, **56**, 210 (1978).

[63] G.S. Park, "Transport Principles—Solution, Diffusion and Permeation in Polymer Membranes," *Synth. Membr.*, **181**, 155 (1986).

[64] G. Parkinson, "Membranes Widen Roles in Gas Separations," *Chemical Engineering*, April (1984).

[65] C. Rain, "Supersieves Hit the Market," *High Technology*, Nov. (1983).

[66] R. Rangarajan, M.A. Mazid, T. Matsuura and S. Sourirajan, "Permeation of Pure Gases Under Pressure Through Asymmetric Porous Membranes. Membrane Characterization and Prediction of Performance," *Ind. Eng. Chem. Proc. Des. Dev.*, **23**, 79 (1984).

[67] R. Rautenbach and R. Albrecht, "Pervaporation and Gas Permeation —Fundamentals of Process Design," *Int. Chem. Eng.*, **27**, 10 (1987).

[68] C.E. Reid and E.G. Breton Jr., "Water and Ion Flow Across Cellulosic Membranes," *J. Appl. Polym. Sci.*, **1**, 133 (1959).

[69] R.L. Riley, J.O. Gardner and U. Merten, "Electron Microscopy of Structure, Cellulose Acetate Membranes," *Science*, **143**, 801 (1964).

[70] R.L. Riley, U. Merten and J.O. Gardner, "Replication Electron Microscopy of Cellulose Acetate Osmotic Membranes," *Desalination*, 1, 30 (1966).

[71] L.T. Rozelle, J.E. Cadotte, K.E. Cobian and C.V. Kopp, "Reverse Osmosis and Synthetic Membranes," *Reverse Osmosis Synth. Memr.*, 249 (1977).

[72] W.J. Schell, C.D. Houston and W.L. Houston, "Membranes Can Efficiently Separate Carbon Dioxide from Mixtures," *Oil and Gas J.*, 81, 52 (1983).

[73] W.J. Schell, "Separation of Coal Hydrogasification of Gases by Permselective Membranes," *ACS Div. Fuel Chem. Preprints*, 20, 253 (1975).

[74] R.L. Schendel and J.D. Seymour, "Expanding Use of Membranes for Carbon Dioxide Removal," *PetroEnergy 84'*, presented in Houston, Texas (1984).

[75] Y. Shindo, T. Hakuta , H. Yoshitome and H. Inoue, "Calculation Methods for Multicomponent Gas Separation by Permeation," *Sep. Sci. Tech.*, 20, 445 (1985).

[76] E. Soles, J.M. Smith and W.R. Parrish, "Gas Transport through Polyethylene Membranes," *A.I.Ch.E.J.*, 28, 474 (1982).

[77] M. Soltanieh and W.N. Gill, "Review of Reverse Osmosis Membranes and Transport Models," *Chem. Eng. Commun.*, 12, 279 (1981).

[78] S. Sourirajan, "Reverse Osmosis and Synthetic Membranes," *National Research Council Canada*, 527 (1977).

[79] V.T. Stannett, W.J. Koros, D.R. Paul, H.K. Lonsdale and R.W. Baker, "Recent Advances in Membrane Science and Technology," *Adv. Polym. Sci.*, 32, 69 (1979).

[80] V.T. Stannett, "The Transport of Gases in Synthetic Polymeric Membranes —An Historic Perspective," *J. Membrane Sci.*, 3, 97 (1978).

[81] S.A. Stern, S.K. Sen and A.K. Rao, "The Permeation of Gases Through Symmetric and Asymmetric (Loeb-Type) Cellulose Acetate Membranes," *J. Macromol. Sci. Phys.*, 10, 507 (1974).

[82] D.J. Stookey, C.J. Patton and G.L. Malcolm, "Membranes Separate Gases Selectively," *Chem. Eng. Prog.*, **82**, 11, 36 (1986).

[83] "Synthetic Membranes: The Next Technology To Watch," *Business Week* Nov. (1984).

[84] A. Tanioka, K. Ishikawa, A. Kakuta, M. Kuramoto and M. Ohno, "Mixed Gases Separation by Fine Porous Freeze-Dried Cellulose Acetate Membrane," *J. Appl. Polym. Sci.*, **29**, 583 (1984).

[85] A. Tanioka, K. Ishikawa, A. Kakuta, M. Kuramoto and M. Ohno, "Pore Size Evaluation for Fine Porous Freeze–Dried Cellulose Acetate Membrane by Gas Separation," *J. Appl. Polym. Sci.*, **30**, 695 (1985).

[86] A.-Y. Tremblay, A. Fouda, A. Lui and S. Sourirajan, "The Use of the Simplex Method to Characterize Dry Cellulose Acetate Membranes for Gas Separations," *Can. J. Chem. Eng.*, Submitted (1987).

[87] A. Tweddle, personal communication.

[88] A. Tweddle, O. Kutowy and A. Baxter, "Equipment and Procedures for Testing Small Coupon Samples of Reverse and Ultrafiltration Membranes," written for National Research Council, Div. of Chem. Jan.(1986).

[89] K.D. Vos and F.O. Burris Jr., "Drying Cellulose Acetate Reverse Osmosis Membranes," *Ind. Eng. Chem. Proc. Des. Dev.*, **8**, 84 (1969).

[90] A. Walch, "Preparation and Structure of Synthetic Membranes," *Desalination*, **46**, 303 (1983).

[91] W.J. Ward III, "Membrane Gas Separations—Why and How," *Synth. Membr.*, **181**, 389 (1986).

[92] W.J. Ward III, "Method for the Casting of Ultrathin Polymer Membranes; Removal of Solvent, Solidification," *U.S. Patent*, 4279855, (1981).

[93] W.J. Ward III, W.R. Browall and R.M. Salemme, "Ultrathin Silicone/Polycarbonate Membranes for Gas Separation Processes," *J. Membr. Sci.*, **1**, 99 (1976).

[94] W.F. Weber and W. Bowman, "Membranes Replacing Other Separation Technologies," *Chem. Eng. Prog.*, **82**, 11, 23 (1986).

[95] U. Werner, "Some Technical and Economical Aspects of Gas Separation by Means of Membranes," *Membr. Gas Sep. Enrich.*, **62**, 43 (1986).

[96] T.L. Vu, B.S. Minhas and S. Sourirajan, "Selection of Polymer Membrane Materials Based on Gas Chromatography Data," *J. Colloid Interface Sci.*, In press, (1988).

Nomenclature

A_1	constant for a given membrane related to porous structure, m^{-3}.
A_2	constant related to surface transport, $kmol/m^3\,s\,Pa^2$.
A_G	gas permeability coefficient, $kmol/m^2\,s\,Pa$.
C_R	coefficient of resistance for transport of adsorbed molecules, $kmol/s\,m^2$.
$\bar{c}_i$	mean speed of gas molecules, m/s.
d_i	collision diameter, m.
$(G_1)_i$	a physicochemical constant.
$(G_2)_i$	a physicochemical constant.
$(G_3)_i$	a physicochemical constant.
$(I_j)_i$	quantities defined in thesis, $j = 1, 5$.
J_i	flux of gas i, $kmol/m^2\,s$.
k	constant representing gas adsorption equilibrium.
M_i	molecular weight of gas i, kg/kmol.
N	Avogadro number.
$N(R)$	number of pores having a radius R, m^{-1}.
N_t	total number of pores.
$\bar{P}_i$	mean pressure across the membrane, Pa.

$[PR]$	total permeation rate of the gas mixture, kmol/m^2 s.
R	pore radius, m.
$\bar{R}_i$	mean pore radius, m.
R	gas constant, m^3 Pa/K kmol.
S	membrane area, m^2.
S_{12}	separation factor for mixture of gas 1 and 2.
T	absolute temperature, K.
X_i	mole fraction of gas i.

Greek symbols:

δ_i	radius correction factor, a costant for gas i for a given membrane material, m.
δ	equivalent thickness of the membrane.
λ	mean free path of gas, m.
ρ_{app}	apparent density of the membrane, kg/m^3.
σ	standard deviation for the pore size distribution, m.
τ	tortuosity factor for the pores.
ϕ_i	characteristic parameter, called the relative surface transport coefficient$(= (A_2)_i/(A_2)_{ref})$, related to gas–membrane interaction.

Appendix A

Errors

A.1 Discussion of Error

A.1.1 Errors in Membrane Testing

Once the coupons were placed within the system, the gas testing was done. If the outlet gas was injected by hand into the gas chromatograph, there would be human error involved. The autosampler eliminated most of this. The average of two readings were used to make this error even smaller. There would be a very small amount of error due to the variation in the feed gas composition. The feed gas mixtures were analyzed by Matheson to a two decimal accuracy. Any variation in the gas compositions would affect the separation factor, and is the most sensitive source of error.

The flowrates were found using soap bubble meters. There would be a small variation due to the uniformity in the diameter of the meters. Also, the shorter the time to take the flowrate reading, the less accurate it would be. More error was involved when reading low flowrates. To reduce the error involved in reading the flowrates, an accurate stop watch was used, the readings were thirty seconds or longer, and an average of three readings were used. A variation in the flowrates would affect the permeation coefficient directly.

Since high pressure regulators were often used, the pressure was hard to regulate. Slow leaks would also lead to minor errors. This variation would affect the permeation coefficient directly. The pressure could be read from the regulator with an error of 3.4 kPa (5 psi).

A small amount of error would also be introduced due to variation of the ambient temperature and pressure. These would affect the study of

gases; however it was felt to be a minor variation.

Sensitivity of Separation Factor to Gas Analysis

The analysis of separation factor is more sensitive for higher mole fractions of carbon dioxide in the feed. The following calculations illustrate the sensitivity.

$$S = \frac{[X_{CO_2}/X_{CH_4}]_P}{[X_{CO_2}/X_{CH_4}]_F} \cong \frac{[X_{CO_2}/(1-X_{CO_2})]_P}{[X_{CO_2}/(1-X_{CO_2})]_F}$$
$$= \left[\frac{1-X_{CO_2}}{X_{CO_2}}\right]_F \left[\frac{X_{CO_2}}{1-X_{CO_2}}\right]_P \quad (A.1)$$

$$\frac{dS}{dX_{CO_2,P}} = \left[\frac{1-X_{CO_2}}{X_{CO_2}}\right]_F \left[\frac{1}{1-X_{CO_2}}\right]_P^2 \quad (A.2)$$

Conditions one are when:

$$X_{CO_2,F} = 0.90 \quad (A.3)$$
$$X_{CO_2,P} = 0.99 \quad (A.4)$$
$$dS = \frac{1}{9}\left(\frac{1}{.01}\right)^2 = 1,111 dX_{CO_2,P} \quad (A.5)$$

Conditions two are when:

$$X_{CO_2,F} = 0.10 \quad (A.6)$$
$$X_{CO_2,P} = 0.50 \quad (A.7)$$
$$dS = 9\left(\frac{1}{.5}\right)^2 = 36 dX_{CO_2,P} \quad (A.8)$$

The ratio of the first to the second conditions is 36 times more sensitive. This indicates more variation of separation factors at low % CH_4 (high % CO_2) in the feed gas. This scatter can be seen in Figure 4.16. The 10 and 20 % CH_4 curves, denoted by the square and circle, have more scatter than the other three curves. Also, the points on the left hand side of Figure 4.17 contains more scatter than the points on the right hand side.

A.1.2 Errors in Wet Membrane Manufacture

There was a certain amount of error due to making the cellulose acetate casting solution. However, error was limited to the accuracy of measuring

out the chemicals. Variations can occur simply due to the way the membrane sheet was cast. Casting must be done as uniformly as possible (i.e. spreading the solution at a constant rate across the glass plate). Even when this is done, variations from one sheet to another will occur due to changes in the solution temperature and equipment (glass plate and doctor's blade) and the room temperature and humidity. These variations can be reduced by making a whole batch at one time. Variations can also be reduced if the evaporation time before gelation, the temperature of the gelation bath and the amount of time in the gelation bath were kept identical for each sheet (i.e. use of accurate stop watches).

The sheet was then cut into coupons. At this point, the coupons with obvious pinholes or bubbles were rejected. This was done with the naked eye on top of a light board. Each of the coupons were then randomly selected and placed in a water bath at five different temperatures. Experimental error arose here due to reading the bath temperature within 1°C. The duration of immersion was ten minutes and again, it is important to be accurate.

A wet test can be performed to ensure that the pure water permeation (i.e. the pore size) of each coupon was comparable to standards. This wet test was done on a few of the coupons and was then considered to be representative of a homogenous batch.

A.1.3 Errors in Drying Membranes

The shrunk coupons were put into separate jars for solvent exchange at room temperature. Each particular solvent combination would be done as a batch, thus eliminating error within any solvent combination. Each solvent exchange or step took one day to reach equilibrium. The coupons were then left in a dessicator to be air dried. Variations due to the reagents, time or temperature in this stage would be small.

A.2 Estimation of Coupon Variation

The experimental design consisted of a possible 40 sequences of five shrinking temperatures, two first solvents and four second solvents ($5 \times 2 \times 4$). Because of the nature of the experiment, a membrane coupon could only be tested in one sequence. Not all sequences were included in this work and only three were duplicated, and then only in the sense that two coupons were processed in parallel through three sequences. The duplicates were

membranes 5-5 and 6-2, Tables B.7 and B.23, and membranes 1-6 and 4-1 plus 6-5 and 4-2 in Tables B.8 and B.24. These results are the only direct evidence of the variation of observations due to wet-membrane coupon variation. A statistical analysis on some of these results yielded a coupon standard variation of about 1.5 and 0.8 $\times 10^{-11}$ for the separation factor and the permeation coefficient respectively. The corresponding error standard variation was lower and estimated to be about 0.32 and 0.15 $\times 10^{-11}$. An estimate of the residual error of the methanol–IPE series of membrane gives a residual standard deviation of 0.84 for the separation factor and 0.42 $\times 10^{-11}$ for the permeation coefficient. These estimates include the deviation due to the coupon. These two sources give order-of-magnitude agreement and support the interpretation of the trends in Figures 4.20, 4.21 and 4.22 concerning the pore formation mechanism.

Analysis of variance for ethanol–CS_2 separation factor at 75 °C and 345 kPa.

Separation factors

% CH_4	coupon 5-5	6-2
10	2.716	1.640
20	3.000	1.204
50	2.026	1.301
80	2.347	1.360

Analysis of variance

source	sum square residual	degrees of freedom	variance	ratio	1 %	5 %
coupon	2.626	1	2.626	24.8	34	10.1
composition	0.333	3	0.111	1.05		
residual	0.317	3	0.106			
global	3.276	7	0.468			

$\sigma_{coupon} = 1.6$

$\sigma_{error} = 0.33$

Analysis of variance for ethanol–CS_2 permeation coefficient $\times 10^{11}$ at 75 °C and 345 kPa.

Permeation coefficients

	coupon	
% CH_4	5-5	6-2
10	0.994	1.530
20	0.874	1.330
50	0.575	1.250
80	0.427	1.140

Analysis of variance

source	sum square residual	degrees of freedom	variance	ratio	1 %	5 %
coupon	0.7081	1	0.7081	25.5	34	10.1
composition	0.2035	3	0.0678	2.44		
residual	0.0833	3	0.0278			
global	0.9949	7	0.142			

$\sigma_{error} = 0.17$

$\sigma_{coupon} = 0.84$

Analysis of variance for ethanol–hexane separation factor at 75 °C and 345 kPa.

Separation factors

	coupon	
% CH_4	1-6	4-1
10	2.904	4.138
20	2.042	3.503
50	2.784	3.375
80	1.957	2.498

Analysis of variance

source	sum square residual	degrees of freedom	variance	ratio	1 %	5 %
coupon	1.828	1	1.828	17.2	34	10.1
composition	1.772	3	0.591	5.6		
residual	0.317	3	0.106			
global	3.917	7	0.560			

$\sigma_{error} = 0.32$

$\sigma_{coupon} = 1.35$

Analysis of variance for ethanol–hexane permeation coefficient $\times 10^{11}$ at 75 °C and 345 kPa.

Permeation coefficients

% CH_4	coupon 1-6	coupon 4-1
10	0.725	0.242
20	0.S62	0.1S7
50	0.S32	0.143
S0	0.436	0.105

Analysis of variance

source	sum square residual	degrees of freedom	variance	ratio	1 %
coupon	0.5929	1	0.5929	40.9	34
composition	0.0S00	3	0.0267	1.S	25
residual	0.0436	3	0.0145	1	
global	0.7165	7	0.1024		

$\sigma_{error} = 0.12$

$\sigma_{coupon} = 0.77$

Analysis of variance for methanol–IPE separation factors Results from Table B.2 were used.

Analysis of variance

source	sum square	degrees of freedom	variance
temperature	1026.391	4	256.59S
pressure	22.094	4	5.524
composition	4.412	3	1.471
residual	62.655	SS	0.7120
global	1115.552	99	11.26S

$\sigma_{error} = 0.S4$

Analysis of variance for methanol–IPE permeation coefficient $\times 10^{11}$. Results from Table B.18 were used.

Analysis of variance

source	sum square	degrees of freedom	variance
temperature	134.482	4	33.621
pressure	0.774	4	0.193
composition	13.224	3	4.408
residual	15.828	88	0.1799
global	164.308	99	1.66

$$\sigma_{error} = 0.42$$

Appendix B

Tables of Results

Table B.1: Separation Factors for Methanol–Triethyl Amine Membranes on Methane–Carbon Dioxide Gas Mixtures

Composition Mole Percent Methane	Pressure kPa	Shrinkage Temperature °C			
		70	80	85	90
		Coupon Number			
		1-4	1-3	4-3	4-5
10	255	4.130	1.307	–	–
	345	4.546	1.626	2.047	1.492
	689	–	–	1.723	1.310
	1034	3.772	1.431	1.182	1.039
	1379	3.009	1.318	1.755	1.262
	1724	3.468	1.130	1.392	1.111
	2068	3.179	0.908	–	–
20	345	4.464	1.174	1.749	1.358
	689	4.655	1.174	1.491	1.195
	1034	3.618	1.371	1.350	1.108
	1379	3.139	1.296	1.223	1.037
	1724	2.821	1.267	1.212	1.010
	2068	3.424	1.312	1.117	0.967
50	345	5.758	1.540	1.479	1.203
	689	3.011	1.196	1.432	1.178
	1034	3.063	1.183	1.257	1.064
	1379	2.641	1.168	1.070	0.965
	1724	2.430	1.125	1.339	1.071
	2068	2.131	1.136	1.148	0.978
80	345	3.419	1.240	1.468	1.132
	689	2.807	1.125	1.261	1.014
	1034	2.610	1.160	1.100	0.937
	1379	2.464	1.117	1.056	0.938
	1724	2.286	1.151	1.217	1.017
	2068	2.143	1.097	1.060	0.958
90	345	4.017	1.321	–	–
	689	2.731	1.116	–	–
	1034	2.354	1.074	–	–
	1379	2.081	1.034	–	–
	1724	1.891	1.078	–	–
	2068	2.006	1.056	–	–

Table B.2: Separation Factors for Methanol–Isopropyl Ether Membranes on Methane–Carbon Dioxide Gas Mixtures

Composition Mole Percent Methane	Pressure kPa	Shrinkage Temperature °C				
		70	75	80	85	90
		Coupon Number				
		1-1	1-2	4-6	4-7	4-4
10	345	10.530	1.640	5.150	1.185	1.766
	689	10.716	2.932	4.313	1.176	1.542
	1034	10.597	2.071	2.511	1.046	1.400
	1379	8.724	1.677	3.911	1.226	1.441
	1724	10.665	1.880	3.106	1.123	1.356
	2068	5.160	2.442	–	–	–
20	345	14.115	2.230	4.434	1.051	1.706
	689	9.674	1.670	3.767	1.024	1.529
	1034	12.130	2.615	3.182	1.026	1.426
	1379	8.634	1.871	2.589	1.020	1.341
	1724	7.004	1.761	2.547	1.004	1.318
	2068	10.781	2.691	2.110	1.003	1.003
50	345	11.534	3.315	3.358	1.045	1.666
	689	10.323	2.958	3.173	1.142	1.397
	1034	8.480	2.291	2.669	1.092	1.335
	1379	7.975	2.168	1.945	1.020	1.247
	1724	7.880	1.900	2.780	1.015	1.259
	2068	5.723	1.661	2.237	0.986	1.206
80	345	12.192	2.343	2.987	1.013	1.720
	689	10.237	2.095	2.572	0.989	1.479
	1034	8.282	2.246	2.104	0.982	1.342
	1379	8.151	2.036	1.883	0.974	1.263
	1724	7.279	2.086	1.883	1.020	1.229
	2068	6.070	1.752	1.882	0.978	1.168
90	345	10.752	2.506	–	–	–
	689	8.848	2.123	–	–	–
	1034	7.174	1.881	–	–	–
	1379	5.698	1.715	–	–	–
	1724	5.162	1.647	–	–	–
	2068	6.242	1.856	–	–	–

Table B.3: Separation Factors for Methanol–Carbon Disulfide Membranes on Methane–Carbon Dioxide Gas Mixtures

Composition Mole percent Methane	Pressure kPa	Shrinkage Temperature °C	
		75	85
		Coupon Number	
		1-5	5-7
10	345	0.986	0.985
	689	0.870	0.918
	1034	1.048	0.871
	1379	1.009	0.920
	1724	1.012	0.894
	2068	1.037	0.886
20	345	1.002	0.995
	689	1.157	0.967
	1034	1.039	0.964
	1379	1.078	0.974
	1724	1.011	0.996
	2068	1.023	–
50	345	0.969	0.778
	689	1.026	0.773
	1034	1.043	0.763
	1379	0.995	0.767
	1724	1.059	0.757
	2068	1.032	0.769
80	345	1.019	0.992
	689	1.013	0.955
	1034	1.031	0.981
	1379	1.015	0.958
	1724	1.007	0.959
	2068	0.996	0.977
90	345	1.037	1.004
	689	0.985	1.028
	1034	0.958	0.977
	1379	0.986	1.018
	1724	0.954	0.921
	2068	0.977	0.971

Table B.4: Separation Factors for Methanol–Hexane Membranes on Methane–Carbon Dioxide Gas Mixtures

Composition Mole Percent Methane	Pressure kPa	Shrinkage Temperature °C				
		70	75	80	85	90
		Coupon Numbers				
		2-8	6-7	5-3	2-4	5-6
10	345	3.854	2.957	2.102	3.843	3.152
	689	3.199	3.107	2.430	3.181	3.445
	1034	2.898	2.483	2.460	2.722	2.920
	1379	2.683	2.908	2.796	2.502	3.261
	1724	–	2.424	2.859	–	2.930
	2068	2.386	1.785	2.591	2.120	2.291
20	345	3.360	2.391	2.285	3.360	–
	689	2.840	2.554	2.201	2.760	2.776
	1034	3.220	2.253	2.250	3.090	2.687
	1379	2.710	2.126	2.617	2.440	3.256
	1724	2.580	2.406	3.028	2.200	3.542
	2068	2.890	1.887	–	2.800	–
50	345	2.325	1.985	1.681	2.183	2.173
	689	2.230	2.024	1.633	2.261	1.926
	1034	2.709	2.018	1.606	2.748	1.789
	1379	2.249	2.323	1.516	2.282	1.606
	1724	1.991	2.354	1.500	2.185	1.543
	2068	1.660	1.907	1.755	1.896	1.809
80	345	3.070	2.154	2.072	2.660	2.513
	689	2.340	1.980	1.939	2.410	2.266
	1034	2.470	1.668	1.901	2.280	2.047
	1379	2.500	1.585	1.786	2.710	1.798
	1724	1.930	1.579	1.668	1.930	1.647
	2068	1.690	1.439	1.894	1.630	1.962
90	345	2.320	2.193	2.059	2.730	2.521
	689	1.930	2.154	1.917	1.925	2.438
	1034	2.290	2.043	1.930	2.170	2.141
	1379	1.900	1.887	1.797	1.890	2.012
	1724	1.610	1.494	1.801	1.700	1.887
	2068	2.030	1.671	1.805	1.910	1.695

Table B.5: Separation Factors for Ethanol–Triethyl Amine Membranes on Methane–Carbon Dioxide Gas Mixtures

Composition Mole Percent Methane	Pressure kPa	Shrinkage Temperature °C			
		70	75	85	90
		Coupon Number			
		6-6	6-8	6-1	5-2
10	345	1.014	2.755	1.070	2.031
	689	1.018	2.707	1.021	2.031
	1034	0.996	2.311	0.991	1.649
	1379	1.037	2.585	1.096	1.889
	1724	1.021	2.162	1.042	1.692
	2068	0.981	1.335	0.992	1.340
20	345	0.889	2.255	0.841	1.818
	689	0.935	2.227	1.016	1.515
	1034	0.916	2.037	0.977	1.426
	1379	0.922	1.977	0.942	1.690
	1724	0.945	1.615	0.986	1.844
	2068	0.922	1.416	0.917	–
50	345	0.972	1.970	0.888	1.304
	689	0.994	1.917	0.970	1.109
	1034	1.003	1.841	0.999	1.021
	1379	1.032	2.106	1.061	0.930
	1724	1.044	2.072	1.012	0.919
	2068	1.011	1.459	1.014	1.091
80	345	0.998	2.043	1.021	1.549
	689	1.020	1.835	1.024	1.337
	1034	0.995	1.639	0.960	1.219
	1379	0.967	1.477	0.989	1.125
	1724	1.002	1.315	0.962	1.069
	2068	0.966	1.169	0.924	1.261
90	345	1.057	2.111	1.022	1.800
	689	1.078	1.951	1.094	1.615
	1034	1.080	1.911	1.022	1.332
	1379	1.090	1.759	1.052	1.309
	1724	0.983	1.232	0.995	1.249
	2068	1.028	1.270	1.016	1.151

Table B.6: Separation Factors for Ethanol–Isopropyl Ether Membranes on Methane–Carbon Dioxide Gas Mixtures

Composition Mole Percent Methane	Pressure kPa	Shrinkage Temperature °C			
		70	80	85	90
		Coupon Number			
		2-3	2-5	1-8	2-2
10	345	2.892	2.085	5.773	4.642
	689	2.503	1.784	3.342	4.074
	1034	2.084	1.615	3.942	3.682
	1379	1.986	1.475	2.555	3.342
	1724	–	–	3.190	–
	2068	1.946	1.385	1.670	2.688
20	345	2.350	1.860	4.059	4.130
	689	1.890	1.590	3.105	3.500
	1034	1.730	1.840	3.354	3.850
	1379	2.150	1.520	2.627	3.350
	1724	1.810	1.450	1.946	2.930
	2068	2.030	1.570	3.129	3.350
50	345	1.492	1.218	5.511	1.918
	689	1.665	1.331	2.850	3.340
	1034	1.834	1.583	3.000	3.270
	1379	1.592	1.313	2.098	2.915
	1724	1.523	1.228	2.225	2.561
	2068	1.457	1.165	1.772	2.178
80	345	1.580	1.620	3.719	2.522
	689	1.370	1.330	2.793	2.294
	1034	1.350	1.440	2.646	2.394
	1379	1.760	1.540	2.201	2.665
	1724	1.320	1.180	2.346	2.074
	2068	1.220	1.110	1.622	1.763
90	345	1.530	1.450	3.618	1.910
	689	1.160	1.140	2.610	1.490
	1034	1.240	1.390	2.162	1.620
	1379	1.150	1.140	1.874	1.410
	1724	1.120	1.050	1.646	1.240
	2068	1.120	1.230	1.968	1.500

Table B.7: Separation Factors for Ethanol–Carbon Disulfide Membranes on Methane–Carbon Dioxide Gas Mixtures

Composition Mole Percent Methane	Pressure kPa	Shrinkage Temperature °C					
		70	75	75	80	85	90
		Coupon Number					
		6-3	5-5	6-2	2-7	6-4	5-4
10	345	2.210	2.716	1.640	6.128	3.384	2.876
	689	2.128	2.650	1.638	5.206	3.330	2.814
	1034	1.649	2.350	1.476	4.291	2.653	2.134
	1379	1.774	2.578	1.655	3.784	2.918	2.521
	1724	1.511	2.485	1.469	–	2.655	2.193
	2068	1.248	2.193	1.427	3.087	2.185	1.599
20	345	1.626	3.000	1.204	5.780	2.131	2.772
	689	1.851	2.499	1.357	4.690	2.301	2.270
	1034	1.592	2.312	1.277	4.770	2.128	2.072
	1379	1.402	2.556	1.235	3.640	2.164	2.610
	1724	1.550	2.736	1.345	3.220	2.214	2.718
	2068	1.294	–	1.190	4.180	1.885	–
50	345	1.573	2.026	1.301	3.975	2.227	1.837
	689	1.451	1.763	1.284	4.068	2.065	1.509
	1034	1.405	1.595	1.303	4.321	2.880	1.355
	1379	1.661	1.476	1.407	3.346	2.265	1.195
	1724	1.577	1.420	1.392	2.821	2.213	1.165
	2068	1.337	1.565	1.280	2.321	1.888	1.434
80	345	1.726	2.347	1.360	5.560	2.226	2.198
	689	1.493	2.077	1.275	4.440	1.985	1.858
	1034	1.321	1.844	1.173	4.490	1.698	1.628
	1379	1.178	1.641	1.140	4.230	1.574	1.410
	1724	1.205	1.500	1.169	2.780	1.641	1.301
	2068	1.131	1.706	1.113	2.250	1.440	1.644
90	345	1.689	2.252	1.435	4.340	2.248	2.244
	689	1.686	2.041	1.312	3.400	2.182	2.018
	1034	1.499	1.908	1.356	4.410	1.877	1.782
	1379	1.424	1.686	1.203	3.050	1.806	1.648
	1724	1.261	1.605	1.152	2.530	1.553	1.518
	2068	1.288	1.482	1.212	3.320	1.656	1.342

Table B.8: Separation Factors for Ethanol–Hexane Membranes on Methane–Carbon Dioxide Gas Mixtures

Composition Mole Percent Methane	Pressure kPa	Shrinkage Temperature °C					
		70	75	75	80	90	90
		Coupon Number					
		2-6	1-6	4-1	5-1	6-5	4-2
10	345	9.809	2.904	4.138	4.005	1.171	1.035
	689	8.636	1.678	3.537	3.821	1.173	1.029
	1034	8.932	1.939	3.099	3.643	1.067	0.993
	1379	9.208	1.562	3.374	3.784	1.159	1.017
	1724	–	1.763	3.101	3.889	1.060	1.007
	2068	7.747	1.215	–	3.642	1.058	–
20	345	8.050	2.042	3.503	4.157	1.011	0.995
	689	8.490	1.082	2.998	3.598	1.083	0.987
	1034	9.790	1.789	2.803	3.354	1.040	0.996
	1379	8.490	1.538	2.593	3.233	2.164	0.995
	1724	7.700	1.202	2.629	3.362	1.069	0.996
	2068	9.290	1.797	2.475	–	0.973	0.996
50	345	6.741	2.784	3.372	2.639	1.006	0.998
	689	7.910	1.560	2.464	2.336	1.021	0.998
	1034	9.521	1.643	2.282	2.170	1.021	0.988
	1379	8.928	1.315	2.091	1.992	1.123	0.988
	1724	7.109	1.287	2.226	1.915	1.146	0.992
	2068	7.013	1.181	2.046	2.062	1.053	0.981
80	345	4.460	1.975	2.498	3.086	1.115	0.981
	689	3.750	1.516	2.410	2.738	1.022	0.991
	1034	3.590	1.504	2.095	2.504	1.017	0.960
	1379	7.140	1.245	1.947	2.294	0.992	1.008
	1724	6.020	1.366	1.951	2.086	1.002	0.985
	2068	5.430	1.151	1.795	2.170	0.945	0.980
90	345	3.500	2.012	–	2.835	1.204	–
	689	2.690	3.000	–	2.939	1.041	–
	1034	3.120	1.294	–	2.679	1.047	–
	1379	2.930	1.207	–	2.436	1.083	–
	1724	2.710	1.096	–	2.295	0.990	–
	2068	2.990	1.270	–	2.234	0.960	–

Table B.9: Permeation Coefficients for Methanol–Triethyl Amine Membranes with Pure Gases in kmol/s.m^2.Pa

Pressure kPa	Shrinkage Temperature °C			
	70	80	85	90
	Coupon Number			
	1-4	1-3	4-3	4-5
Helium Gas				
345	0.705×10^{-11}	0.183×10^{-10}	0.517×10^{-10}	0.718×10^{-10}
689	0.811×10^{-11}	0.209×10^{-10}	0.623×10^{-10}	0.696×10^{-10}
1034	0.932×10^{-11}	0.246×10^{-10}	0.598×10^{-10}	0.760×10^{-10}
1379	0.105×10^{-10}	0.267×10^{-10}	0.570×10^{-10}	0.702×10^{-10}
1724	0.111×10^{-10}	0.278×10^{-10}	0.532×10^{-10}	0.646×10^{-10}
2068	0.117×10^{-10}	0.293×10^{-10}	0.503×10^{-10}	0.973×10^{-10}
Carbon Dioxide Gas				
345	0.459×10^{-11}	0.874×10^{-11}	0.237×10^{-10}	0.306×10^{-10}
689	0.581×10^{-11}	0.124×10^{-10}	0.226×10^{-10}	0.312×10^{-10}
1034	0.703×10^{-11}	0.137×10^{-10}	0.261×10^{-10}	0.361×10^{-10}
1379	0.955×10^{-11}	0.176×10^{-10}	0.278×10^{-10}	0.389×10^{-10}
1724	0.113×10^{-10}	0.194×10^{-10}	0.337×10^{-10}	0.461×10^{-10}
2068	0.139×10^{-10}	0.222×10^{-10}	0.417×10^{-10}	0.567×10^{-10}
Methane Gas				
345	0.149×10^{-11}	0.847×10^{-11}	0.162×10^{-10}	0.281×10^{-10}
689	0.152×10^{-11}	0.856×10^{-11}	0.166×10^{-10}	0.282×10^{-10}
1034	–	–	0.170×10^{-10}	0.302×10^{-10}
1379	0.204×10^{-11}	0.126×10^{-10}	0.182×10^{-10}	0.332×10^{-10}
1724	0.215×10^{-11}	0.135×10^{-10}	0.207×10^{-10}	0.388×10^{-10}
2068	0.236×10^{-11}	0.146×10^{-10}	0.214×10^{-10}	0.401×10^{-10}

Table B.10: Permeation Coefficients for Methanol–Isopropyl Ether Membranes with Pure Gases in kmol/s.m^2.Pa

Pressure kPa	Shrinkage Temperature °C				
	70	75	80	85	90
	Coupon Number				
	1-1	1-2	4-6	4-7	4-4
	Helium Gas				
345	0.160×10^{-10}	0.224×10^{-10}	0.253×10^{-10}	0.971×10^{-10}	0.208×10^{-11}
689	0.174×10^{-10}	0.247×10^{-10}	0.285×10^{-10}	0.918×10^{-10}	0.321×10^{-11}
1034	0.194×10^{-10}	0.281×10^{-10}	0.331×10^{-10}	0.788×10^{-10}	0.384×10^{-11}
1379	0.203×10^{-10}	0.308×10^{-10}	0.354×10^{-10}	0.712×10^{-10}	0.441×10^{-11}
1724	0.212×10^{-10}	0.328×10^{-10}	0.371×10^{-10}	0.645×10^{-10}	0.497×10^{-11}
2068	0.217×10^{-10}	0.324×10^{-10}	0.397×10^{-10}	0.938×10^{-10}	0.547×10^{-11}
	Carbon Dioxide Gas				
345	0.906×10^{-11}	0.109×10^{-10}	0.140×10^{-10}	0.442×10^{-10}	0.266×10^{-11}
689	0.110×10^{-10}	0.149×10^{-10}	0.159×10^{-10}	0.418×10^{-10}	0.268×10^{-11}
1034	0.144×10^{-10}	0.162×10^{-10}	0.194×10^{-10}	0.431×10^{-10}	0.336×10^{-11}
1379	0.190×10^{-10}	0.210×10^{-10}	0.222×10^{-10}	0.444×10^{-10}	0.332×10^{-11}
1724	0.227×10^{-10}	0.234×10^{-10}	0.262×10^{-10}	0.471×10^{-10}	0.363×10^{-11}
2068	0.264×10^{-10}	0.266×10^{-10}	0.348×10^{-10}	0.408×10^{-10}	0.454×10^{-11}
	Methane Gas				
345	0.316×10^{-12}	0.352×10^{-11}	0.330×10^{-11}	0.708×10^{-10}	0.240×10^{-11}
689	0.432×10^{-12}	0.450×10^{-11}	0.349×10^{-11}	0.600×10^{-10}	0.269×10^{-11}
1034	–	0.475×10^{-11}	0.390×10^{-11}	0.584×10^{-10}	0.310×10^{-11}
1379	0.642×10^{-12}	0.542×10^{-11}	0.436×10^{-11}	0.587×10^{-10}	0.343×10^{-11}
1724	0.684×10^{-12}	0.553×10^{-11}	0.487×10^{-11}	0.619×10^{-10}	0.403×10^{-11}
2068	0.749×10^{-12}	0.675×10^{-11}	0.526×10^{-11}	0.610×10^{-10}	0.432×10^{-11}

Table B.11: Permeation Coefficients for Methanol–Carbon Disulfide Membranes with Pure Gases in kmol/s.m^2.Pa

Pressure kPa	Shrinkage Temperature °C	
	75	85
	Coupon Number 1-5	5-7
Helium Gas		
345	0.121×10^{-09}	0.131×10^{-09}
689	0.119×10^{-09}	0.141×10^{-09}
1034	0.120×10^{-09}	0.152×10^{-09}
1379	0.118×10^{-09}	0.168×10^{-09}
1724	0.118×10^{-09}	0.181×10^{-09}
2068	0.117×10^{-09}	0.187×10^{-09}
Carbon Dioxide Gas		
345	-	0.689×10^{-10}
689	-	0.576×10^{-10}
1034	-	-
1379	-	0.643×10^{-10}
1724	-	-
2068	-	0.696×10^{-10}
Methane Gas		
345	0.719×10^{-10}	0.105×10^{-09}
689	0.692×10^{-10}	0.105×10^{-09}
1034	0.639×10^{-10}	0.103×10^{-09}
1379	0.657×10^{-10}	0.109×10^{-09}
1724	0.663×10^{-10}	0.109×10^{-09}
2068	0.683×10^{-10}	0.117×10^{-09}

Table B.12: Permeation Coefficients for Methanol–Hexane Membranes with Pure Gases in kmol/s.m^2.Pa

Pressure kPa	Shrinkage Temperature °C				
	70	75	80	85	90
	Coupon Number				
	2-8	6-7	5-3	2-4	5-6
	Helium Gas				
345	0.248×10^{-10}	0.487×10^{-10}	0.121×10^{-10}	0.458×10^{-10}	0.330×10^{-10}
689	0.293×10^{-10}	0.565×10^{-10}	0.133×10^{-10}	0.528×10^{-10}	0.355×10^{-10}
1034	0.318×10^{-10}	0.590×10^{-10}	0.141×10^{-10}	0.554×10^{-10}	0.372×10^{-10}
1379	0.250×10^{-10}	0.626×10^{-10}	0.149×10^{-10}	0.450×10^{-10}	0.402×10^{-10}
1724	0.320×10^{-10}	0.632×10^{-10}	0.158×10^{-10}	0.531×10^{-10}	0.429×10^{-10}
2068	0.335×10^{-10}	0.638×10^{-10}	0.170×10^{-10}	0.557×10^{-10}	0.452×10^{-10}
	Carbon Dioxide Gas				
345	0.994×10^{-11}	0.202×10^{-10}	0.581×10^{-11}	0.168×10^{-10}	0.122×10^{-10}
689	0.121×10^{-10}	0.246×10^{-10}	0.612×10^{-11}	0.212×10^{-10}	0.206×10^{-10}
1034	0.146×10^{-10}	0.260×10^{-10}	0.829×10^{-11}	0.2550-10	-
1379	0.149×10^{-10}	0.313×10^{-10}	0.876×10^{-11}	0.262×10^{-10}	0.230×10^{-10}
1724	0.193×10^{-10}	0.423×10^{-10}	-	0.346×10^{-10}	-
2068	0.226×10^{-10}	0.454×10^{-10}	0.111×10^{-10}	0.415×10^{-10}	0.291×10^{-10}
	Methane Gas				
345	0.353×10^{-11}	0.667×10^{-11}	0.267×10^{-11}	0.451×10^{-11}	0.417×10^{-11}
689	0.390×10^{-11}	0.763×10^{-11}	0.287×10^{-11}	0.486×10^{-11}	0.471×10^{-11}
1034	0.425×10^{-11}	0.854×10^{-11}	0.291×10^{-11}	0.516×10^{-11}	0.498×10^{-11}
1379	0.480×10^{-11}	0.926×10^{-11}	0.317×10^{-11}	0.584×10^{-11}	0.562×10^{-11}
1724	0.497×10^{-11}	0.995×10^{-11}	0.319×10^{-11}	0.591×10^{-11}	0.590×10^{-11}
2068	0.521×10^{-11}	0.108×10^{-10}	0.343×10^{-11}	0.650×10^{-11}	0.649×10^{-11}

Table B.13: Permeation Coefficients for Ethanol–Triethyl Amine Membranes with Pure Gases in kmol/s.m^2.Pa

Pressure kPa	Shrinkage Temperature °C				
	70	70	75	85	90
	Coupon Number				
	2-1	6-6	6-8	6-1	5-2
	Helium Gas				
345	0.291×10^{-09}	0.469×10^{-10}	0.256×10^{-10}	0.865×10^{-10}	0.417×10^{-10}
689	0.274×10^{-09}	0.553×10^{-10}	0.305×10^{-10}	0.111×10^{-09}	0.466×10^{-10}
1034	0.245×10^{-09}	0.561×10^{-10}	0.332×10^{-10}	0.117×10^{-09}	0.506×10^{-10}
1379	0.232×10^{-09}	0.580×10^{-10}	0.371×10^{-10}	0.125×10^{-09}	0.528×10^{-10}
1724	0.142×10^{-09}	0.577×10^{-10}	0.381×10^{-10}	0.131×10^{-09}	0.553×10^{-10}
2068	0.136×10^{-09}	0.581×10^{-10}	0.391×10^{-10}	0.138×10^{-09}	0.561×10^{-10}
	Carbon Dioxide Gas				
345	0.622×10^{-10}	0.222×10^{-10}	0.126×10^{-10}	0.483×10^{-10}	0.179×10^{-10}
689	0.517×10^{-10}	0.212×10^{-10}	0.157×10^{-10}	0.532×10^{-10}	0.183×10^{-10}
1034	0.451×10^{-10}	0.203×10^{-10}	0.165×10^{-10}	0.526×10^{-10}	0.227×10^{-10}
1379	0.384×10^{-10}	0.287×10^{-10}	0.199×10^{-10}	0.572×10^{-10}	0.261×10^{-10}
1724	0.371×10^{-10}	0.326×10^{-10}	0.270×10^{-10}	0.722×10^{-10}	–
2068	0.393×10^{-10}	0.329×10^{-10}	0.356×10^{-10}	0.700×10^{-10}	0.337×10^{-10}
	Methane Gas				
345	0.103×10^{-09}	0.427×10^{-10}	0.556×10^{-11}	0.926×10^{-10}	0.125×10^{-10}
689	0.687×10^{-10}	0.420×10^{-10}	0.641×10^{-11}	0.848×10^{-10}	0.145×10^{-10}
1034	0.543×10^{-10}	0.422×10^{-10}	0.670×10^{-11}	0.890×10^{-10}	0.149×10^{-10}
1379	0.473×10^{-10}	0.433×10^{-10}	0.747×10^{-11}	0.880×10^{-10}	0.169×10^{-10}
1724	0.432×10^{-10}	0.440×10^{-10}	0.815×10^{-11}	0.922×10^{-10}	0.176×10^{-10}
2068	0.378×10^{-10}	0.445×10^{-10}	0.142×10^{-10}	0.937×10^{-10}	0.193×10^{-10}

Table B.14: Permeation Coefficients for Ethanol–Isopropyl Ether Membranes with Pure Gases in kmol/s.m^2.Pa

Pressure kPa	Shrinkage Temperature °C			
	70	80	85	90
	Coupon Number			
	2-3	2-5	1-8	2-2
Helium Gas				
345	0.704×10^{-10}	0.619×10^{-10}	0.149×10^{-10}	0.569×10^{-10}
689	0.808×10^{-10}	0.707×10^{-10}	0.170×10^{-10}	0.646×10^{-10}
1034	0.842×10^{-10}	0.744×10^{-10}	0.201×10^{-10}	0.672×10^{-10}
1379	0.875×10^{-10}	0.733×10^{-10}	0.216×10^{-10}	0.593×10^{-10}
1724	0.913×10^{-10}	0.771×10^{-10}	0.227×10^{-10}	0.663×10^{-10}
2068	0.946×10^{-10}	0.806×10^{-10}	0.234×10^{-10}	0.683×10^{-10}
Carbon Dioxide Gas				
345	0.211×10^{-10}	0.214×10^{-10}	0.116×10^{-10}	0.189×10^{-10}
689	0.279×10^{-10}	0.270×10^{-10}	0.141×10^{-10}	0.238×10^{-10}
1034	0.342×10^{-10}	0.336×10^{-10}	0.172×10^{-10}	0.293×10^{-10}
1379	0.409×10^{-10}	0.360×10^{-10}	0.218×10^{-10}	0.317×10^{-10}
1724	0.524×10^{-10}	0.463×10^{-10}	0.250×10^{-10}	0.408×10^{-10}
2068	0.630×10^{-10}	0.571×10^{-10}	0.360×10^{-10}	0.491×10^{-10}
Methane Gas				
345	0.152×10^{-10}	0.134×10^{-10}	0.211×10^{-11}	0.930×10^{-11}
689	0.164×10^{-10}	0.146×10^{-10}	0.265×10^{-11}	0.956×10^{-11}
1034	0.175×10^{-10}	0.162×10^{-10}	0.276×10^{-11}	0.111×10^{-10}
1379	0.218×10^{-10}	0.177×10^{-10}	0.340×10^{-11}	0.116×10^{-10}
1724	0.227×10^{-10}	0.192×10^{-10}	0.362×10^{-11}	0.123×10^{-10}
2068	0.237×10^{-10}	0.204×10^{-10}	0.399×10^{-11}	0.132×10^{-10}

Table B.15: Permeation Coefficients for Ethanol–Carbon Disulfide Membranes with Pure Gases in kmol/s.m^2.Pa

Pressure kPa	Shrinkage Temperature °C					
	70	75	75	80	85	90
	Coupon Number					
	6-3	5-5	6-2	2-7	6-4	5-4
	Helium Gas					
345	0.491×10^{-10}	0.188×10^{-10}	0.355×10^{-10}	0.348×10^{-10}	0.230×10^{-10}	0.344×10^{-10}
689	0.617×10^{-10}	0.207×10^{-10}	0.458×10^{-10}	0.407×10^{-10}	0.284×10^{-10}	0.390×10^{-10}
1034	0.624×10^{-10}	0.219×10^{-10}	0.462×10^{-10}	0.438×10^{-10}	0.292×10^{-10}	0.423×10^{-10}
1379	0.653×10^{-10}	0.236×10^{-10}	0.487×10^{-10}	0.281×10^{-10}	0.322×10^{-10}	0.468×10^{-10}
1724	0.668×10^{-10}	0.254×10^{-10}	0.488×10^{-10}	0.414×10^{-10}	0.327×10^{-10}	0.511×10^{-10}
2068	0.704×10^{-10}	0.271×10^{-10}	0.498×10^{-10}	0.454×10^{-10}	0.333×10^{-10}	0.533×10^{-10}
	Carbon Dioxide Gas					
345	0.237×10^{-10}	0.915×10^{-11}	0.168×10^{-10}	0.150×10^{-10}	0.128×10^{-10}	0.164×10^{-10}
689	0.259×10^{-10}	0.956×10^{-11}	0.185×10^{-10}	0.177×10^{-10}	0.143×10^{-10}	0.180×10^{-10}
1034	0.283×10^{-10}	0.132×10^{-10}	0.188×10^{-10}	0.216×10^{-10}	0.154×10^{-10}	0.252×10^{-10}
1379	0.325×10^{-10}	0.146×10^{-10}	0.188×10^{-10}	0.213×10^{-10}	0.176×10^{-10}	0.278×10^{-10}
1724	0.417×10^{-10}	–	0.240×10^{-10}	0.287×10^{-10}	0.231×10^{-10}	–
2068	0.445×10^{-10}	0.186×10^{-10}	0.251×10^{-10}	0.339×10^{-10}	0.239×10^{-10}	0.356×10^{-10}
	Methane Gas					
345	0.112×10^{-10}	0.359×10^{-11}	0.120×10^{-10}	0.156×10^{-11}	0.446×10^{-11}	0.593×10^{-11}
689	0.125×10^{-10}	0.429×10^{-11}	0.129×10^{-10}	0.183×10^{-11}	0.527×10^{-11}	0.695×10^{-11}
1034	0.138×10^{-10}	0.464×10^{-11}	0.142×10^{-10}	0.198×10^{-11}	0.567×10^{-11}	0.746×10^{-11}
1379	0.155×10^{-10}	0.546×10^{-11}	0.155×10^{-10}	0.239×10^{-11}	0.652×10^{-11}	0.861×10^{-11}
1724	0.184×10^{-10}	0.565×10^{-11}	0.169×10^{-10}	0.266×10^{-11}	0.700×10^{-11}	0.902×10^{-11}
2068	0.199×10^{-10}	0.653×10^{-11}	0.178×10^{-10}	0.286×10^{-11}	0.769×10^{-11}	0.106×10^{-10}

Table B.16: Permeation Coefficients for Ethanol–Hexane Membranes with Pure Gases in kmol/s.m^2.Pa

Pressure kPa	Shrinkage Temperature °C					
	70	75	75	80	90	90
	Coupon Number					
	2-6	1-6	4-1	5-1	6-5	4-2
	Helium Gas					
345	0.112×10^{-10}	0.134×10^{-10}	0.460×10^{-11}	0.443×10^{-11}	0.944×10^{-10}	0.108×10^{-09}
689	0.140×10^{-10}	0.201×10^{-10}	0.533×10^{-11}	0.520×10^{-11}	0.113×10^{-09}	0.106×10^{-09}
1034	0.155×10^{-10}	0.243×10^{-10}	0.547×10^{-11}	0.580×10^{-11}	0.113×10^{-09}	0.114×10^{-09}
1379	0.122×10^{-10}	0.258×10^{-10}	0.596×10^{-11}	0.626×10^{-11}	0.118×10^{-09}	0.129×10^{-09}
1724	0.157×10^{-10}	0.272×10^{-10}	0.646×10^{-11}	0.689×10^{-11}	0.122×10^{-09}	0.122×10^{-09}
2068	0.171×10^{-10}	0.279×10^{-10}	0.681×10^{-11}	0.749×10^{-11}	0.124×10^{-09}	0.137×10^{-09}
	Carbon Dioxide Gas					
345	0.635×10^{-11}	0.819×10^{-11}	0.242×10^{-11}	0.268×10^{-11}	0.452×10^{-10}	0.443×10^{-10}
689	0.728×10^{-11}	0.128×10^{-10}	0.273×10^{-11}	0.288×10^{-11}	0.465×10^{-10}	0.409×10^{-10}
1034	0.897×10^{-11}	0.165×10^{-10}	0.309×10^{-11}	0.3200-11	0.509×10^{-10}	0.422×10^{-10}
1379	0.925×10^{-11}	0.210×10^{-10}	0.338×10^{-11}	0.462×10^{-11}	0.558×10^{-10}	0.458×10^{-10}
1724	0.121×10^{-10}	0.244×10^{-10}	0.398×10^{-11}	0.509×10^{-11}	0.676×10^{-10}	0.509×10^{-10}
2068	0.153×10^{-10}	0.355×10^{-10}	0.460×10^{-11}	0.645×10^{-11}	0.707×10^{-10}	0.577×10^{-10}
	Methane Gas					
345	0.228×10^{-11}	0.176×10^{-11}	0.915×10^{-12}	0.993×10^{-12}	0.373×10^{-10}	0.714×10^{-10}
689	0.151×10^{-11}	0.579×10^{-11}	0.101×10^{-11}	0.109×10^{-11}	0.426×10^{-10}	0.709×10^{-10}
1034	0.167×10^{-11}	0.638×10^{-11}	0.116×10^{-11}	0.116×10^{-11}	0.456×10^{-10}	0.760×10^{-10}
1379	0.175×10^{-11}	0.860×10^{-11}	0.138×10^{-11}	0.140×10^{-11}	0.493×10^{-10}	0.834×10^{-10}
1724	0.190×10^{-11}	0.931×10^{-11}	0.153×10^{-11}	0.146×10^{-11}	0.535×10^{-10}	0.949×10^{-10}
2068	0.197×10^{-11}	0.105×10^{-10}	0.165×10^{-11}	0.166×10^{-11}	0.592×10^{-10}	0.980×10^{-10}

Table B.17: Permeation Coefficients for Methanol–Triethyl Amine Membranes on Methane–Carbon Dioxide Gas Mixtures in kmol/s.m^2.Pa

Composition Mole Percent Methane	Pressure kPa	Shrinkage Temperature °C			
		70	80	85	90
		Coupon Number			
		1-4	1-3	4-3	4-5
10	345	0.513×10^{-11}	0.794×10^{-11}	0.235×10^{-10}	0.316×10^{-10}
	689	0.511×10^{-11}	0.730×10^{-11}	0.249×10^{-10}	0.337×10^{-10}
	1034	0.586×10^{-11}	0.132×10^{-10}	0.267×10^{-10}	0.356×10^{-10}
	1379	0.685×10^{-11}	0.151×10^{-10}	0.281×10^{-10}	0.398×10^{-10}
	1724	0.823×10^{-11}	0.172×10^{-10}	0.280×10^{-10}	0.412×10^{-10}
	2068	0.887×10^{-11}	0.192×10^{-10}	–	–
20	345	0.420×10^{-11}	0.965×10^{-11}	0.215×10^{-10}	0.305×10^{-10}
	689	0.489×10^{-11}	0.116×10^{-10}	0.226×10^{-10}	0.325×10^{-10}
	1034	0.540×10^{-11}	0.125×10^{-10}	0.242×10^{-10}	0.356×10^{-10}
	1379	0.584×10^{-11}	0.140×10^{-10}	0.260×10^{-10}	0.390×10^{-10}
	1724	0.606×10^{-11}	0.153×10^{-10}	0.296×10^{-10}	0.441×10^{-10}
	2068	0.720×10^{-11}	0.159×10^{-10}	0.298×10^{-10}	0.450×10^{-10}
50	345	0.311×10^{-11}	0.895×10^{-11}	0.154×10^{-10}	0.243×10^{-10}
	689	0.239×10^{-11}	0.990×10^{-11}	0.184×10^{-10}	0.277×10^{-10}
	1034	0.270×10^{-11}	0.107×10^{-10}	0.183×10^{-10}	0.292×10^{-10}
	1379	0.285×10^{-11}	0.118×10^{-10}	0.195×10^{-10}	0.308×10^{-10}
	1724	0.307×10^{-11}	0.125×10^{-10}	0.210×10^{-10}	0.346×10^{-10}
	2068	0.329×10^{-11}	0.134×10^{-10}	0.229×10^{-10}	0.385×10^{-10}
80	345	0.137×10^{-11}	0.767×10^{-11}	0.144×10^{-10}	0.287×10^{-10}
	689	0.173×10^{-11}	0.100×10^{-10}	0.170×10^{-10}	0.318×10^{-10}
	1034	0.194×10^{-11}	0.111×10^{-10}	0.180×10^{-10}	0.199×10^{-10}
	1379	0.217×10^{-11}	0.121×10^{-10}	0.191×10^{-10}	0.224×10^{-10}
	1724	0.225×10^{-11}	0.129×10^{-10}	0.137×10^{-10}	0.252×10^{-10}
	2068	0.240×10^{-11}	0.135×10^{-10}	0.135×10^{-10}	0.288×10^{-10}
90	345	0.127×10^{-11}	0.797×10^{-11}	–	–
	689	0.150×10^{-11}	0.100×10^{-10}	–	–
	1034	0.174×10^{-11}	0.112×10^{-10}	–	–
	1379	0.197×10^{-11}	0.123×10^{-10}	–	–
	1724	0.213×10^{-11}	0.134×10^{-10}	–	–
	2068	0.232×10^{-11}	0.142×10^{-10}	–	–

Table B.18: Permeation Coefficients for Methanol–Isopropy Ether Membranes on Methane–Carbon Dioxide Gas Mixtures in kmol/s.m^2.Pa

Composition Mole Percent Methane	Pressure kPa	Shrinkage Temperature °C				
		70	75	80	85	90
		Coupon Number				
		1-1	1-2	4-6	4-7	4-4
10	345	0.746×10^{-11}	0.108×10^{-10}	0.150×10^{-10}	0.375×10^{-10}	0.258×10^{-11}
	689	0.844×10^{-11}	0.123×10^{-10}	0.162×10^{-10}	0.334×10^{-10}	0.287×10^{-11}
	1034	0.102×10^{-10}	0.146×10^{-10}	0.174×10^{-10}	0.321×10^{-10}	0.321×10^{-11}
	1379	0.112×10^{-10}	0.166×10^{-10}	0.185×10^{-10}	0.332×10^{-10}	0.362×10^{-11}
	1724	0.147×10^{-10}	0.180×10^{-10}	0.190×10^{-10}	0.340×10^{-10}	0.352×10^{-11}
	2068	0.152×10^{-10}	0.202×10^{-10}	–	–	–
20	345	0.696×10^{-11}	0.965×10^{-11}	0.121×10^{-10}	0.499×10^{-10}	0.275×10^{-11}
	689	0.701×10^{-11}	0.107×10^{-10}	0.124×10^{-10}	0.476×10^{-10}	0.246×10^{-11}
	1034	0.841×10^{-11}	0.116×10^{-10}	0.135×10^{-10}	0.470×10^{-10}	0.328×10^{-11}
	1379	0.876×10^{-11}	0.123×10^{-10}	0.146×10^{-10}	0.483×10^{-10}	0.362×10^{-11}
	1724	0.872×10^{-11}	0.128×10^{-10}	0.173×10^{-10}	0.479×10^{-10}	0.408×10^{-11}
	2068	0.115×10^{-10}	0.142×10^{-10}	0.165×10^{-10}	0.486×10^{-10}	0.409×10^{-11}
50	345	0.337×10^{-11}	0.645×10^{-11}	0.618×10^{-11}	0.335×10^{-10}	0.216×10^{-11}
	689	0.268×10^{-11}	0.517×10^{-11}	0.746×10^{-11}	0.245×10^{-10}	0.289×10^{-11}
	1034	0.306×10^{-11}	0.553×10^{-11}	0.760×10^{-11}	0.241×10^{-10}	0.296×10^{-11}
	1379	0.300×10^{-11}	0.579×10^{-11}	0.785×10^{-11}	0.245×10^{-10}	0.328×10^{-11}
	1724	0.325×10^{-11}	0.600×10^{-11}	0.890×10^{-11}	0.462×10^{-10}	0.349×10^{-11}
	2068	0.303×10^{-11}	0.639×10^{-11}	0.950×10^{-11}	0.481×10^{-10}	0.400×10^{-11}
80	345	0.110×10^{-11}	0.320×10^{-11}	0.457×10^{-11}	0.387×10^{-10}	0.227×10^{-11}
	689	0.123×10^{-11}	0.391×10^{-11}	0.523×10^{-11}	0.352×10^{-10}	0.304×10^{-11}
	1034	0.141×10^{-11}	0.410×10^{-11}	0.536×10^{-11}	0.210×10^{-10}	0.260×10^{-11}
	1379	0.144×10^{-11}	0.437×10^{-11}	0.571×10^{-11}	0.229×10^{-10}	0.352×10^{-11}
	1724	0.157×10^{-11}	0.461×10^{-11}	0.580×10^{-11}	0.260×10^{-10}	0.368×10^{-11}
	2068	0.156×10^{-11}	0.479×10^{-11}	0.626×10^{-11}	0.285×10^{-10}	0.400×10^{-11}
90	345	0.681×10^{-12}	0.315×10^{-11}	–	–	–
	689	0.804×10^{-12}	0.357×10^{-11}	–	–	–
	1034	0.922×10^{-12}	0.383×10^{-11}	–	–	–
	1379	0.989×10^{-12}	0.413×10^{-11}	–	–	–
	1724	0.115×10^{-11}	0.430×10^{-11}	–	–	–
	2068	0.125×10^{-11}	0.445×10^{-11}	–	–	–

Table B.19: Permeation Coefficients for Methanol–Carbon Disulfide Membranes on Methane–Carbon Dioxide Gas Mixtures in kmol/s.m^2.Pa

Composition Mole percent Methane	Pressure kPa	Shrinkage Temperature °C	
		75	85
		Coupon Number	
		[illegible]	5-7
10	345	0.454×10^{-10}	0.673×10^{-10}
	689	0.437×10^{-10}	0.611×10^{-10}
	1034	0.408×10^{-10}	0.645×10^{-10}
	1379	0.409×10^{-10}	0.660×10^{-10}
	1724	0.400×10^{-10}	0.673×10^{-10}
	2068	0.398×10^{-10}	0.724×10^{-10}
20	345	0.410×10^{-10}	0.716×10^{-10}
	689	0.406×10^{-10}	0.593×10^{-10}
	1034	0.406×10^{-10}	0.731×10^{-10}
	1379	0.409×10^{-10}	0.754×10^{-10}
	1724	0.406×10^{-10}	0.814×10^{-10}
	2068	0.406×10^{-10}	–
50	345	0.484×10^{-10}	0.830×10^{-10}
	689	0.497×10^{-10}	0.792×10^{-10}
	1034	0.485×10^{-10}	0.817×10^{-10}
	1379	0.486×10^{-10}	0.870×10^{-10}
	1724	0.476×10^{-10}	0.880×10^{-10}
	2068	0.478×10^{-10}	0.900×10^{-10}
80	345	0.533×10^{-10}	0.945×10^{-10}
	689	0.548×10^{-10}	0.872×10^{-10}
	1034	0.564×10^{-10}	0.904×10^{-10}
	1379	0.554×10^{-10}	0.920×10^{-10}
	1724	0.562×10^{-10}	0.955×10^{-10}
	2068	0.559×10^{-10}	0.101×10^{-09}
90	345	0.612×10^{-10}	0.843×10^{-10}
	689	0.614×10^{-10}	0.829×10^{-10}
	1034	0.119×10^{-10}	0.804×10^{-10}
	1379	0.600×10^{-10}	0.877×10^{-10}
	1724	0.598×10^{-10}	0.901×10^{-10}
	2068	0.606×10^{-10}	0.920×10^{-10}

Table B.20: Permeation Coefficients for Methanol–Hexane Membranes on Methane–Carbon Dioxide Gas Mixtures in kmol/s.m^2.Pa

Composition Mole Percent Methane	Pressure kPa	Shrinkage Temperature °C				
		70	75	80	85	90
		Coupon Numbers				
		2-8	6-7	5-3	2-4	5-6
10	345	0.131×10^{-10}	0.186×10^{-10}	0.609×10^{-11}	0.236×10^{-10}	0.131×10^{-10}
	689	0.122×10^{-10}	0.233×10^{-10}	0.585×10^{-11}	0.212×10^{-10}	0.129×10^{-10}
	1034	0.124×10^{-10}	0.241×10^{-10}	0.608×10^{-11}	0.224×10^{-10}	0.146×10^{-10}
	1379	0.128×10^{-10}	0.290×10^{-10}	0.681×10^{-11}	0.229×10^{-10}	0.162×10^{-10}
	1724	–	0.301×10^{-10}	0.740×10^{-11}	–	0.174×10^{-10}
	2068	0.140×10^{-10}	0.310×10^{-10}	0.830×10^{-11}	0.248×10^{-10}	0.191×10^{-10}
20	345	0.856×10^{-11}	0.140×10^{-10}	0.563×10^{-11}	0.159×10^{-10}	–
	689	0.923×10^{-11}	0.150×10^{-10}	0.472×10^{-11}	0.165×10^{-10}	0.108×10^{-10}
	1034	0.948×10^{-11}	0.165×10^{-10}	0.598×10^{-11}	0.167×10^{-10}	0.129×10^{-10}
	1379	0.101×10^{-10}	0.178×10^{-10}	0.625×10^{-11}	0.176×10^{-10}	0.145×10^{-10}
	1724	0.106×10^{-10}	0.208×10^{-10}	0.734×10^{-11}	0.181×10^{-10}	0.176×10^{-10}
	2068	0.115×10^{-10}	0.224×10^{-10}	–	0.207×10^{-10}	–
50	345	0.538×10^{-11}	0.105×10^{-10}	0.433×10^{-11}	0.871×10^{-11}	0.776×10^{-11}
	689	0.572×10^{-11}	0.107×10^{-10}	0.401×10^{-11}	0.959×10^{-11}	0.766×10^{-11}
	1034	0.654×10^{-11}	0.123×10^{-10}	0.405×10^{-11}	0.107×10^{-10}	0.762×10^{-11}
	1379	0.671×10^{-11}	0.135×10^{-10}	0.431×10^{-11}	0.108×10^{-10}	0.837×10^{-11}
	1724	0.667×10^{-11}	0.144×10^{-10}	0.437×10^{-11}	0.110×10^{-10}	0.870×10^{-11}
	2068	0.683×10^{-11}	0.149×10^{-10}	0.458×10^{-11}	0.116×10^{-10}	0.994×10^{-11}
80	345	0.455×10^{-11}	0.686×10^{-11}	0.322×10^{-11}	0.625×10^{-11}	0.549×10^{-11}
	689	0.477×10^{-11}	0.795×10^{-11}	0.293×10^{-11}	0.657×10^{-11}	0.530×10^{-11}
	1034	0.502×10^{-11}	0.876×10^{-11}	0.323×10^{-11}	0.703×10^{-11}	0.578×10^{-11}
	1379	0.213×10^{-11}	0.908×10^{-11}	0.335×10^{-11}	–	0.612×10^{-11}
	1724	0.131×10^{-11}	0.102×10^{-10}	0.350×10^{-11}	0.529×10^{-11}	0.648×10^{-11}
	2068	0.253×10^{-11}	0.108×10^{-10}	0.355×10^{-11}	0.543×10^{-11}	0.715×10^{-11}
90	345	0.349×10^{-11}	0.668×10^{-11}	0.244×10^{-11}	0.486×10^{-11}	0.441×10^{-11}
	689	0.393×10^{-11}	0.736×10^{-11}	0.261×10^{-11}	0.520×10^{-11}	0.455×10^{-11}
	1034	0.459×10^{-11}	0.823×10^{-11}	0.259×10^{-11}	0.624×10^{-11}	0.474×10^{-11}
	1379	0.479×10^{-11}	0.914×10^{-11}	0.284×10^{-11}	0.647×10^{-11}	0.530×10^{-11}
	1724	0.541×10^{-11}	0.100×10^{-10}	0.294×10^{-11}	0.698×10^{-11}	0.565×10^{-11}
	2068	0.583×10^{-11}	0.103×10^{-10}	0.313×10^{-11}	0.762×10^{-11}	0.635×10^{-11}

Table B.21: Permeation Coefficients for Ethanol–Triethyl Amine Membranes on Methane–Carbon Dioxide Gas Mixtures in kmol/s.m².Pa

Composition Mole Percent Methane	Pressure kPa	Shrinkage Temperature °C			
		70	75	85	90
		Coupon Number			
		6-6	6-8	6-1	5-2
10	345	0.300×10^{-10}	0.133×10^{-10}	0.578×10^{-10}	0.189×10^{-10}
	689	0.289×10^{-10}	0.146×10^{-10}	0.623×10^{-10}	0.159×10^{-10}
	1034	0.288×10^{-10}	0.158×10^{-10}	0.647×10^{-10}	0.188×10^{-10}
	1379	0.306×10^{-10}	0.187×10^{-10}	0.648×10^{-10}	0.207×10^{-10}
	1724	0.313×10^{-10}	0.198×10^{-10}	0.672×10^{-10}	0.229×10^{-10}
	2068	0.335×10^{-10}	0.276×10^{-10}	0.711×10^{-10}	0.253×10^{-10}
20	345	0.303×10^{-10}	0.102×10^{-10}	0.624×10^{-10}	0.177×10^{-10}
	689	0.306×10^{-10}	0.927×10^{-11}	0.454×10^{-10}	0.152×10^{-10}
	1034	0.300×10^{-10}	0.104×10^{-10}	0.475×10^{-10}	0.198×10^{-10}
	1379	0.310×10^{-10}	0.117×10^{-10}	0.541×10^{-10}	0.216×10^{-10}
	1724	0.318×10^{-10}	0.174×10^{-10}	0.686×10^{-10}	0.246×10^{-10}
	2068	0.333×10^{-10}	0.199×10^{-10}	0.733×10^{-10}	–
50	345	0.330×10^{-10}	0.788×10^{-11}	0.655×10^{-10}	0.148×10^{-10}
	689	0.316×10^{-10}	0.860×10^{-11}	0.664×10^{-10}	0.149×10^{-10}
	1034	0.333×10^{-10}	0.875×10^{-11}	0.679×10^{-10}	0.162×10^{-10}
	1379	0.320×10^{-10}	0.952×10^{-11}	0.664×10^{-10}	0.177×10^{-10}
	1724	0.326×10^{-10}	0.137×10^{-10}	0.883×10^{-10}	0.183×10^{-10}
	2068	0.338×10^{-10}	0.147×10^{-10}	0.871×10^{-10}	0.197×10^{-10}
80	345	0.380×10^{-10}	0.491×10^{-11}	0.102×10^{-09}	0.132×10^{-10}
	689	0.388×10^{-10}	0.592×10^{-11}	0.920×10^{-10}	0.135×10^{-10}
	1034	0.372×10^{-10}	0.654×10^{-11}	0.754×10^{-10}	0.146×10^{-10}
	1379	0.370×10^{-10}	0.707×10^{-11}	0.743×10^{-10}	0.157×10^{-10}
	1724	0.393×10^{-10}	0.123×10^{-10}	0.107×10^{-09}	0.169×10^{-10}
	2068	0.382×10^{-10}	0.130×10^{-10}	0.107×10^{-09}	0.177×10^{-10}
90	345	0.408×10^{-10}	0.474×10^{-11}	0.928×10^{-10}	0.860×10^{-11}
	689	0.403×10^{-10}	0.566×10^{-11}	0.802×10^{-10}	0.100×10^{-10}
	1034	0.396×10^{-10}	0.628×10^{-11}	0.786×10^{-10}	0.109×10^{-10}
	1379	0.412×10^{-10}	0.701×10^{-11}	0.825×10^{-10}	0.123×10^{-10}
	1724	0.414×10^{-10}	0.122×10^{-10}	0.856×10^{-10}	0.128×10^{-10}
	2068	0.425×10^{-10}	0.126×10^{-10}	0.908×10^{-10}	0.137×10^{-10}

Table B.22: Permeation Coefficients for Ethanol–Isopropyl Ether Membranes on Methane–Carbon Dioxide Gas Mixtures in kmol/s.m^2.Pa

Composition Mole Percent Methane	Pressure kPa	Shrinkage Temperature °C			
		70	80	85	90
		Coupon Number			
		2-3	2-5	1-8	2-2
10	345	0.259×10^{-10}	0.299×10^{-10}	0.736×10^{-11}	0.100×10^{-10}
	689	0.258×10^{-10}	0.291×10^{-10}	0.919×10^{-11}	0.104×10^{-10}
	1034	0.316×10^{-10}	0.311×10^{-10}	0.112×10^{-10}	0.115×10^{-10}
	1379	0.320×10^{-10}	0.332×10^{-10}	0.128×10^{-10}	0.119×10^{-10}
	1724	–	–	0.156×10^{-10}	–
	2068	0.372×10^{-10}	0.385×10^{-10}	0.165×10^{-10}	0.143×10^{-10}
20	345	0.196×10^{-10}	0.228×10^{-10}	0.726×10^{-11}	0.723×10^{-11}
	689	0.236×10^{-10}	0.237×10^{-10}	0.822×10^{-11}	0.776×10^{-11}
	1034	0.237×10^{-10}	0.260×10^{-10}	0.964×10^{-11}	0.853×10^{-11}
	1379	0.269×10^{-10}	0.282×10^{-10}	0.103×10^{-10}	0.960×10^{-11}
	1724	0.286×10^{-10}	0.298×10^{-10}	0.108×10^{-10}	0.985×10^{-11}
	2068	0.314×10^{-10}	0.321×10^{-10}	0.132×10^{-10}	0.114×10^{-10}
50	345	0.141×10^{-10}	0.176×10^{-10}	0.616×10^{-11}	0.453×10^{-11}
	689	0.173×10^{-10}	0.189×10^{-10}	0.418×10^{-11}	0.538×10^{-11}
	1034	0.199×10^{-10}	0.204×10^{-10}	0.528×10^{-11}	0.506×10^{-11}
	1379	0.208×10^{-10}	0.217×10^{-10}	0.514×10^{-11}	0.559×10^{-11}
	1724	0.217×10^{-10}	0.232×10^{-10}	0.553×10^{-11}	0.615×10^{-11}
	2068	0.229×10^{-10}	0.251×10^{-10}	0.568×10^{-11}	0.625×10^{-11}
80	345	0.147×10^{-10}	0.156×10^{-10}	0.233×10^{-11}	0.483×10^{-11}
	689	0.156×10^{-10}	0.164×10^{-10}	0.313×10^{-11}	0.532×10^{-11}
	1034	0.189×10^{-10}	0.171×10^{-10}	0.373×10^{-11}	0.555×10^{-11}
	1379	0.988×10^{-11}	0.111×10^{-10}	0.387×10^{-11}	0.370×10^{-11}
	1724	0.985×10^{-11}	0.106×10^{-10}	0.441×10^{-11}	0.333×10^{-11}
	2068	0.117×10^{-10}	0.981×10^{-11}	0.445×10^{-11}	0.437×10^{-11}
90	345	0.132×10^{-10}	0.130×10^{-10}	0.238×10^{-11}	0.873×10^{-11}
	689	0.148×10^{-10}	0.142×10^{-10}	0.300×10^{-11}	0.972×10^{-11}
	1034	0.193×10^{-10}	0.162×10^{-10}	0.339×10^{-11}	0.110×10^{-10}
	1379	0.208×10^{-10}	0.179×10^{-10}	0.372×10^{-11}	0.118×10^{-10}
	1724	0.221×10^{-10}	0.199×10^{-10}	0.409×10^{-11}	0.130×10^{-10}
	2068	0.237×10^{-10}	0.220×10^{-10}	0.442×10^{-11}	0.137×10^{-10}

Table B.23: Permeation Coefficients for Ethanol–Carbon Disulfide Membranes on Methane–Carbon Dioxide Gas Mixtures in kmol/s.m^2.Pa

Composition Mole Percent Methane	Pressure kPa	Shrinkage Temperature °C					
		70	75	75	80	85	90
		Coupon Number					
		6-3	5-5	6-2	2-7	6-4	5-4
10	345	0.207×10^{-10}	0.994×10^{-11}	0.153×10^{-10}	0.164×10^{-10}	0.122×10^{-10}	0.166×10^{-10}
	689	0.238×10^{-10}	0.944×10^{-11}	0.168×10^{-10}	0.149×10^{-10}	0.142×10^{-10}	0.168×10^{-10}
	1034	0.257×10^{-10}	0.101×10^{-10}	0.186×10^{-10}	0.153×10^{-10}	0.137×10^{-10}	0.188×10^{-10}
	1379	0.289×10^{-10}	0.111×10^{-10}	0.206×10^{-10}	0.155×10^{-10}	0.159×10^{-10}	0.227×10^{-10}
	1724	0.318×10^{-10}	0.124×10^{-10}	0.216×10^{-10}	-	0.171×10^{-10}	0.245×10^{-10}
	2068	0.345×10^{-10}	0.133×10^{-10}	0.231×10^{-10}	0.166×10^{-10}	0.182×10^{-10}	-
20	345	0.175×10^{-10}	0.874×10^{-11}	0.133×10^{-10}	0.101×10^{-10}	0.786×10^{-11}	0.147×10^{-10}
	689	0.165×10^{-10}	0.751×10^{-11}	0.141×10^{-10}	0.103×10^{-10}	0.891×10^{-11}	0.123×10^{-10}
	1034	0.183×10^{-10}	0.970×10^{-11}	0.156×10^{-10}	0.114×10^{-10}	0.966×10^{-11}	0.159×10^{-10}
	1379	0.205×10^{-10}	0.108×10^{-10}	0.176×10^{-10}	0.115×10^{-10}	0.106×10^{-10}	0.180×10^{-10}
	1724	0.234×10^{-10}	0.126×10^{-10}	0.184×10^{-10}	0.118×10^{-10}	0.124×10^{-10}	0.221×10^{-10}
	2068	0.264×10^{-10}	-	0.200×10^{-10}	0.129×10^{-10}	0.132×10^{-10}	-
50	345	0.136×10^{-10}	0.575×10^{-11}	0.125×10^{-10}	0.508×10^{-11}	0.659×10^{-11}	0.988×10^{-11}
	689	0.147×10^{-10}	0.573×10^{-11}	0.136×10^{-10}	0.513×10^{-11}	0.733×10^{-11}	0.967×10^{-11}
	1034	0.163×10^{-10}	0.629×10^{-11}	0.146×10^{-10}	0.668×10^{-11}	0.810×10^{-11}	0.106×10^{-10}
	1379	0.176×10^{-10}	0.725×10^{-11}	0.152×10^{-10}	0.658×10^{-11}	0.870×10^{-11}	0.115×10^{-10}
	1724	0.196×10^{-10}	0.758×10^{-11}	0.163×10^{-10}	0.635×10^{-11}	0.919×10^{-11}	0.121×10^{-10}
	2068	0.213×10^{-10}	0.830×10^{-11}	0.179×10^{-10}	0.663×10^{-11}	0.987×10^{-11}	0.142×10^{-10}
80	345	0.104×10^{-10}	0.427×10^{-11}	0.114×10^{-10}	0.294×10^{-11}	0.497×10^{-11}	0.721×10^{-11}
	689	0.126×10^{-10}	0.447×10^{-11}	0.132×10^{-10}	0.281×10^{-11}	0.570×10^{-11}	0.755×10^{-11}
	1034	0.140×10^{-10}	0.506×10^{-11}	0.141×10^{-10}	0.331×10^{-11}	0.622×10^{-11}	0.830×10^{-11}
	1379	0.156×10^{-10}	0.552×10^{-11}	0.149×10^{-10}	0.179×10^{-11}	0.661×10^{-11}	0.909×10^{-11}
	1724	0.176×10^{-10}	0.608×10^{-11}	0.156×10^{-10}	0.200×10^{-11}	0.722×10^{-11}	0.973×10^{-11}
	2068	0.185×10^{-10}	0.654×10^{-11}	0.167×10^{-10}	0.119×10^{-11}	0.773×10^{-11}	0.111×10^{-10}
90	345	0.108×10^{-10}	0.361×10^{-11}	0.138×10^{-10}	0.177×10^{-11}	0.479×10^{-11}	0.582×10^{-11}
	689	0.124×10^{-10}	0.381×10^{-11}	0.126×10^{-10}	0.196×10^{-11}	0.538×10^{-11}	0.661×10^{-11}
	1034	0.139×10^{-10}	0.428×10^{-11}	0.138×10^{-10}	0.257×10^{-11}	0.588×10^{-11}	0.708×10^{-11}
	1379	0.162×10^{-10}	0.495×10^{-11}	0.150×10^{-10}	0.311×10^{-11}	0.667×10^{-11}	0.789×10^{-11}
	1724	0.175×10^{-10}	0.537×10^{-11}	0.161×10^{-10}	0.332×10^{-11}	0.707×10^{-11}	0.892×10^{-11}
	2068	0.187×10^{-10}	0.615×10^{-11}	0.172×10^{-10}	0.371×10^{-11}	0.761×10^{-11}	0.991×10^{-11}

Table B.24: Permeation Coefficients for Ethanol–Hexane Membranes on Methane–Carbon Dioxide Gas Mixtures in kmol/s.m^2.Pa

Composition Mole Percent Methane	Pressure kPa	Shrinkage Temperature °C					
		70	75	75	80	90	90
		Coupon Number					
		2-6	1-6	4-1	5-1	6-5	4-2
10	345	0.577×10^{-11}	0.725×10^{-11}	0.242×10^{-11}	0.262×10^{-11}	0.407×10^{-10}	0.448×10^{-10}
	689	0.550×10^{-11}	0.106×10^{-10}	0.270×10^{-11}	0.270×10^{-11}	0.415×10^{-10}	0.493×10^{-10}
	1034	0.544×10^{-11}	0.135×10^{-10}	0.303×10^{-11}	0.301×10^{-11}	0.462×10^{-10}	0.526×10^{-10}
	1379	0.563×10^{-11}	0.154×10^{-10}	0.288×10^{-11}	0.345×10^{-11}	0.526×10^{-10}	0.576×10^{-10}
	1724	–	0.177×10^{-10}	0.311×10^{-11}	0.376×10^{-11}	0.574×10^{-10}	0.601×10^{-10}
	2068	0.652×10^{-11}	0.201×10^{-10}	–	0.435×10^{-11}	0.624×10^{-10}	–
20	345	0.391×10^{-11}	0.862×10^{-11}	0.187×10^{-11}	0.226×10^{-11}	0.354×10^{-10}	0.480×10^{-10}
	689	0.376×10^{-11}	0.106×10^{-10}	0.234×10^{-11}	0.205×10^{-11}	0.390×10^{-10}	0.507×10^{-10}
	1034	0.409×10^{-11}	0.118×10^{-10}	0.263×10^{-11}	0.272×10^{-11}	0.414×10^{-10}	0.577×10^{-10}
	1379	0.408×10^{-11}	0.132×10^{-10}	0.286×10^{-11}	0.268×10^{-11}	0.428×10^{-10}	0.640×10^{-10}
	1724	0.454×10^{-11}	0.144×10^{-10}	0.324×10^{-11}	0.371×10^{-11}	0.492×10^{-10}	0.740×10^{-10}
	2068	0.495×10^{-11}	0.169×10^{-10}	0.330×10^{-11}	–	0.530×10^{-10}	0.723×10^{-10}
50	345	0.206×10^{-11}	0.832×10^{-11}	0.143×10^{-11}	0.170×10^{-11}	0.350×10^{-10}	0.506×10^{-10}
	689	0.131×10^{-11}	0.803×10^{-11}	0.150×10^{-11}	0.179×10^{-11}	0.379×10^{-10}	0.604×10^{-10}
	1034	0.158×10^{-11}	0.897×10^{-11}	0.171×10^{-11}	0.189×10^{-11}	0.425×10^{-10}	0.628×10^{-10}
	1379	0.831×10^{-12}	0.967×10^{-11}	0.179×10^{-11}	0.206×10^{-11}	0.451×10^{-10}	0.670×10^{-10}
	1724	0.107×10^{-11}	0.104×10^{-10}	0.199×10^{-11}	0.217×10^{-11}	0.478×10^{-10}	0.727×10^{-10}
	2068	0.127×10^{-11}	0.112×10^{-10}	0.216×10^{-11}	0.237×10^{-11}	0.494×10^{-10}	0.790×10^{-10}
80	345	0.189×10^{-11}	0.436×10^{-11}	0.105×10^{-11}	0.145×10^{-11}	0.361×10^{-10}	0.555×10^{-10}
	689	0.186×10^{-11}	0.693×10^{-11}	0.132×10^{-11}	0.133×10^{-11}	0.405×10^{-10}	0.459×10^{-10}
	1034	0.182×10^{-11}	0.798×10^{-11}	0.140×10^{-11}	0.142×10^{-11}	0.430×10^{-10}	0.530×10^{-10}
	1379	0.528×10^{-12}	0.856×10^{-11}	0.162×10^{-11}	0.151×10^{-11}	0.447×10^{-10}	0.587×10^{-10}
	1724	0.696×10^{-12}	0.986×10^{-11}	0.166×10^{-11}	0.168×10^{-11}	0.483×10^{-10}	0.623×10^{-10}
	2068	0.654×10^{-12}	0.105×10^{-10}	0.175×10^{-11}	0.181×10^{-11}	0.479×10^{-10}	0.904×10^{-10}
90	345	0.153×10^{-11}	0.523×10^{-11}	–	0.762×10^{-12}	0.366×10^{-10}	–
	689	0.174×10^{-11}	0.678×10^{-11}	–	0.918×10^{-12}	0.388×10^{-10}	–
	1034	0.178×10^{-11}	0.776×10^{-11}	–	0.106×10^{-11}	0.429×10^{-10}	–
	1379	0.185×10^{-11}	0.889×10^{-11}	–	0.137×10^{-11}	0.481×10^{-10}	–
	1724	0.188×10^{-11}	0.986×10^{-11}	–	0.122×10^{-11}	0.498×10^{-10}	–
	2068	0.196×10^{-11}	0.106×10^{-10}	–	0.139×10^{-11}	0.504×10^{-10}	–

Appendix C

Model Figures

The results can be seen in Figures C.1 to C.3. The Surface-Force-Pore-Flow mechanism is used to represent the gas separation by permeation under pressure through asymmetric membranes. Under this mechanism, the transport model (developed further by Minhas) predicted the membrane performance. Figure C.1 shows experimental separation factor versus calculated separation factor. Experimental versus calculated of the permeation coefficient, Figure C.2 is slightly skewed to one side. The last figure, Figure C.3 is a plot of experimental mole percent methane versus calculated mole percent methane in the permeate gas.

Table C.1: Average Pore Radius in Angtroms Calculated using a Triangular Distribution with Pure Helium Gas

Second Solvents Used	Shrinkage Temperature °C	First Solvents					
		Methanol			Ethanol		
		Coupon Number	Radius	Standard Deviation	Coupon Number	Radius	Standard Deviation
Triethyl-amine	70	1-4	2.50	1.60	6-6	11.50	8.25
	70	–	–	–	2-1	8.00	1.10
	75	–	–	–	6-8	11.50	5.50
	80	1-3	6.25	1.30	–	–	–
	85	4-3	6.00	1.25	6-1	13.00	7.00
	90	4-5	18.50	18.50	5-2	4.00	4.00
Isopropyl-ether	70	1-1	4.00	1.50	2-3	5.50	1.40
	75	1-2	5.75	1.10	–	–	–
	80	4-6	25.50	9.00	2-5	7.25	1.30
	85	4-7	11.00	2.50	1-8	5.75	1.30
	90	4-4	7.50	2.25	2-2	9.75	1.10
Carbon disulfide	70	–	–	–	6-3	12.50	10.75
	75	1-5	24.50	1.01	5-5	45.00	18.00
	75	–	–	–	6-2	13.50	5.75
	80	–	–	–	2-7	9.50	1.00
	85	5-7	5.00	1.75	6-4	12.00	6.00
	90	–	–	–	5-4	4.00	3.00
Hexane	70	2-8	10.75	1.01	2-6	10.75	1.00
	75	6-7	9.50	9.00	1-6	7.75	1.10
	75	–	–	–	4-1	3.50	3.00
	80	5-3	50.00	20.50	5-1	7.00	6.50
	85	2-4	10.75	1.01	–	–	–
	90	5-6	37.50	25.25	6-5	12.00	12.00
	90	–	–	–	4-2	29.00	12.50

Table C.2: Average Pore Radius in Angtroms Calculated using a Lognormal Distribution with Pure Helium Gas

Second Solvents Used	Shrinkage Temperature °C	First Solvents					
		Methanol			Ethanol		
		Coupon Number	Radius	Standard Deviation	Coupon Number	Radius	Standard Deviation
Triethyl-amine	70	1-4	2.50	1.60	6-6	6.25	1.30
	70	–	–	–	2-1	8.00	1.10
	75	–	–	–	6-8	6.25	1.20
	80	1-3	6.25	1.30	–	–	–
	85	4-3	7.25	1.20	6-1	6.50	1.30
	90	4-5	10.25	1.10	5-2	4.50	1.40
Isopropyl-ether	70	1-1	4.00	1.50	2-3	5.50	1.40
	75	1-2	5.75	1.10	–	–	–
	80	4-6	6.00	1.30	2-5	7.25	1.30
	85	4-7	11.50	1.20	1-8	5.75	1.30
	90	4-4	7.25	1.10	2-2	9.75	1.10
Carbon disulfide	70	–	–	–	6-3	6.75	1.30
	75	1-5	24.50	1.01	5-5	3.00	1.80
	75	–	–	–	6-2	7.00	1.20
	80	–	–	–	2-7	9.50	1.00
	85	5-7	5.25	1.10	6-4	6.50	1.20
	90	–	–	–	5-4	5.25	1.10
Hexane	70	2-8	10.75	1.01	2-6	10.75	1.00
	75	6-7	5.75	1.30	1-6	7.75	1.10
	75	–	–	–	4-1	5.50	1.50
	80	5-3	4.50	1.60	5-1	6.25	1.40
	85	2-4	10.75	1.01	–	–	–
	90	5-6	1.00	2.30?	6-5	5.50	1.40
	90	–	–	–	4-2	25.75	1.50

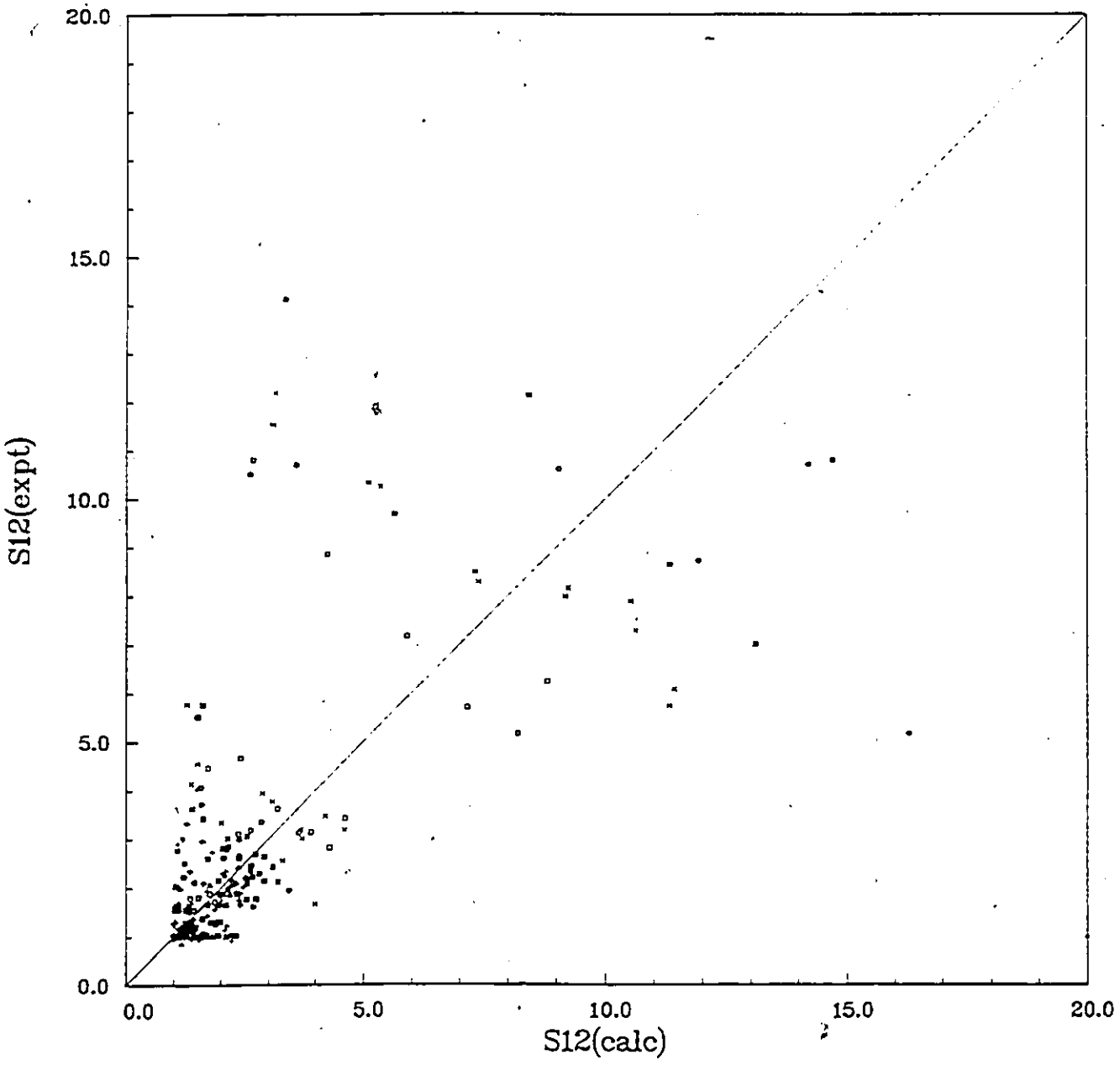

Figure C.1: Experimental Separation Factor Versus Calculated Separation Factor.

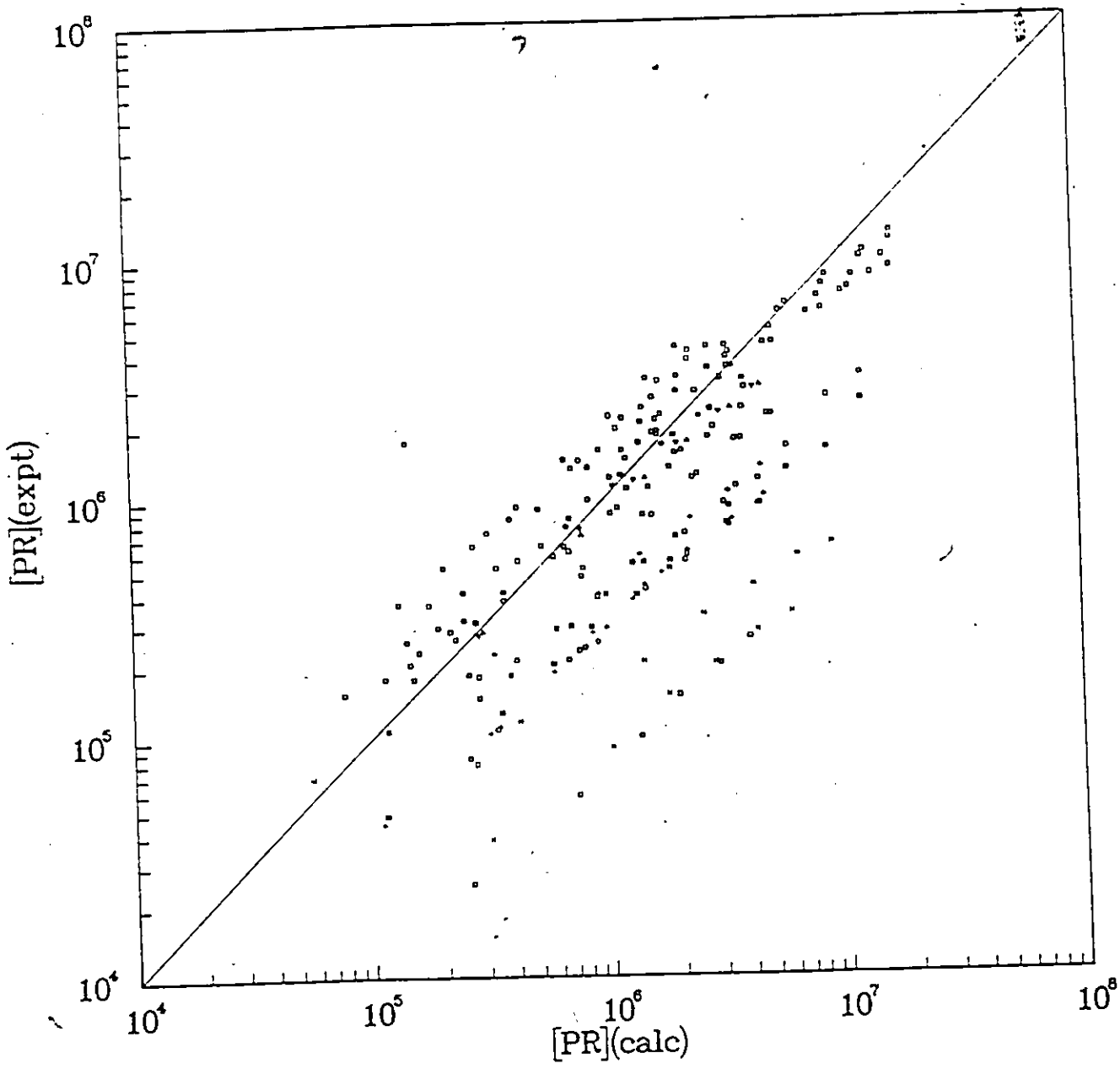

Figure C.2: Experimental Permeation Coefficient Versus Calculated Permeation Coefficient.

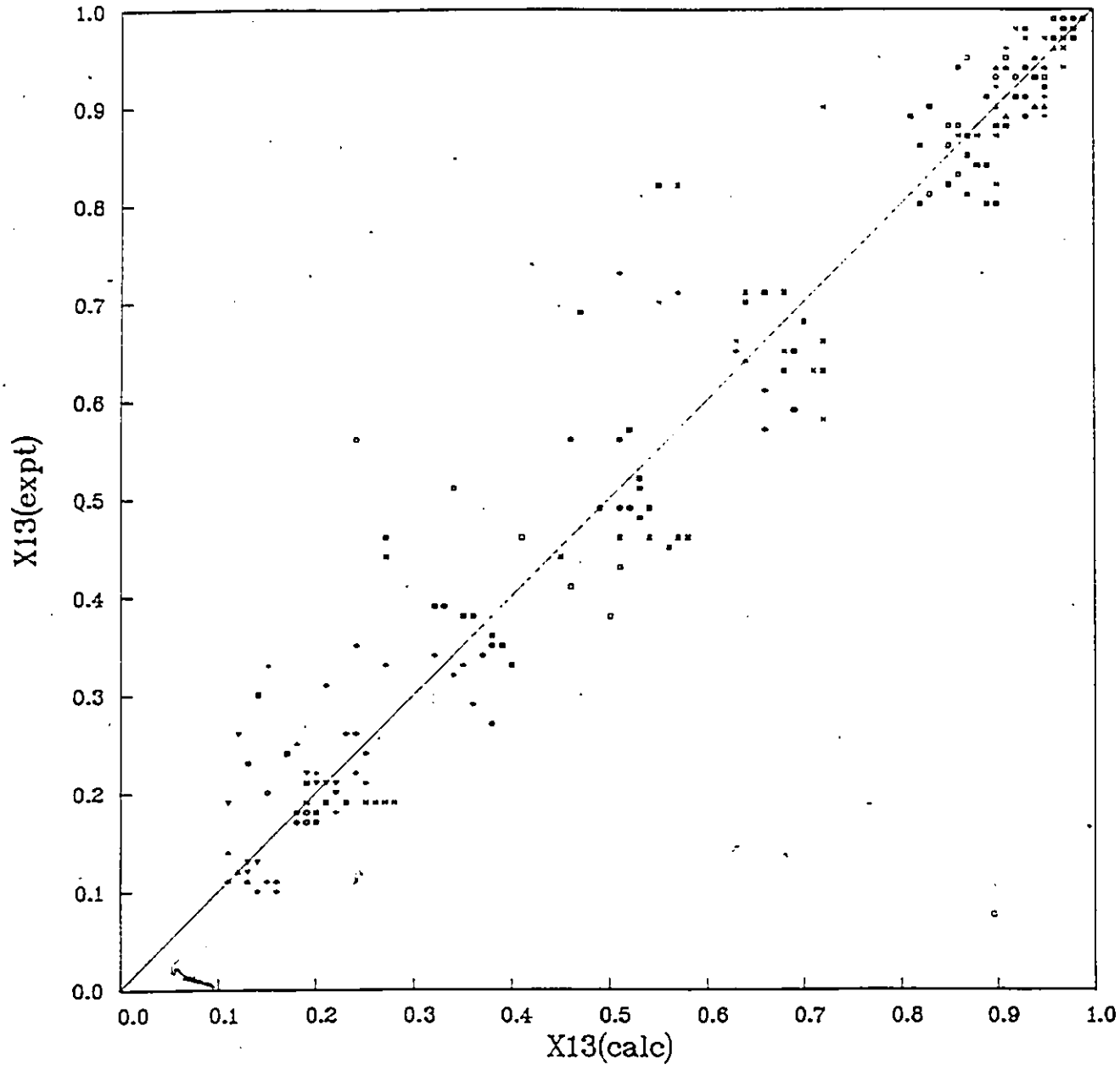

Figure C.3: Experimental Mole Percent Methane Versus Calculated Mole Percent Methane.

Abstract

The development by Loeb and Sourirajan of an asymmetric membrane with a thin separating layer and a larger porous layer made membranes as a liquid separation technique feasible. However, these membranes have a high water content. A good method for removing the water and keeping the structure intact is necessary in order to yield a dry membrane suitable for gas separation.

The solvent exchange technique is used in this study to dry asymmetric cellulose acetate membranes. The effects of various factors in the drying procedure are investigated. The separation factors and permeation coefficients of a CO_2–CH_4 gas mixture are used to evaluate the performance of the dried membranes. A pore formation mechanism is proposed.